3-D CRUSTAL STRUCTURE OF THE SİMAV-KÜTAHYA AND SURROUNDING REGIONS

by

Nuray Duran

B.S, Geophysical Engineering, Kocaeli University, 2007

Submitted to the Kandilli Observatory and Earthquake
Research Institute in partial fulfillment of
the requirements for the degree of
Master of Science

Graduate Program in Geophysics

Boğaziçi University

2017

3-D CRUSTAL STRUCTURE OF THE SİMAV-KÜTAHYA AND SURROUNDING REGIONS

APPROVED BY:

Asst. Prof. Dr. Ali Özgün Konca ……
(Thesis Supervisor)

Prof. Dr. Nurcan Meral Özel ……

Prof. Dr. Şerif Barış ……
(Kocaeli University)

DATE OF APPROVAL: 19/04/2017

ACKNOWLEDGEMENTS

Firstly, I would like to express my sincere gratitude to my thesis supervisor, Ass. Prof. Dr. Ali Özgün Konca and Prof. Dr. Nurcan Meral Özel for their guidance, help and support during my thesis study.

I am grateful to the director of Kocaeli University, Earth and Space Sciences Research Center, Prof. Dr. Şerif Barış for his comments, suggestions, guidance and support during my thesis.

I have benefited from the data and catalogs of National Earthquake Monitoring Centre, KOERI and Disaster and Emergency Management Precidensy, AFAD. I thank the all staff in there.

My special thanks are to Prof. Dapeng Zhao from Tohoku University Research Center for Prediction of Earthquakes & Volcanic Eruptions Graduate School of Science, for permission to use his tomography code TOMOG3D. I also would like to Prof. Dr. Junichi Nakajima from Tokyo Institute of Gechnology, for providing me some his codes and GMT scripts.

My other special thanks are to Boğaziçi University Res. Assist. Dr. Gülten Polat for her patience, support, comments and friendship. I would like to thank to Ass. Prof. Dr. Berna Tunç, Res. Ass. Dr. Deniz Çaka from Kocaeli University who spent their invaluable time with me. They helped me about running and teaching computer programs, technical difficulties and made useful suggestions.

Lastly, my special thanks are for my mother Şayegan Duran, my father Hüseyin Duran, my elder sister İlkay Duran Altınışık and my brother-in-law Mehmet Altınışık. Without their patience, support and understanding I would not be able to complete this thesis.

ABSTRACT

3-D CRUSTAL STRUCTURE OF THE SİMAV-KÜTAHYA AND SURROUNDING REGIONS

Kütahya and surroundings are quite complex structures from a tectonic and geological perspective. On May 19, 2011, an earthquake of magnitude M = 5.9 occurred in Simav.

The purpose of this thesis is determination of the 3-D seismic velocity structure applying the local earthquake tomography method, using earthquakes that occurred between the years 2010 and 2015 in Kütahya Simav and surroundings. The signifigance of this study is that the first 1-D and 3-D tomographic inversion for Simav, Kütahya and surroundings is done by this study. The region's 1-D velocity model, 3-D velocity model and crustal structure are obtained.

In this study, the 3-D velocity distribution up to 30 km depth of upper crust of the study area is determined with tomographic inversion methods. For this purpose, by creating data sets, travel time of phases were prepared by tomographic inversion format, appropriate model structure has been created, Vp, Vs and Vp/Vs models that obtained with appropriate resolution parameters and tomographic inversion, has been interpreted with geological and tectonic features of the area.

At 30 km depth, P and S waves velocity structure of Kütahya, Simav and surroundings were obtained. The Graben system of the region is supported by the velocity cross-section obtained. The depth of the graben is determined as 20 km. The relationship between the hypocentre of the recorded earthquakes in the region and Vp, Vs, and Vp/Vs anomalies has been revealed with horizontal and vertical cross-sections. Comments are made about the structural differences of the region’s P wave and S wave velocity information and the physical properties of the rock’s Vp/Vs ratio information. Fault systems, potential fault zones and earthquake activity of the region are discussed with the combined results of the study.

ÖZET

SİMAV-KÜTAHYA VE ÇEVRESİNİN 3 BOYUTLU KABUK YAPISININ BELİRLENMESİ

Kütahya ve civarı tektonik ve jeolojik açıdan açıdan oldukça karmaşık bir yapıya sahiptir. Simav'da 19 Mayıs 2011'de M=5.9 büyüklüğünde bir deprem meydana gelmiştir.

Bu tezin amacı, 2010 – 2015 yılları arasında Kütahya Simav bölgesi ve çevresinde meydana gelen depremleri kullanarak, yerel deprem tomografisi yöntemi ile bölgenin 3-B sismik hız yapısının belirlenmesidir. Bu çalışmanın önemi Simav, Kütahya ve çevresi için yapılmış olan ilk 3-B tomografi çalışmasıdır. Bu bağlamda bölgenin 1-B hız modeli, 3-B hız modeli ve kabuk yapısı elde edilmiştir.

Bu çalışmada, çalışma bölgesinin 30 km derinliğe kadar olan üst kabuğuna ait 3-boyutlu sismik hız dağılımı, tomografik ters çözüm yöntemleri ile belirlenmiştir. Bu amaçla, önce veri setleri oluşturularak fazlara ait seyahat zamanlarının tomografik ters çözüm formatında hazırlanması, uygun model yapısının oluşturulması, uygun çözüm parametreleri ile tomografik ters çözüm işlemlerinin yapılmıştır. Aynı zamanda elde edilen Vp, Vs ve Vp/Vs modellerinin, bölgenin jeolojik ve tektonik özellikleri ile birlikte yorumlanması, tez kapsamında uygulanmıştır.

Bu çalışma sonucunda, Kütahya Simav bölgesi ve civarının 30 km'ye kadar olan P ve S dalga hızı yapısı ve Vp/Vs oranları elde edilmiştir. Elde edilen hız kesitleri ile bölgenin graben sistemi desteklenmiştir. Grabenin yaklaşık derinliği 20 km olarak belirlenmiştir. Bölgede kaydedilen depremlerin odakları ile Vp, Vs ve Vp/Vs anomalileri arasındaki ilişki alınan derinlik kesitleri ile ortaya konmuştur. Bölgeye ait P- dalga hızı, S- dalga hızı bilgisi bölgenin yapısal farklılıkları hakkında, Vp/Vs oranı bilgisi ise kayaçların fiziksel özellikleri hakkında yorum yapılabilmesini sağlamıştır. Bölgeye ait fay sistemleri, olası fay zonları ve depremsellik çalışma sonuçları ile birleştirilerek tartışılmıştır.

TABLE OF CONTENTS

ACKNOWLEDGEMENTS iii
ABSTRACT iv
ÖZET v
TABLE OF CONTENTS vi
LIST OF FIGURES ix
LIST OF TABLES xiv
LIST OF SYMBOLS xv
LIST OF ABBREVIATIONS xvi
1. INTRODUCTION 1
2. TECTONIC STRUCTURE AND GEOLOGY 2
2.1. Tectonic Structure of Kütahya Simav Region 2
2.2. Geology 5
3. SEISMICITY AND DATA 7
3.1. Seismicity of Simav and Surrounding Regions 7
3.2. Data and Solution Quality 10
4. 3-D VELOCITY TOMOGRAPHY 12
4.1. Seismic Tomography Methods 12
4.1.1. According to the Type of Source 12
4.1.2. According to Distance Between the Source and the Receiver 13
4.1.3. According to Types of Data 14
4.2. Local Earthquake Tomography (LET) 14
4.2.1. Modelling of Velocity Structure 15
4.2.2. Ray Tracing and Travel Time 19
4.2.3. 3-D Inversion 21
4.2.4. Evaluation of Resolution Quality 24
5. METHODOLOGY OF TOMOGRAPHY 26
5.1. 1-D Local Earthquake Tomography 26

5.1.1. Calculation Steps of the 1-D Minimum Velocity Model 26
5.1.3.1. Establishing the Priori 1-D Model(s) 26
5.1.3.2. Establishing the Geometry and the Velocity Intervals of Potential 1-D Model(s)..... 27
5.1.3.3. Relocation and Final Selection of Events 28
5.2. 3-D Tomography Program TOMOG3D 28
5.2.1. Synthetic Checkerboard Resolution Test 29
5.2.2. Ray Density Approach 31
5.3. Calculation Steps of 1-D Minimum Velocity Model for Kütahya, Simav and Surrounding Areas 32
6. 3-D TOMOGRAPHIC INVERSION FOR THE KÜTAHYA, SİMAV AND SURROUNDING REGIONS 37
6.1. Data Selection 37
6.2. Velocity Model Parameterization 43
6.3. Control Parameters 43
6.4. Resolution Tests 45
6.4.1. Synthetic Checkerboard Resolution Test 45
6.4.2. Ray Density 47
6.5. Results of 3-D Tomographic Inversions 49
6.5.1. P Phase Results 49
6.5.2. S Phase Results 53
6.5.3. Vp/Vs Results 56
7. DISCUSSION AND CONCLUSIONS 62
REFERENCES 67
APPENDIX A 82
Data Selection Criterias: 82
Station Distributions For 3 Different Data Sets: 83
Original Data Sets For 1-D Relocation: 84
Selected Earthquake Distribution For 3-D Inversion: 85
Grid Distribution Results: 86
Checkerboard Resolution Test Results: 86

Ray Density Results: 87
P Wave 3-D Tomography Results: 90
S Wave 3-D Tomography Results: 94
Vp/Vs Ratio 3-D Tomography Results: 98

LIST OF FIGURES

Figure 2.1. Simplified tectonic map of Turkey and surrounding regions (Koçyiğit and Deveci, 2007). 3

Figure 2.2. Graben distribution in the western Anatolia and major structural and tectonic elements of western Anatolia Neotectonics of Turkey –asynthesis. Red labeled points show the major towns and cities in the area. (Bozkurt, 2001) 3

Figure 2.3. Detailed tectonic features of the study area (Koçyiğit, 1984) 4

Figure 2.4. Geological map of Simav and surrounding regions (Aydan and Kumsar, 2011; modified from Oygür and Erler, 2000). 6

Figure 3.1. Seismicity map of Turkey between 1900-2015 (KOERI, 2015). Circle indicates stuy area. 8

Figure 4.1. Modelling of earth structure for (a) local rays and (b) teleseismic rays (from Hirahara, 1993) 13

Figure 4.2. Flow chart of the calculation steps of the study (modified from Kaypak, 2007). 15

Figure 4.3. (a) Stable velocity blocks (Aki and Lee, 1976), (b) lateral variant layers, (c) model consisting from a grid of nodes (Thurber, 1983). Dashed lines show the fields calculated by interpolation. 16

Figure 4.4. Eight grid points surrounding Q (from Zhao, 1991) 17

Figure 4.5. (a) Shoot method, (b) simple representation of the bending method 20

Figure 4.6. 3-D schematic representation of ray paths between hypocenter and seismic stations for the study region. Blue triangles represent seismic stations and red stars show hypocenters, gray lines show ray paths (from Kaypak 2002).....23

Figure 4.7. Schematic representation of ray number approach 24

Figure 5.1. 1-D velocity model obtained from VELEST software of the study region. Continuous lines represent P waves and dashed lines represents S waves.....28

Figure 5.2. Horizontal view of P-wave checkerboard results with after inversion. 30

Figure 5.3. Ray density distribution map.....31

Figure 5.4. Schematic view of the adapted 1-D velocity model from VELEST results. Solid lines represent P-wave velocity, dashed lines denote S-wave velocity. 33

Figure 5.5. Schematic view of Wadati diagram. P_time is the P arrival time, S-time is the S arrival time, O_time is the Origin time of the earthquake. 34

Figure 6.1. Schematic view of seismic station distribution used for tomographic inversion. 38

Figure 6.2. Initial (original) seismicity distribution for the combined data.....40

Figure 6.3. Seismicity map of selected events from the combined data set for inversion...42

Figure 6.4. (a) Damping factor (b) Travel Time Residuals. 44

Figure 6.5. Plan (above map) and E-W cross sectional view(below) of variable grid distribuiton. 46

Figure 6.6. Results for the checkerboard resolution test for P wave. The depth of each layer is shown on the upper right of each map. 47

Figure 6.7. Ray density for each grid for the combined data. 48

Figure 6.8. P wave velocity perturbations perturbations.obtained by the inversion for the integrated data and location. Blue and red colors represent high and low velocity perturbations. 51

Figure 6.9. S wave velocity perturbations got by the inversion for the integrated data. 54

Figure 6.10. Horizontal cross section of Vp/Vs ratio's values obtained by the inversion. Blue and yellow colors show low and high Vp/Vs ratio. 56

Figure 6.11. In the E-W direction along 39.15°N vertical cross section of velocity perturbation for (a) the P wave, (b) the S wave and (c) Vp/Vs. 59

Figure 6.12. In the N-S direction along 29.10°E vertical cross section of velocity perturbation for (a) the P wave, (b) the S wave and (c) Vp/Vs ratio. 61

Figure A.1. Schematic view of used 1-D velocity models for location of earthquakes for AFAD(left), KOERI(middle), and Combined data set(right). Solid lines denote P-wave velocity, dashed lines denote the S-wave velocity. 82

Figure A.2. Schematic view of Wadati diagram for AFAD(left), KOERI(middle), and Combined data set(right). 83

Figure A.3. Map view of the station distribution of the study region for AFAD(left), KOERI(middle), Combined data set(right) 83

Figure A.4. Seismicity and station distribution of original data for AFAD(left), KOERI(middle), Combined data set (right). Red triangles show seismic stations and black dots show earthquakes. 84

Figure A.5. Initial data sets for AFAD(left), KOERI(middle), Combined data(right). 84

Figure A.6. Number of recorded earthquakes by each seismic station for AFAD(left), KOERI(middle), Combined data set(right). 85

Figure A.7. Selected earthquakes for inversion AFAD(left), KOERI(middle), Combined earthquake data(right). 85

Figure A.8. Map view of horizontal and vertical grid distributons for AFAD(left), KOERI (middle), Combined data(right). 86

Figure A.9. Map view of checkerboard resolution tests for AFAD(left), KOERI (middle), Combined data(right). 86

Figure A.10. (a) AFAD (b) KOERI (c) Combined data ray density for each grids. 87

Figure A.11. (a) AFAD (b) KOERI (c) Combined data horizontal cross-section of Vp distribution 90

Figure A.12. (a) AFAD (b) KOERI (c) Combined data vertical cross-section of Vp distribution along 29.10°E longitude 92

Figure A.13. (a) AFAD (b) KOERI (c) Combined data vertical cross-section of Vp distribution along 39.15°N latitude 93

Figure A.14. (a) AFAD (b) KOERI (c) Combined data horizontal cross-section of Vs distribution. 94

Figure A.15. (a) AFAD (b) KOERI (c) Combined data vertical cross-section of Vs distribution along 29.10° E longitude 96

Figure A.16. (a) AFAD (b) KOERI (c) Combined data vertical cross-section of Vs distribution along 39.15°N latitude. 97

Figure A.17. (a) AFAD (b) KOERI (c) Combined data horizontal cross-section of Vp/Vs ratio distribution. 98

Figure A.18. (a) AFAD (b) KOERI (c) Combined data vertical cross-section of Vp/Vs ratio distribution along 29.10°E longitude 100

Figure A.19. (a) AFAD (b) KOERI (c) Combined data vertical cross-section of Vp/Vs distribution along 39.15°N latitude 101

LIST OF TABLES

Table 3.1. Historical earthquakes occurring on the Alaşehir-Simav fault system (from AFAD) 9

Table 3.2. Moderate and strong earthquakes (M≥4.5) occurred on the Alaşehir-Simav Fault System (combined from KOERI and AFAD database) 9

Table 5.1. 1-D P-wave Velocity Model (VELEST) 28

Table 5.2. Adopted 1-D wave Velocity Model from Velest result 33

Table 6.1. Statistics of data 39

Table A.1. Initial 1-D velocity model for relocation procedure for AFAD(left), KOERI(middle), Combined data set(right) 82

LIST OF SYMBOLS

NE	North-East
SW	South-West
s	Station coordinates
t_{calc}	Theoretical arrival times
t_{res}	Residual travel-time
t_{obs}	Observed travel times
Δ	Functions of differences
Δh_k	Hypocentral parameters
Δm_i	Velocity parameters
H	Matrix of partial derivatives of travel time with respect to hypocentral parameters
h	Hypocentral adjustments
M	Partial derivatives of travel time with respect to model parameters
m	Model parameter adjustments
e	Travel time errors
A	All partial derivatives
d	Hypocentral and model parameter adjustments
IP	Index of latitude direction
JP	Index of longitude direction
KP	Index of depth direction
VAi	Velcoity of the grid node of I surrounding Q point
WH(i)	Weighting parameter of the distance between Q and grid points v(s) : wave velocity
u	Slowness
τ_i	Weighting parameter of the distance between Q and grid points
r	Residuel

LIST OF ABBREVIATIONS

1D	One Dimensional
2D	Two Dimensional
3D	Three Dimensional
AFAD	Disaster and Emergency Management Presidency
CSEM	Centre of Seismology European-Mediterranean
KOERI	Kandilli Observatory and Earthquake Research Center
MARNET	Marmara Seismic Network
TÜBİTAK	The Scientific and Technological Research Council of Turkey
USGS	United States Geological Survey
zSacWin	KOERI Earthquake Solution Software
TOMOG3D	Software of 3-D Tomography
VELEST	Software of 1-D Velocity Model
HYPO71	Software for Determining Hypocenter and Magnitude
HYPOCENTER	Software for Determining Hypocenter and Magnitude
SEISAN	Earthquake Analysis Software for Windows
NORDIC	Norwegian Seismic Network Format
RMS	Root Mean Square
ART	Algebraic Reconstruction Technique
SIRT	Simultaneous Iterative Reconstruction Technique
LSQR	Sparse Equations and Least Squares
JHD	Joint Hypocenter Determination
PR	Poisson’s Ratio
Low-V	Low-velocity

1. INTRODUCTION

Previous geologic and tectonic studies Kütahya, Simav and surroundings have a complex structure (Zeschke 1954, Seyitoğlu 1997, Koçyiğit and Deveci 2005, 2007, Koçyiğit 1984, Aydan and Kumsar 2011, İnan et al, 2011, Emre et al, 2011). M=5.9 main shock occurred on 19 May 2011 at 23:15 local time. The intensity of the earthquake near the epicenter was determined as (Io=VI-VII). The hypocenter determined by the Regional Earthquake and Tsunami Monitoring Center (KOERI) of Boğaziçi University, Kandilli Observatory and Earthquake Research Institute (KOERI) is located at 39.139S - 29.102E, with 8-km depth (KOERI, 2011). Examining the 20 years preceding the main shock, the seismicity is less than compared with the surrounding areas. The Simav earthquake occurred without any prominent foreshock. In the four months period after the main shock, aftershock activity decreased quickly and at the end of a period of eight months earthquake activity had settled.

For the study area, many tectonic, seismic and geological have been conducted by different organizations and researchers. The signifigance of this study is that it is the first study about 1-D and 3-D tomography research for Kütahya, Simav and surroundings. In this context, the region's 1-D velocity model, 3-D velocity model and crustal structure are obtained.

In the first stage of this thesis, literature review was conducted regarding on the region of interest and geological, tectonic studies were briefly reviewed.

2. TECTONIC STRUCTURE AND GEOLOGY

2.1. Tectonic Structure of Kütahya Simav Region

Simav is located in the western part of Turkey and exposed to the extensonal tectonic regime. In western Turkey there are approximately eight prominent E-W trending grabens shown. In Figures 2.3 and 2.4 and the most known are; Alaşehir, Menderes and Simav grabens are well konown. The Simav graben is located in the North of NE-SW trending Demirci and Selendi basins and shows a WNW-ESE trend between Söğütçük and Simav town. The Simav graben has a topographical expression, with approximately 1100 m of elevation separating the rift shoulders (Seyitoğlu, 1997). According to Seyitoğlu (1997), the graben is one of the latest products of North-South extensional tectonics that began lates Oligocene-early Miocene times. There is another basin located in the north of the Simav basin between Akdağ and Karadağ and joins the WNW-ESE trending Simav graben at a high angle. The tectonic structure and seismotectonics of the Simav graben and surrounding regions have been studied by many earth scientists such as Zeschke (1954) and Seyitoğlu (1997).

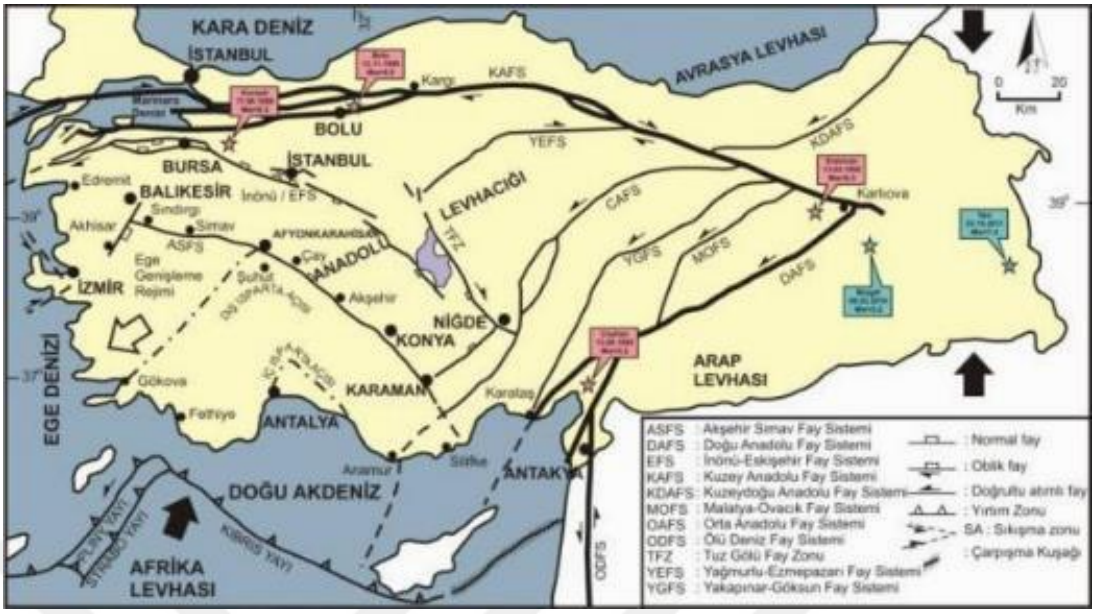


Figure 2.1. Simplified tectonic map of Turkey and surrounding regions (Koçyiğit and Deveci, 2007).

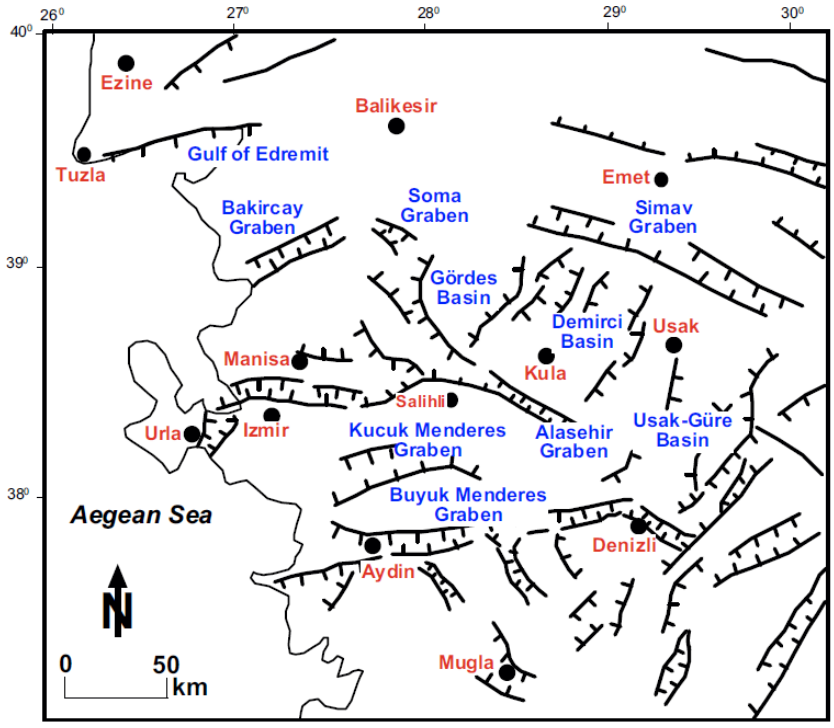


Figure 2.2. Graben distribution in the western Anatolia and major structural and tectonic elements of western Anatolia Neotectonics of Turkey –asynthesis. Red labeled points show the major towns and cities in the area. (Bozkurt, 2001)

As can be seen from the tectonic map of the Western Anatolia region shown in Figure 2.2, the graben structures bounded with a number of sub-parallel normal faults show an extension regime in the region. Geologic and tectonic studies (Koçyiğit and Deveci 2005, 2007, Koçyiğit 1984, İnan et al, 2011, Emre et al, 2011) show that some earthquakes such as 1899 Buyuk Menderes, 1928 Torbali, 1955 Balat, 1969 Alasehir, 1969 Simav, 1970 Gediz and 1995 Dinar earthquakes were produced by the normal faulting system developed in the region. However, the Simav earthquake of 19 May 2011 was associated with the Simav Graben (Bekler et al, 2011, Demirci 2013, Emre et al, 2011, Inan et al, 2011).

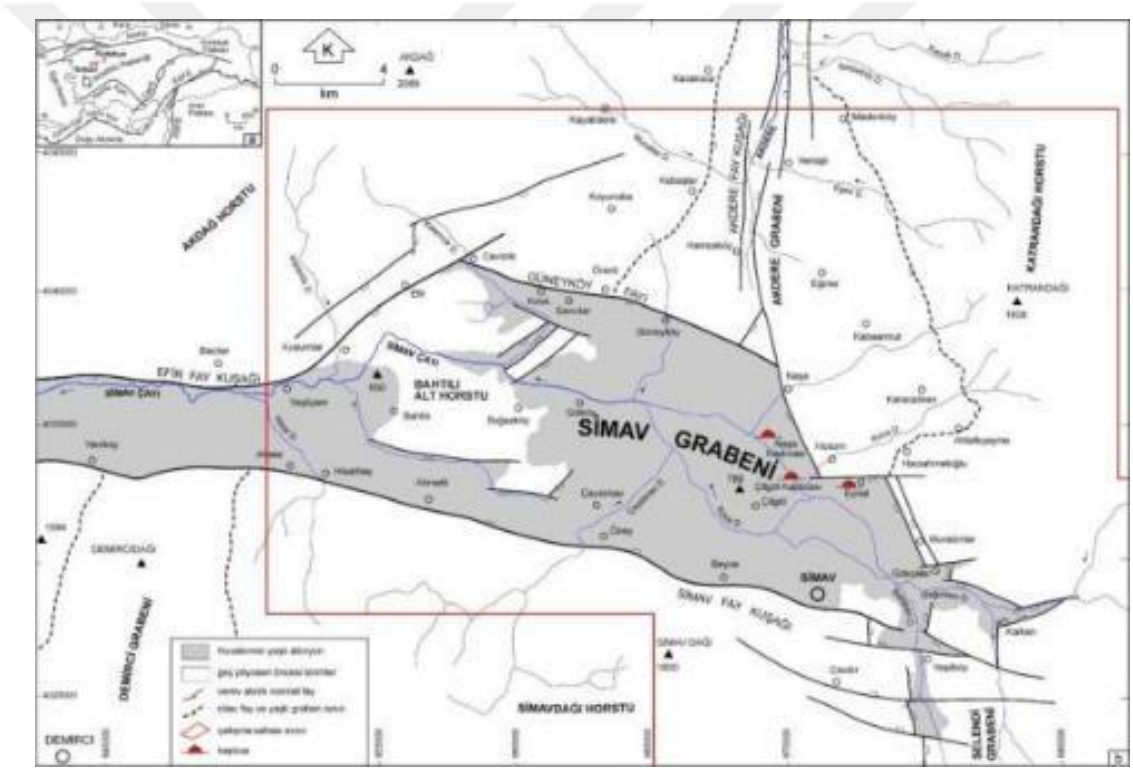


Figure 2.3. Detailed tectonic features of the study area (Koçyiğit, 1984)

Kocyigit (1984) shows that continuation tectonic movements in Simav and surrounding regions are highly deformed but graben and basin systems in these regions are fairly formed (Figure 2.3). Koçyiğit (1984) also demonstrated that active faults can be seen in different geologic and tectonic formations. Shaded regions indicated in Figure 2.3 represent Quaternary aged alluviums.

This region lies between Southeast Karaman and Northwest Sındırgı and is called the Alaşehir-Simav Fault system (Koçyiğit and Deveci, 2005). This fault system is known to be about 10-30 km wide and 500 km long. Addititonally, it has a NE-SW trending continuous oblique normal fault. To define the seismogenic zone beneath the area, series of graben-host and faults are investigated. The region is situated in the north-western part of the Gediz Graben. This region is one of the important tectonic units of the Western Anatolia extension regime. The epicenter of the Demirci earthquake was placed in the Simav Fault Zone which is surrounded by active faults with WNW-ESE directions. (Koçyiğit and Deveci, 2007, Üçer, 2000).

2.2. Geology

In this section, detailed geological information about the study area is given. As mentioned before, two graben systems in the region are formed in late Oligocene-early Miocene (see Figure 2.4). The main graben system consists of Konya, Akşehir-Afyon, Sincanlı, Ağaçköy, Gediz, Simav and Sındırgı. The secondary graben system comprises Karamık, Sivaslı, Banaz, Emet, Kocaçay and Emet depressions. The main and secondary graben systems have two different deposits (Figure 2.5). The main grabens have old graben depoists, while secondary grabens have younger graben deposits. Geologic studies (e.g., Akdeniz and Konak 1979, Koçyiğit 1984, Seyitoğlu 1997, Koçyiğit and Deveci 2005, Doğan and Emre 2006) indicated that older graben deposits are highly deformed but covered by younger deposits. The older deposits were formed by andesit-basaltic volcanics and covered by lake and river deposits containing coal and borax. Younger deposits were mainly formed by coarse-grained deposits and sedimants (Akdeniz and Konak 1979, Seyitoğlu 1997, Koçyiğit and Deveci 2007, Aydan and Kumsar 2011). In this section the well known active faults such as Emet and Simav faults are also described. In addition to these faults, Akşehir, Karagöztepe, Sivaslı-Banaz, Muratdağı and Gökler faults can be considered. Koçyiğit and Deveci (2005) indicated that the Alaşehir-Simav Fault system is seismically very active. Ambraseys and Tchalenko, (1972) pointed out that Simav and Akşehir fault systems are located in the Alaşehir-Simav Fault system and have created many historical and recent

earthquakes causing noticabe surface rupture and represent seismic activity very clearly. It means that the fault systems are seismically very activity.

The Simav graben is located in the northeastern region of the Menderes massif which is subjected to the extensional tectonic regime (Şaroğlu, 1992, Koçyiğit and Deveci, 2005, Emre et al, 2011, Aydan and Kumsar, 2011). This region of the massif is represented by Precambrian–Tertiary aged rock units. The Simav detachment Fault separates footwall and hangingwall rock units which show different lithologic, metamorphism and deformation characteristics (Figure 2.5). The footwall rock units consist of medium-high grade metamorphites, pegmatoids and granitoids. The hangingwall rock units contain schist-marble and ophiolitic mélange units. All these units are covered by Neogene-Quaternary sedimentary and volcanic rocks (Aydan and Kumsar, 2011; Oygür and Erler, 2000) (Figure 2.5).

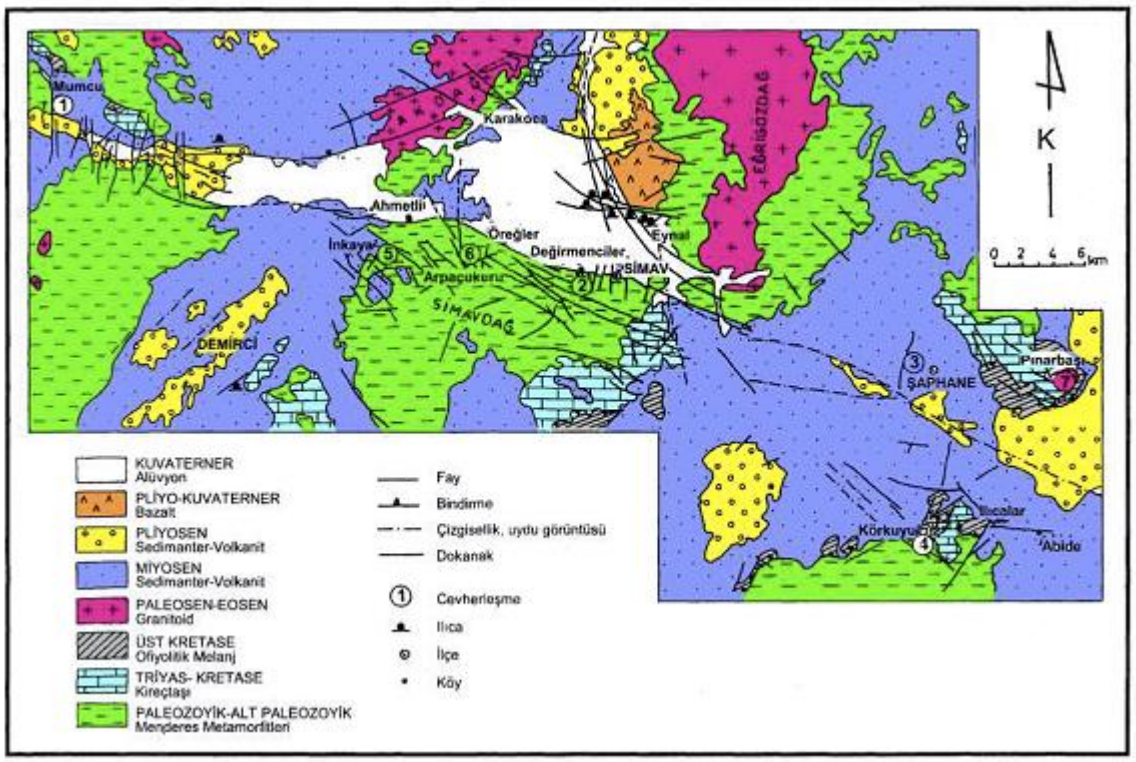


Figure 2.4. Geological map of Simav and surrounding regions (Aydan and Kumsar, 2011; modified from Oygür and Erler, 2000).

3. SEISMICITY AND DATA

Generally it is observed that the high seismic activities in the region occur on the E-W tectonic line and on its branches (Eyidoğan and Jackson, 1985; Bekler et al, 2011; Demirci 2013). As seen in Figure 2.4, Gediz, Emet and Simav Fault Zones are the main tectonic structures in the study area. On the 17 February 2009 an earthquake with a ML=5.0 occurred in the region. Intermediate earthquakes can be expected for this region because it is seismically very active. Also, the instrumental records indicated that on 28 March 1970 Gediz earthquake with Mw=7.2 occurred in the region. In addition to this event, the 1928 Emet earthquake M6.2 and 1970 Çavdarhisar earthquake M5.9 can be considered as other important events occurring in this region.

3.1. Seismicity of Simav and Surrounding Regions

As described in Section 2, the Eurasian and the Arabian–African Plates applied an intensive compressional force to the Anatolian Plate and as a result, the North Anatolia Fault (NAF) and the East Anatolian Fault (EAF) in Northeast-Southwest direction were developed. These two main fault systems are conjugated in Karlıova (Figure 2.1). The active faults mainly control the seismic activity of Turkey. The seismic activity of Turkey from 1900 to 2013 is shown in Figure 3.1 based on the KOERI catalogue. As seen, particularly many micro earthquake clusters appeared in Western Anatolia, Marmara region and in Eastern Anatolia. In addition, similar patterns are observed in the study area.

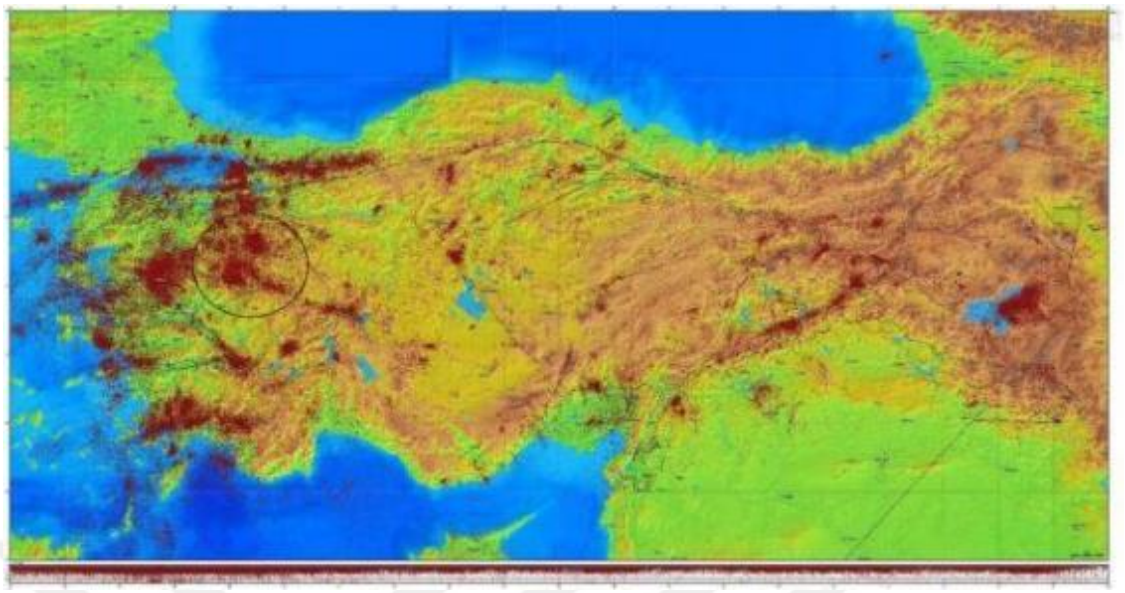


Figure 3.1. Seismicity map of Turkey between 1900-2015 (KOERI, 2015). Circle indicates stuy area.

As observed from previous studies, earthquakes generally occurring in Simav and surrounding regions are mainly activation of WNW-ESE elongated Alaşehir-Simav Fault systems and NNE-SSW elongated secondary faults cutting the Alaşehir-Simav Fault system.

Before and after the instrumental period, many moderate and strong earthquakes were observed in this zone. These earthquakes indicate that that the Alaşehir-Simav Fault system is an active tectonic zone. Historical earthquakes are listed in Table 3.1. As observed, almost all recorded events are moderate size and a few seem to be devastating earthquakes. The largest event occurred in Dinar in 1895 (www.deprem.gov.tr). There are no earthquakes between the years 94-1766 (www.deprem.gov.tr). This seems to be neither a seismic gap, nor quiescence of seismicity. This is not a natural seismicity pattern due to tectonic activity and occurrence of many moderate size earthquakes in these regions**.** Probably there were some moderate size earthquakes in the region but no written documents available or all these documents were destroyed by wars and fires (udim.koeri.boun.edu.tr). Many earthquakes occurred in the region after 1900 because the instrumental period started from this date. These events are given in Table 3.2.

Table 3.1. Historical earthquakes occurring on the Alaşehir-Simav fault system (from AFAD)

Date	**Location**	**Intensity**
B.C.88	Dinar	Unknown
53	Dinar and its surroundings	VIII
94	Afyonkarahisar and its surroundings	VIII
1766	Şuhut	VIII
1795	Afyonkarahisar	VIII
1862	Afyonkarahisar and Şuhut	VIII
1873	Afyonkarahisar	VI
03.05.1875	Dinar and Çivril	IX
13.05.1876	Afyonkarahisar	VI

Table 3.2. Moderate and strong earthquakes (M≥4.5) occurred on the Alaşehir-Simav Fault System (combined from KOERI and AFAD database)

Date	**Time**	**Location**	**Intensity**	**M**	**Loss of Life**	**Damaged Buildings**
04.10.1914		Bolvadin	-	5.1	-	-
26.09.1921		Argıthanı-Akşehir	-	5.4	-	-
07.08.1925	08:46	Dinar-Afyon	VIII	5.9	3	2043
24.06.1944		Kütahya-Abide	-	6.0	-	-
21.02.1946		Ilgın ─Argıthanı	-	5.5	-	-
25.03.1969		Manisa-Demirci	-	5.0	-	-
28.03.1970	23:02	Gediz-Kütahya	IX	7.2	1086	19291
19.04.1970	15:29	Gediz -Kütahya	VIII	5.8	-	1360
01.10.1995		Dinar	-	6.1	-	-
08.09.2000		Savaştepe	-	4.7	-	-
15.12.2000	18:44	Sultandağı-Afyon	VII	5.8	6	547
03.02.2002	09:11	Çay-Sultandağı	VII	6.4	44	622
19.05.2011	23:15	Simav	VI	5.9	3	-

3.2. Data and Solution Quality

Tomographic methods usually involve some sort of iterative algorithm to invert the travel times (Dines and Lytle, 1979; Peterson *et al*., 1985). A problem with these techniques is a trade-off between resolution and stability of the solutions.

In other words, an important part of a seismic tomography study is the assessment of the solution quality. Regions of good resolution need to be separated from poorly resolved ones (Kissling et al. 2001). In contrast to classical methods such as hit count or derivative weight sum (DWS), the full resolution matrix contains information about the interdependence between model parameters which influence the model resolution (Michelini and McEvilly 1991). The spread function derived from the resolution matrix is a measure of how strong and peaked the resolution is at each node (Toomey & Foulger 1989; Eberhart-Phillips & Michael 1998).

Ray density (number of rays passing through a block) is changing quality of the resolution of seismic velocity calculation. If some region has smaller number of rays for different reasons (e.g. high GAP values, number of recorded seismic stations or a few number of earthquakes occurred in a wide region, etc smaller events), than, the resolution will decrease and the reliability of the tomography results to become coarse. To obtain fine tomographic results it is necessary to have good quality data. The data quality strongly depends on the distribution of seismic stations, high ray density, fine phase readings, higher number of phases and as well as low rms values or better solution quality of earthquakes. Eberhart-Phillips 1990 and 1993, pointed out that the better tomographic results need to have better ray coverage, good station coverage, accurate located earthquakea and simple 1-D starting model. So, 3 dimensional tomography studies can calculate better velocity structure for regions with dense ray distribution, many earthquakes and dense station coverage.

Also, the station distribution and distance between seismic stations are important parameter of calculating high resolution tomographic images. There are higher number of stations in Simav and Kütahya regions, however there are only a few stations in the southern

part of Simav. The distribution of larger distance between seismic stations will affect the resolution of the velocity results. Therefore, it can be expectedthat the resolution of southern part of the study area displays coarse velocity perturbation ands is not reliable. Many aftershocks occurred after the Simav earthquake. The largest aftershock is a M5.7 earthquake. Seismic activity of the study region routinely observed by KOERI and AFAD. There was another temporary seismic network is deployed by Çanakkale Onsekiz Mart University (COMU), but I could not get get their phase data so that my dataset does not include these phases.

During the study, two different data sets from KOERI and AFAD were used to obtain 3-D crustal structure of the Simav and Kütahya region. After carefull examination both data sets I noticed that some earthquakes are recorded only by KOERI networks and only by AFAD network. So, I decided to integrate a new data set from both national data sets. I integrated KOERI data from January 2010 to July 2015 with AFAD from May 2010 to April 2012 to improve station-earthquake distribution and ray-coverage of the study area. The station distribution map is given in Figure 6.1. Data combination procedure is as follows:

(1) All phases recorded by two different networks for the same event were combined.
(2) If the event appears on the only one data set (either in KOERI or AFAD catalog) this event was accepted as a new event and then this phase information was added to the integrated phase database and all earthquakes with these phase information with the VELEST (Kissling, 1995) 1-D model were located.

Finally, three different earthquake catalogs were used to reveal 3-D crustal structure of the study area. Location and relocation of earthquakes in the all three data sets are made with HYPO71 (Lee and Lahr, 1972) and HYPOCENTER location algorithms (Lienert et al, 1986) respectively. In following sections only results of the integrated data set will be given. All results belong to three different sets will be given in Appendix sections of the thesis for comparisons of the results.

4. 3-D VELOCITY TOMOGRAPHY

4.1. Seismic Tomography Methods

In this section, a brief description about seismic tomography methods is presented. Seismic tomography is divided into crust and upper mantle blocks to determine velocity perturbations which is described as the deviations of the velocity from the initial velocity model of each block and analysis of wave velocity collected from various depths on the cross-sections in the studied blocks. As mentioned above, the distribution of seismic velocity of the Earth's inner exists in 3-D and can be made in local, regional, and global scales. Seismic tomography can be applied by using very different inversion techniques such as using artificial or natural source, body waves (P and S), surface waves (Rayleigh and Love) and using free oscillations (e.g., Hirahara, 1993). Tomography methods can be classified under different headings: (1) according to the type of resource, (2) according to distance between the source and the receiver, and (3) according to the types of data.

4.1.1. According to the Type of Source

As mentioned above, seismic tomography is divided into natural source and artificial sources. For natural source tomography the data set should be obtained from the earthquake and noise, whereas the data set for controlled source tomography is obtained from weight drop, vibration devices, dynamite and similar explosives. Body waves or surface waves are used in natural source tomography. In tomography applied by using natural sources, earth structure can be viewed as much deeper than other tomography obtained using controlled sources because inversion of focus and velocity parameters is simultaneously performed, even though the source location is not exactly known.

In general shallow segments of the earth structure can be well defined by using controlled sources. By using powerful explosives more information about the depth of the Earth's crust can be obtained. In recent tomography studiesboth natural and controlled sources data sets have been together used with hybrid algorithms.

4.1.2. According to Distance Between the Source and the Receiver

Tomography studies are divided into three classes according to size of the source-receiver distance and size of the study area. These methods consist of local, regional and global tomographies.

In local earthquake tomography studies, local earthquakes are used and usually small study areas are chosen. As seen in Figure 4.1 (a), earthquakes and stations must be within same model space. Using travel time of seismic waves, determination of upper crust seismic velocity structure on the regional scale is the main principle of local earthquake tomography. Regional earthquake tomography is generally applied to larger areas. Global earthquake tomography generally deals with the whole earth structure. According to the epicentral distance of the used earthquake, tomography is divided into local earthquake tomography and teleseismic tomography. According to the size and quality of the input data set, modelling of the region is necessary.

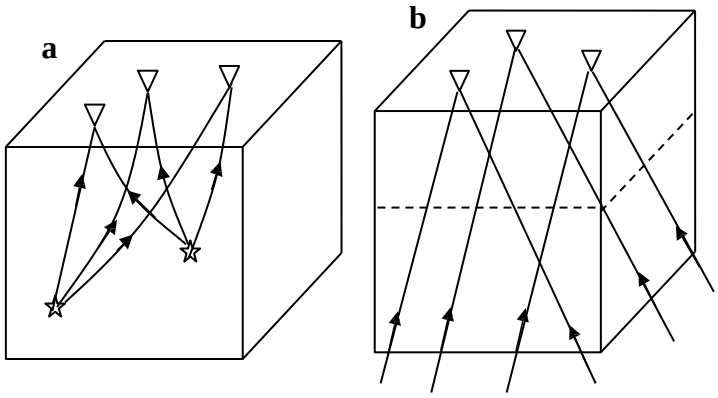


Figure 4.1. Modelling of earth structure for (a) local rays and (b) teleseismic rays (from Hirahara, 1993)

For teleseismic tomography studies, long period seismic waves are used so that the Earth's interior can be investigated on the global scale. As seen in Figure 4.1 (b), stations are within the model and earthquakes are out of a model. Thus the 3-D velocity structure of crust and upper mantle is determined.

4.1.3. According to Types of Data

In this method seismic slowness is calculated using travel time of seismic waves along the ray path between source and receiver and the velocity structure of the media is determined with inversion techniques. In this type earthquake tomography recorded phases of earthquakes are generally used. Recently, inome tomography studies, digitial seismic waveforms have been used for the inversion. In waveform tomography, detailed information about the Earth's interior can be obtained applying an inversion to waveforms because amplitudes of the seismic signal are sensitive to velocity variations in the studied region.

4.2. Local Earthquake Tomography (LET)

Recent tomography studies indicate that local earthquake tomography (LET) is a routine application for use in seismically active regions covered by a dense seismic network. Local earthquake tomography methods have these steps:

- **a.** Modelling of velocity structure,
- **b.** Calculating travel time and ray path,
- **c.** 3-D inversion,
- **d.** Determination of the quality of the solution.

Figure 4.2 shows the implementation steps of the local earthquake tomography.

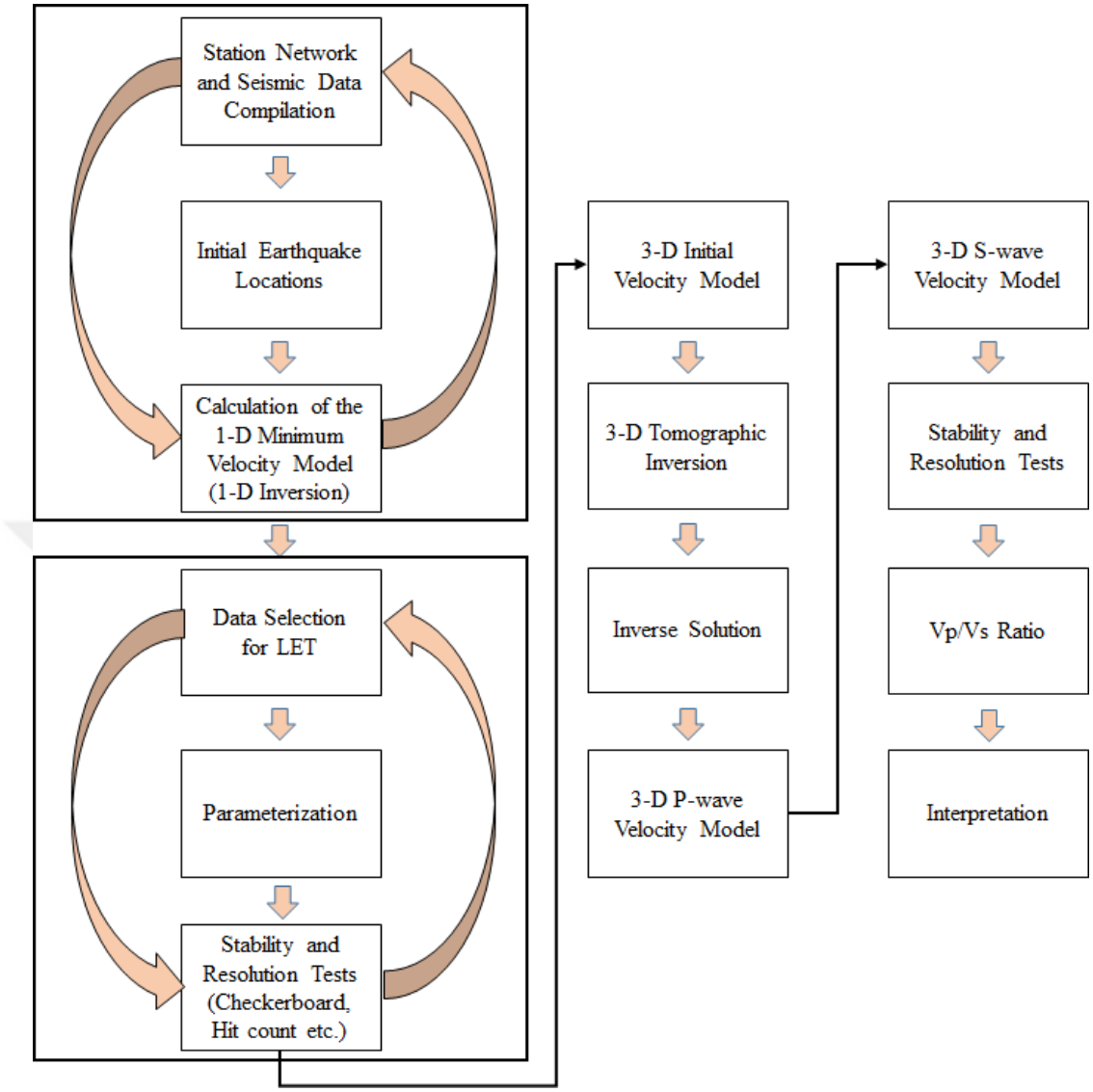


Figure 4.2. Flow chart of the calculation steps of the study (modified from Kaypak, 2007).

4.2.1. Modelling of Velocity Structure

In local earthquake tomography studies, first of all the 3-D environment is divided into little blocks and parameterized in a way that at least one ray could pass through each block. In tomography studies, the variation in the velocity of the study area can be obtained quickly and with high resolution.

It is very important that the parameters are formed by taking the distribution and number of earthquake stations and the distribution of the recorded earthquakes in the region into consideration. Parameterization of the model involves transforming the environment into a geometric form, in other words, turning the environment into a geometric structure where the velocities are the parameters. There are various approaches for this process. The first approach is the constant-velocity blocks given in Aki and Lee (1976) and shown in figure 4.3(a). Considering that the earth's crust has a very complex structure, it failed to yield satisfactory results in modelling as the traditional layer and block approach did not allow change in velocity from one block to the other. The discrete block approach of Hawley et al. (1981) is shown in figure 4.3 (b). In this approach the environment is divided into layers with constant velocities in the vertical direction and the horizontal velocity variation was obtained with the interpolation among the vertical nodal lines. The disadvantage of this approach is that it is insensitive to the vertical velocity variation. The approach displayed in figure 4.3 (c) is a model developed by Thurber (1983) that allows velocity variation in all directions through B-spline interpolation among nodes.

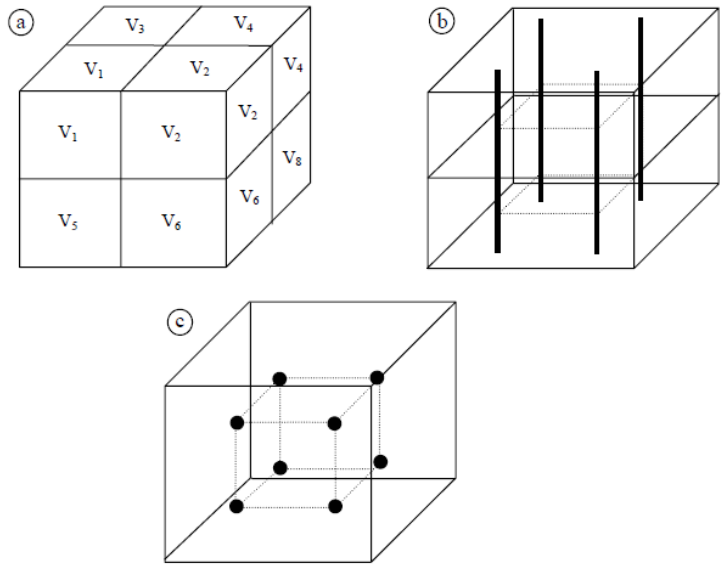


Figure 4.3. (a) Stable velocity blocks (Aki and Lee, 1976), (b) lateral variant layers, (c) model consisting from a grid of nodes (Thurber, 1983). Dashed lines show the fields calculated by interpolation.

Zhao et al. (1990), adapted the 2-D model parameterizing the Moho and Conrad discontinuities developed by Horiuchi et al. (1982) into a 3-D model. There are ways to find out the depth velocity distributions of velocity discontinuities. The first one is using the latitudes and longitudes as a continuous function like power series, which was the method used by Horiuchi et al. (1982) and Zhao et al. (1990). The other way is to calculate the depth of the discontinuity in any location within the study area and the four grids surrounding this location with linear depth interpolation, as the depth distributions of the grid points are known.

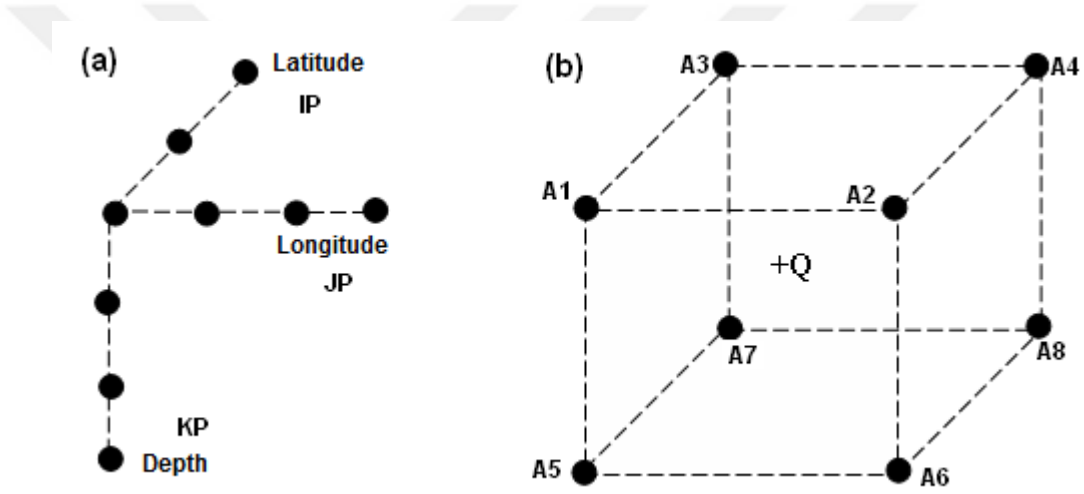


Figure 4.4. Eight grid points surrounding Q (from Zhao, 1991)

After Thurber (1983), Zhao (1991) divided layers under of the study area. For each layer he created 3-D grid mesh to express a 3-D velocity structure (Figure 4.4). In this approach, coordinates of eight grid points that enclose the point Q in the model space. Coordinates can be represented by three parameters, IP, JP and KP. Assuming Q is located in a layer in the upper crust. IP is the index of grid point in a latitude direction. IP=1 for the southmost grid, IP=NPC for the northmost grid. Similary, JP is the index of grid point in longitude direction and KP is the index of grid point in depth direction. (see Zhao, 1991 for detail information about this).

Let’s define

IP1=IP+1

JP1=JP+1

KP1=KP+1

The coordinates of the 8 grid points surrounding Q can be written as:

A1(IP, JP, KP)

A2(IP1,JP, KP

A3(IP, JP1, KP)

A4(IP1, JP1, KP)

A5(IP, JP, KP1)

A6(IP1, JP, KP1)

A7(IP, JP1, KP1)

A8(IP1, JP1, KP1)

The coordinates o A1, A2,…and A8 should be evaluated. Then, the velocity of point Q is calculated by interpolation of velocity of the 8 grid points:

$$VQ = V_{A1} * WH(1) + V_{A2} * WH(2) + \cdots \ldots \ldots + V_{A8} * WH(8) = V_{Ai} * WH(i) \quad (4.1)$$

V_{Ai}, is the velocity of the A_i grid point surrounding Q. *WH* (i) is a weight in the range 0-1 according to distance of point Q to the grid point. Larger weights are assigned to grid points closer to Q and small weights to those points farther away. The velocity at any point of the m layer is calculated using the interpolation function.

$$(\emptyset, \lambda, h) = \sum_{i=1}^{2} \sum_{j=1}^{2} \sum_{k=1}^{2} v_m(\emptyset_i, \lambda_j, h_k) \left[\left(1 - \left|\frac{\emptyset - \emptyset_i}{\emptyset_2 - \emptyset_1}\right|\right)\left(1 - \left|\frac{\lambda - \lambda_j}{\lambda_2 - \lambda_1}\right|\right)\left(1 - \left|\frac{h - h_k}{h_2 - h_1}\right|\right)\right] \quad (4.2)$$

ϕ is latitude, λ is longitude, h is depth from surface, $\emptyset_i$, λ_j, h_k are coordinates of grid points and $v_m(\emptyset_i, \lambda_j, h_k)$ are velocities at grid points. In the method used by Zhao (1991), the velocity belonging to a block is obtained by interpolating the velocities at eight surrounding grid points. In terms of being sensitive to velocity variation, this method estimates velocities closer to the truth is than can be obtained from other models in both lateral and vertical directions.

4.2.2. Ray Tracing and Travel Time

Ray tracing is the process of calculating the ray paths and travel times between the source-receiver pair. To date many ray tracing methods have been developed and are divided into two methods: complete and approximate ray tracing methods. In terms of calculation these methods may be classified as shooting, bending, approximate and finite-difference.

The calculation speed of the approximate ray tracing methods is high but as the travel times are miscalculated, the travel time residuals, focal partial derivatives and the partial derivatives of the velocity model will also be miscalculated. Therefore, the direction of the ray exiting the source and the ray path alone will be faulty (Thurber, 1993).

In the shooting method, rays are sent from a fixed source at different take-off angles and the initial boundary value problem is solved iteratively until one of these rays reaches the receiver. In the bending method, first a straight ray path is formed between the station and the focus and then it is bent until the shortest travel time is reached in accordance with Fermat's principle.

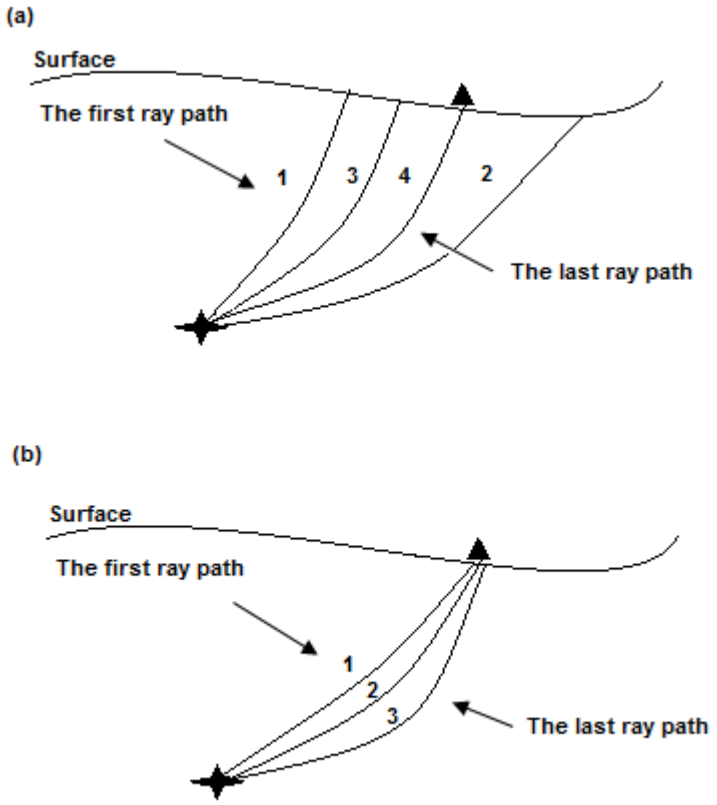


Figure 4.5. (a) Shoot method, (b) simple representation of the bending method

Um and Thurber (1987) developed the pseudo-bending method where the initial ray path is formed and this ray path is bent until Fermat's principle is achieved. The obtained ray path is entered as the beginning in the pseudo-bending method and bending is continued until the most appropriate ray path for the variation in velocity is obtained. The pseudo ray bending technique does not work where velocity discontinuities exist: it is applied only to maintain the velocity model.

Zhao (1991) developed a 3-D ray tracing technique that uses the pseudo-bending method iteratively and applies Snell's law in velocity discontinuities. The principle of this algorithm is the estimation of the initial ray path using the geometric interpretation of the ray equation and reducing the ray piece by piece. This algorithm yields the ray path in 3-D

form without error no matter what the epicenter distance is. The details of ray observation techniques and formulas can be found in (Zhao et.al., 1992, Zhao, 1991).

4.2.3. 3-D Inversion

According to ray theory, travel times in earthquake location problems, a velocity model is applied to the data set and the best origin time and location for an earthquake is determined. This is the process of minimizing the error vector iteratively using the smallest grids until the best result is obtained. It is the same in the simultaneous inversion but the same process is also performed for the velocity structure. In the simultaneous inversion, the error vector does not depend on a single earthquake. First, the ray paths and travel times are calculated. Then, inversion is performed after the ray tracing procedure. In the inversion process, the derivatives of the travel times are evaluated and more accurate earthquake locations are obtained;

$$t_{obs} = \tau_i + \int_s^0 \frac{ds}{v(s)} = \tau_i + \int_{source}^{station} uds \tag{4.3}$$

Here, *v(s)* is the wave velocity, u is the wave slowness, τ_i is the origin time of the earthquake, and t_{teo} is the theoretical travel time. The theoretical travel time is a non-linear function of the station coordinates, focal parameters that contains the coordinates pertaining to the origin time and epicenter (τ_i, x_k) and seismic velocities throughout the path between the epicenter and the station (Kissling et.al., 1994).

Epicenter parameters, origin time, ray paths and the structure of the environment are unknown parameters. Instead, the only parameters that can be observed are the arrival times. That is why in order for the epicenter and velocity parameters to be obtained, first of all, rays are sent between the source and receiver in accordance with a ray tracing method. Using a hypothetical rough velocity model, the above equation is used and the epicenter parameters (τ_i^*, x_k^*) and theoretical arrival times t_{teo} are calculated.

$$t_{teo} = \tau_i^* + \int_{source}^{station} u^* ds \tag{4.4}$$

Here, u^* represents the hypothetical initial wave slowness. The difference between the observed and theoretical travel times is called the travel time residual. Travel time residuals are calculated in order to minimize the errors regarding the location of the epicenter, origin time and the effects of the velocity heterogeneity outside the study area.

$$r_{ij} = t_{obs} - t_{teo} \tag{4.5}$$

If the residual times are expressed in standard errors of residual times, epicenter and velocity parameters, then the following equation is obtained:

$$r_{ij} = \sum_{k=1}^{3} \frac{\partial T_{ij}}{\partial X_k} \Delta X_k + \Delta\tau_i + \int_{source}^{station} uds \tag{4.6}$$

The partial derivatives of the epicenter $\partial T_{ij}/\partial X_k$ are the ratio of the components of the ray vector in the epicenter region to the seismic slowness. If the velocity structure is written discretely, the following equation is obtained:

$$r_{ij} = \sum_{k=1}^{3} \frac{\partial T_{ij}}{\partial X_k} \Delta X_k + \Delta\tau_i + \sum_{l=1}^{L} \frac{\partial T_{ij}}{\partial m_L} \Delta m_l \tag{4.7}$$

Here, *ml l=1,2,....,L* are the parameters of the discrete velocity model. If the above equation is written in matrix representation, then:

$$r = Ad \tag{4.8}$$

Here, r represents the travel time residuals, A represents the partial derivatives matrix and d represents the correction vector of epicenter and velocity parameters. A correction component containing the errors caused by the use of a wrong velocity model and epicenter parameters and that cannot be obtained through correction should also be added:

$$r = Ad + e \tag{4.9}$$

The A matrix in the equation can be split into two matrixes containing the partial derivatives pertaining to velocity parameters and with the error vector:

$$r = H\Delta h + M\Delta m + e \tag{4.10}$$

Here, H is the matrix of the partial derivatives of the travel time corresponding to focal parameters, Δh is the correction vector of focal parameters, M is the matrix of the partial derivatives of travel times corresponding to velocity parameters, Δm is the correction vector of velocity model and e is the residuel vector of travel times. Equation (4.8) is also so called the coupled hypocentre-velocity model problem.

In the first developed model of Aki et. al. (1974), matrix inversion was found through the damped least squares method: later, many iterative inversion algorithms such as ART and SIRT were developed. Paige and Saunders (1982) developed the LSQR (Least Square) method and this method started to be used in seismic tomography studies frequently. TOMOG3D, the tomography program used in this study, performs the inversion process using the LSQR algorithm of Paige and Saunders (1982) in calculating the equation (4.8). The ray paths between seismic stations and earthquake hypocenters in a 3-D view is given in Figure 4.6.

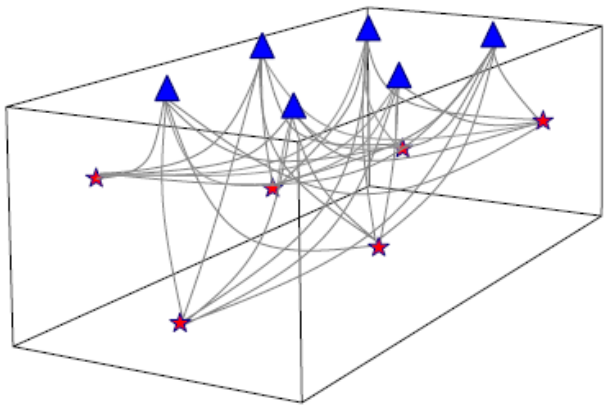


Figure 4.6. 3-D schematic representation of ray paths between hypocenter and seismic stations for the study region. Blue triangles represent seismic stations and red stars show hypocenters, gray lines show ray paths (from Kaypak 2002).

4.2.4. Evaluation of Resolution Quality

In order to obtain reliable results from the tomography, the resolution power of the data set should be determined. Commonly used models include the needle sensitivity test, checkerboard resolution test (CRT), restoring resolution test (RRT), and needle test and ray hit count approach.

In the ray hit count approach, the number of rays passing through each block is taken into consideration and the number of rays passing through one block determines the resolution. The higher the number of rays passing through one block means the higher the resolution: fewer rays or none means that the resolution is poor, meaning they are insoluble blocks. Schematic representations of ray number approach are indicated in Figure 4.7. In block 3, resolution quality is expected as a higher than block 4.

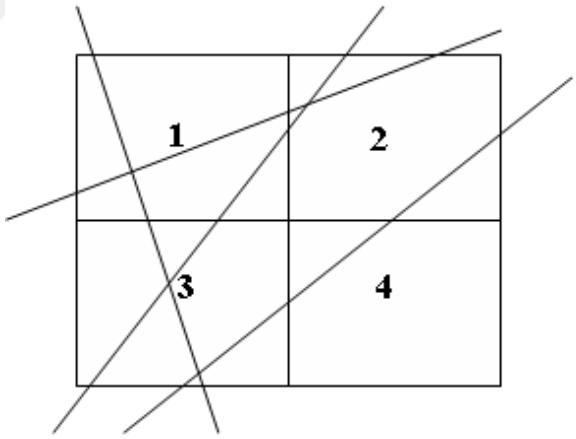


Figure 4.7. Schematic representation of ray number approach

In most tomographic studies several different resolution analyses are performed including the checkerboard resolution test (CRT), restore resolution test (RRT), spike test and ray density or ray path coverage tests. The ones most used are the checkerboard test and ray density functions. According to Iyer and Hirahara, (1993), in the CRT (Humpreys and Clayton, 1988) alternating high and low velocity anomalies are assigned to the 3-D blocks

or grids and the test residual data corresponding to the actual ray paths are computed by 3-D ray tracing in this model. Then, these data are inverted and the comparison of the solution with the original checkerboard velocity pattern provides an estimate of the resolution power of the data set. The details of other resolution tests are found in Iyer and Hirahara (1993). In this work, I performed only CRT and ray density tests to check the solution quality of the inversion results.

5. METHODOLOGY OF TOMOGRAPHY

5.1. 1-D Local Earthquake Tomography

VELEST software was performed by Kissling et al., 1994. (Kissling, 1995). This program can be used to solve problems such as:

1. The coupled hypocenter-velocity model problem for local earthquakes, quarry blasts, and shots; for fixed velocity model and station corrections VELEST in simultaneous mode performs the joint-hypocenter-determination (JHD).
2. The location problem for local earthquakes, blasts, and shots.

5.1.1. Calculation Steps of the 1-D Minimum Velocity Model

1-D Minimum P-wave velocity model is calculated by a four steps process. The calculation steps of a minimum 1-D model have been developed through the application of Equation (3) in many areas of both simple and complex crustal structure around the world (Kissling et al, 1994).

5.1.3.1. Establishing the Priori 1-D Model(s). All *a priori* information regarding the area under study should be obtained (layer velocities and thicknesses), as previously described in Section 5.1.2. This information may include seismic reflection and refraction studies or a general crustal model. The media should be defined by several layers of increasing velocity with depth (Kissling et al, 1994). Upper crust thicknesses should be about two to three kilometres and in the lower crust about four to five kilometres. According to *a priori* information or a general crustal model these are estimated layer velocities. At least three different initial velocity models should be tried for any model geometry (layer thickness) to probe the dependence of the solution on the initial model. One of these layers has extremely low crustal velocities, another has extremely high crustal velocities and the

third has intermediate crustal velocities (Velest User's Guide). After this step, this model is called an “a-priori” 1-D velocity model.

5.1.3.2. Establishing the Geometry and the Velocity Intervals of Potential 1-D Model(s). The best events with the most highest quality P arrivals in the data set were selected to cover the entire area. These events were relocated by VELEST using the appropriate damping values for each model parameter. The final damping values are selected as trial-error method and taking into consideration of rms results, location results and the recommended original damping values given in VELEST User’s manual (Kissling, E., 1995). This procedure was repeated several times with updated (new) velocities, station delays and hypocentral parameters. In addition, adjacent layers with similar velocities were combined during the inversion.

The procedure in this second step was also applied to the combined layers. In most cases, low velocity layers were avoided due to the instabilities they introduce to the problem. Kissling et al., (1994) suggest that shot or blast data (controlled-sources) should not be used in the inversion. Rather such data can be used to test the performance of the final minimum 1-D model. It is possible to proceed to the next step if the following criteria are met:

- Earthquake locations, station delays and velocity values do not vary considerably in subsequent runs: RMS values of all events indicate a considerable reduction;
- Calculated 1-D velocity model and the station corrections make geological sense.

If all these requirements are fulfilled the resulting model can be called the “updated *a-priori* 1-D model with corresponding station residuals” (Kissling et al., 1994). Well-located events recorded by both KOERI and AFAD networks were selected using the criteria of recorded by at least 12 stations with $rms \leq 0.5$ s, hypocentral errors ≤ 5 km and a maximum gap of 180°. The maximum gap is an important parameter for selection that ensures that events are well localizable by the local network. GAP is the angle between two outermost stations with an event position. If GAP is greater than 180 degrees, it means the event is outside of the seismometer network and the event position is unstable. The resulting data-

set is comprised of 1302 earthquakes, with a total of 38861 P and 3946 S observations. The final 1-D velocity model for the study region is given below in Table 5.1 and Figure 5.2.

Table 5.1. 1-D P-wave Velocity Model (VELEST)

Depth(km)	Vp (km/sc)	Vs
0	3.750	2.485
3.0	4.850	2.803
5.0	5.740	3.318
11.0	6.050	3.497
21.0	6.250	3.612
29.0	6.550	3.786
35.0	7.250	4.191

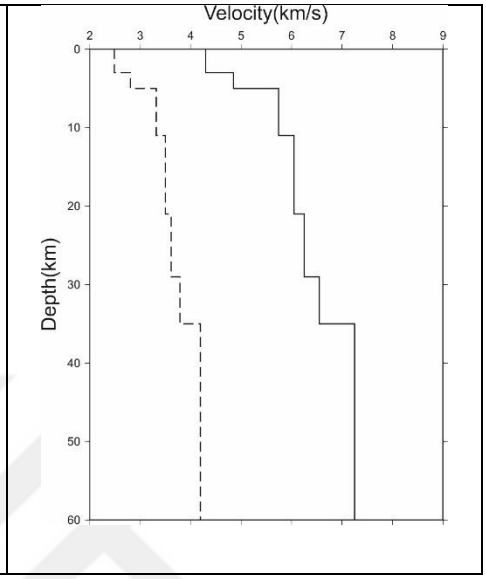


Figure 5.1. 1-D velocity model obtained from VELEST software of the study region. Continuous lines represent P waves and dashed lines represents S waves.

5.1.3.3. Relocation and Final Selection of Events. Using the updated *a priori* 1-D model with station residuals with HYPO71 or with HYPOCENTER in the single event mode, all events were relocated. However, there are no significant differences between the two results.

5.2. 3-D Tomography Program TOMOG3D

TOMOG3D (Zhao, 1992) software was used for 3-D tomographic inversion for Kütahya, Simav and surroundings. The computer algorithm TOMOG3D, written in FORTRAN 77 is designed to use arrival time data from local earthquakes recorded by a network of seismic stations to derive a 3-D seismic velocity model for the crust beneath the seismic network.

Not with standing its similarity to previous algorithms, TOMOG3D has several outstanding advantages:

a) It adopts a quite realistic model that has several complicated velocity discontinuities (CVDs) and velocities between these CVDs have variations in 3-D;

b) It contains a robust and efficient 3-D ray tracing technique to calculate travel times and ray paths in such a complex model;

c) Because of the above features, in addition to first P and S waves, TOMOG3D can combine arrival time data of later phases, i.e., waves converted or reflected at the CVDs. This is extremely important information which was discarded in previous 3-D studies. This feature was not used in this thesis. I used only P and S phases.

d) Finally, unlike other programs (e.g. Thurber's SIMULPS) which can only work for arrays smaller than 50-km by 50-km, TOMOG3D is expected to perform well for regions with sizes from several hundred metres to several thousand kilometres, partly due to the spherical coordinates system used.

Because of these advantages, TOMOG3D is considered to be a powerful tool for investigating the shallow and deep structure in regions such as subduction zones, fault zones and continents with large depth variations of the Conrad and the Moho discontinuities. TOMOG3D is particularly useful for very complex regions where conventional methods do not work well.

5.2.1. Synthetic Checkerboard Resolution Test

Before starting inversion with real values, synthetic models are produced to determine the resolution power of the data set, which areas in the structure have high resolution, and model parameters. The inversion is done using the real station and earthquake locations.

A checkerboard pattern is tried to determine the control parameters required for the inversion process and to determine the best grid intervals. The grid distribution is mainly created by manually as considering distribution of seismic stations and earthquake density.

This process is a trial-error steps and after having synthetic test results are satisfied in some conditions. Then grid distribution is defined and fixed for the inversion.

I tried to use different grid spacing for deciding the better grid distribution horizontal and vertical direction. In this procedure, I changed grid spacing as 0.30°, 0.20° and 0.10° in the N-S and E-W directions for performing resolution tests and inverted the selected data set. Finally, I selected the most suitable 3-D grid spacing. The spacing is dense in the areas with many earthquakes and denser station coverage, and sparse in the regions which have rare station coverage and less earthquakes distribution. The 3-D grid nodes obtained are alternately assigned ±%10 positive and negative velocity differences. According to this model, the travel times are calculated to make synthetic data. The synthetic checkerboard model may be reapplied for 5, 10, 15 and 25 km depths in the regions with frequent station distributions.

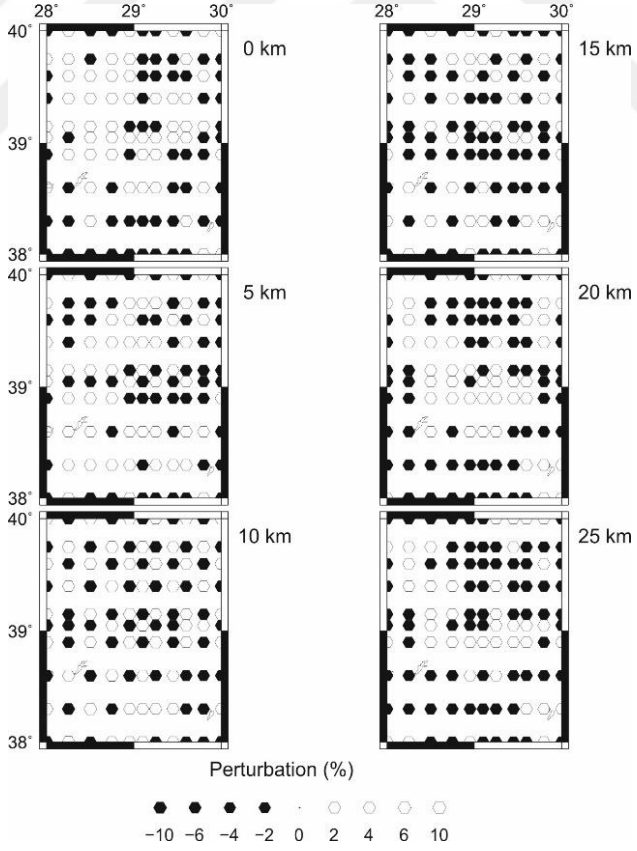


Figure 5.2. Horizontal view of P-wave checkerboard results with after inversion.

5.2.2. Ray Density Approach

Ray density approach is performed to determine the density of the number of rays passing through the blocks. The blocks where the number of rays passing is inadequate are the areas with poor resolution and the areas with very few or no ray passing through are considered insoluble. The insoluble, low-resolution and high-resolution block examples are shown in Figure 5.4 with horizontal cross-sections considered at various depths.

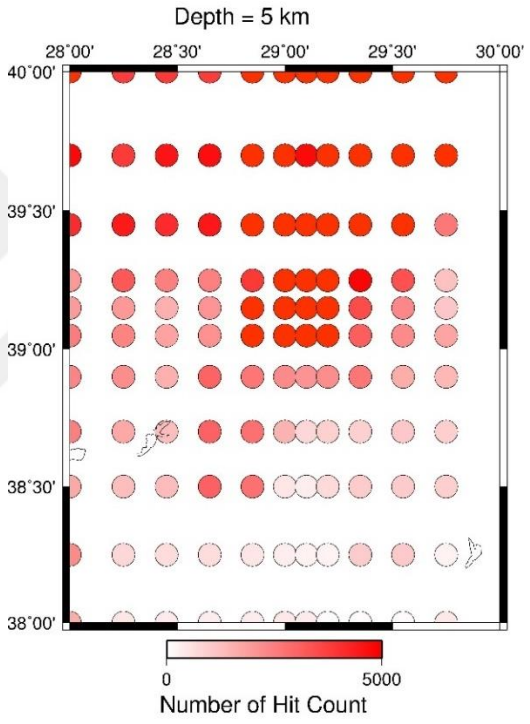


Figure 5.3. Ray density distribution map

5.3. Calculation Steps of 1-D Minimum Velocity Model for Kütahya, Simav and Surrounding Areas

In local earthquake tomography, the 1-D initial velocity model is preferred as it is a good velocity model to define crustal structure of a study is area. Moreover, publications such as Eberhart-Philips (1990, 1993), Barış et al., 2005, Tunç et al., 2009 and Gökalp (2007) state that a simple 1-D velocity model yields much better results compared with a very complex 1-D velocity model. In this study, various 1-D velocity models were reproduced for the investigated region and a simple one among these that produced the least amount of residual was accepted as the final model. The data sets obtained for the Simav region and its surroundings were processed separately and a 1-D velocity model pertaining to the region was produced using the VELEST algorithm and HYPOCENTER software are used earthquake locations for the combined data set and AFAD data set were obtained with this 1-D velocity models. In this stage, SEISAN software was preferred and this software was installed and run on a Windows operating system. The current software was written in FORTRAN. Since the source codes are also available it is possible to make changes in the program if necessary. For the Velest algorithm, all data sets were separately converted into HYPO71 format and these data were again converted into the Norwegian format from HYPO71 format via the format converter software within the SEISAN package. The 3-D tomography software however, only accepts data in its own format. In the LET study, AFAD and the combined data sets were first converted into HYPO71 format and these data converted into TOMOG3D format.

VELEST (Kissling et al., 1994) software was used for the 1-D velocity model of the region to be created. In this software, the hundred of multi-layered initial models with different velocity values are formed and these were used instead of the velocity models used by the institutions operating earthquake networks. These initial models were put through inversion with 9 iterations and the solution was ended when the rms value was minimized. I evaluated the obtained layer and velocity structure and combined the close velocities and changed the layer thicknesses. Then, I input the final crustal velocity model into VELEST

as a new initial model and the iterative inversion process was repeated. I compared the results obtained and determined the most appropriate velocity model for the region with the lowest rms values. The earthquakes were relocated with 1-D velocity model obtained through VELEST and I entered this velocity model and earthquake information into the tomography program as input data. However, TOMOG3D software allows a maximum 4-layer 1-D velocity model as crustal velocity model and does not run velocity models over 4 layers. For such a study, all source codes are required to be re-written and changed. For this reason, iterations were made again in the velocity model obtained via VELESTt and converted into 4-layered model and the 7-layered crustal-velocity model obtained via VELEST was decreased to 4 layers; thus, the final crustal-velocity model was thus achieved. This final 1-D model is given below in Table 6.1 and Figure 5.5. Besides, earthquakes were located via the 1-D velocity model developed by Kalafat and Gürbüz (1987) and routinely used in KOERI network; this 1-D velocity model was entered into TOMOG3D program as input model and 3-D velocity model was obtained.

Table 5.2. Adopted 1-D wave Velocity Model from Velest result

Depth (km)	***Vp (km/s)***	***Vs (km/s)***
0	4.850	2.800
5.0	5.700	3.295
11.0	6.300	3.642
32.0	7.450	4.306

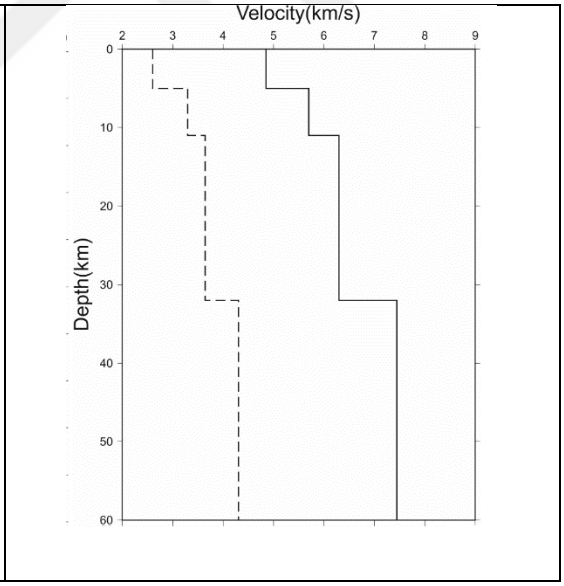


Figure 5.4. Schematic view of the adapted 1-D velocity model from VELEST results. Solid lines represent P-wave velocity, dashed lines denote S-wave velocity.

The locations were made with different velocity models and the error rates were compared. As a result of the comparison, location parameters are similar for two different location softwares. Vp/Vs=1.73 value as generally used by KOERI for the routine locations

of the local seismic events in western Turkey was accepted and S-wave velocity was used in the relocation of the epicenter. Wadati method is used to confirm the accepted Vp/Vs ratio (seen in Figure 5.6). The Wadati diagram produced 1.732 value for the combned data set and this value is stated to be consistent with the reference values used for different earthquake zones.

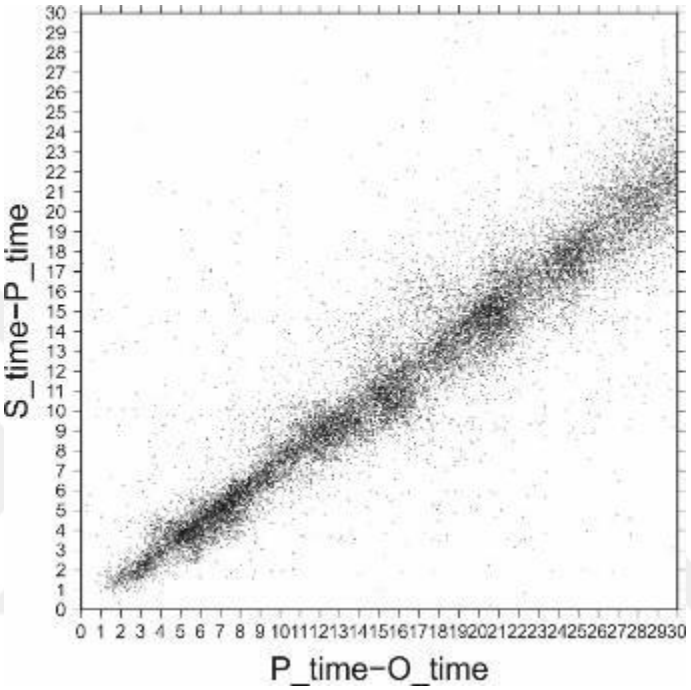


Figure 5.5. Schematic view of Wadati diagram. P_time is the P arrival time, S-time is the S arrival time, O_time is the Origin time of the earthquake.

After the 1-D velocity model is decided and the earthquakes with this model are relocated, the produced dataset isconverted into the data format of the TOMOG3D program. For 3-D earthquake tomography, the steps are mainly followed and the obtained results are listed below:

1- Data conversion: At this stage, the earthquake list, phase readings and earthquake station information in HYPO71 format were converted into the format used by the TOMOG3D software.

2- Selection of earthquakes: To perform 3-D velocity inversion the initial data set should be reduced by using certain criterias explained in section 5.2.1.

3- Grid selection: In order to obtain high resolution seismic images of the study area one should define the grid spacing in horizontal and vertical directions by considering station coverage and density of earthquakes. The biggest advantage of the TOMOG3D algorithm is that it allows identification of blocks with different sizes in both horizontal and vertical directions. Thus, the velocity variation can be calculated as close as possible to the real velocity values not only for horizontal layers but also for dipping layers.

4- Model creation: the model grid nodes should be created for checkerboard test and 3-D inversion according to latitude, longitude and depth nodes obtained from grid selection procedure.

5- Damping parameters: In this step, different damping parameters are tested.

6- Input parameters selection: It is necessary to know that the number of selected events, number of phases, number of seismic stations, number of iterations, dimensions of the study area and mubner of unknown parametrs for the inversion. All these values are explained in the read.me files of the code.

7- Checkerboard test: To check the best grid spacing and damping parameters of the tomography inversion sythetic test should be performed. After CRT test results should be compared with the initial model and if the results are not good enough then process should be started from 3rd step.

8- Drawing checkerboard results: The rsults of CRT test should be drawn and inspected.

9- Calculate P-wave 3-D inversion: To obtain 3-D P-wave velocity and crustal structure, seismic tomography is performed by 3-D inversion and all earthquakes are relocated with the new 3-D velocity model.

10- Draw P-wave results: Results of 3-D velocity perturbation with horizontal and vertical layers are drawn. In this step, also some cross-section of the velocity perturbation are obtained.

11- Calculate S-wave 3-D inversion: To obtain 3-D S-wave velocity and crustal structure, seismic tomography is performed by 3-D inversion and all earthquakes are relocated with the new 3-D velocity model.

12- Draw S-wave results: Results of 3-D velocity perrubation with horizontal and vertical layers are drawn. In this step, also some cross-section of the velocity perturbation.are obtained

13- Vp/Vs calculation: Vp/Vs ratios are obtained from the results of P-wave and S-wave inversions. To obtain Vp/Vs ratios, Vp results divided by Vs results for each grid.

14- Draw Vp/Vs ratio results: Results of 3-D velocity perrubation with horizontal and vertical layers are drawn. In this step, also some cross-section of the velocity perturbation.are obtained.

15- Interpretations of the results: In this step, all tomographic perturbation results should be compared with other results from geophysical observations, tectonic models, geological structures, geothermal sites and fault structures and as well as distribution of moderate and large earthquakes.

6. 3-D TOMOGRAPHIC INVERSION FOR THE KÜTAHYA, SİMAV AND SURROUNDING REGIONS

6.1. Data Selection

After the 19 May 2011 Simav earthquake, firstly, I essayed to combine the seismic phase data arrival from the networks and various studies for the period from January 2010 to April 2015 for the study area. Data selection criteria are the same as the previously performed one-dimensional velocity inversion.

The station distribution, distance between seismic stations and number of earthquakes are important parameters of calculating high resolution tomographic images. There are higher number of seismic stations in Kütahya and surroundings, but there are a few seismic stations only in the south and southeast of Simav for KOERI and AFAD networks. I combined all these stations into a new data set and station distribution is shown in Figure 6.1 for the combined data set. I expected that the resolution of southern part of the study area displays coarse velocity perturbations so that it is not so reliable due to insufficient station and earthquake density. Many aftershocks occurred after the Simav earthquake (19 May 2011, M5.9). The largest after shock is a M5.7 earthquake. Seismic activity of the study region is routinely observed by KOERI and Disaster and AFAD. Another temporary seismic network is deployed by COMU, but I could not obtain their phase data to conduct seismic tomography studies in the framework of this thesis. To obtain 3-D crustal structure of the Simav and Kütahya region I used two different data sets from KOERI and AFAD. After careful examination of both data sets I realized that some earthquakes are recorded only by KOERI network or only by AFAD network, so I decided to combine a new data set from both national data sets. I combined KOERI data from January 2010 to May 2015 with AFAD from May 2010 to June 2012 to improve station-earthquake distribution and ray-coverage of the study area. The data combination procedure is as follows: I combined all phases recorded by two different networks for the same event. If the event appears in only one data set (either in KOERI catalogue or AFAD catalogue), I accepted it as a new event and added this phase

information to the combined catalogue and relocated all the phase information with the VELEST 1-model. Three different earthquake catalogues used to reveal 3-D crustal structure of the study area were obtained from KOERI and the combined catalogue. Location and relocation of earthquakes in all three data sets were made with HYPO71PC (Lee and Lahr, 1972) and HYPOCENTER algorithms (Lienert et al, 1986).

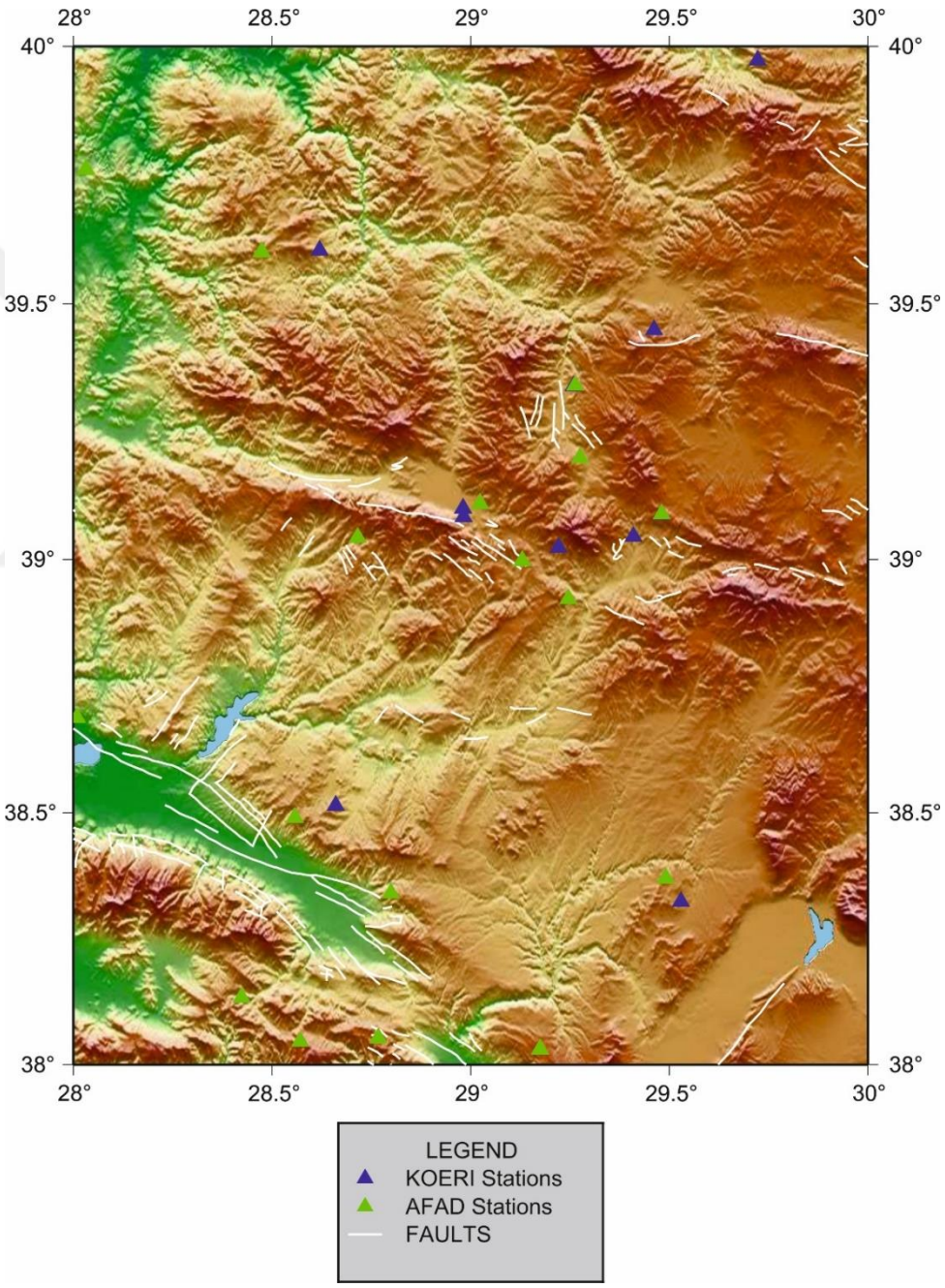


Figure 6.1. Schematic view of seismic station distribution used for tomographic inversion.

As known, resolution sensitivity or solution quality is very important in all tomographic studies. Data quality is significantly associated with the azimuthal gap values (GAP) between the earthquakes and the stations. If the GAP value is bigger than 180º, the data quality decreases. In order to increase the resolution, the earthquakes with a GAP value equal to or lower than 180º, with a phase count below 10 and rms value above 0.7 seconds were removed from the data group. So, I used all data for tomographic inversion satisfy the above criterias.

All calculation for 1-D velocity model, hypocentral relocation and 3-D velocity inversion to the all data are performed with three different sets. Simav earthquake and aftershocks and the earthquake solutions for this region were recorded by the two national networks established in Turkey. The data set consists of the data from the national network operated by KOERI, the data from the national earthquake network of AFAD and the combined data from both networks were obtained. The combination data procedure given as flows: if the same earthquake is recorded by two different networks then their phase readings are merged into same phase list and accepted as a new event. If an earthquake is recorded by only one network either AFAD or KOERI, this phase list added as a new event to the data base. This procedure repeated for all events and final data set is located by four layers 1-D model obtained by VELESTKOERI. After relocation procedure relocated events used for 3-D velocity inversion. The observation periods and number of P and S phase readings in these three data sets are different from each other. In Table 6.1, the observation period, the number of original earthquake number, the number of earthquakes selected from the total data set and the number of P and S phases for these earthquakes are listed:

Table 6.1. Statistics of data

Agency Name	**Period of data**	**Number of Events**	**Selected Events**	**Number of P Phases**	**Number of S- Phases**
AFAD	May 2010-April 2012	8652	2871	33809	27048
KOERI	Jan. 2010-July 2015	11138	4086	68073	9763
Combined	Jan. 2010-July 2015	16062	4788	93117	30217

All results from three datasets are given in Appendix section. In the next section, results obtained from the integrated data will be presented.

In Figure 6.2, the seismicity distribution of original data set is given for the study area. The combined data set has 16062 events for the 1-D model calculation and relocation procedure.

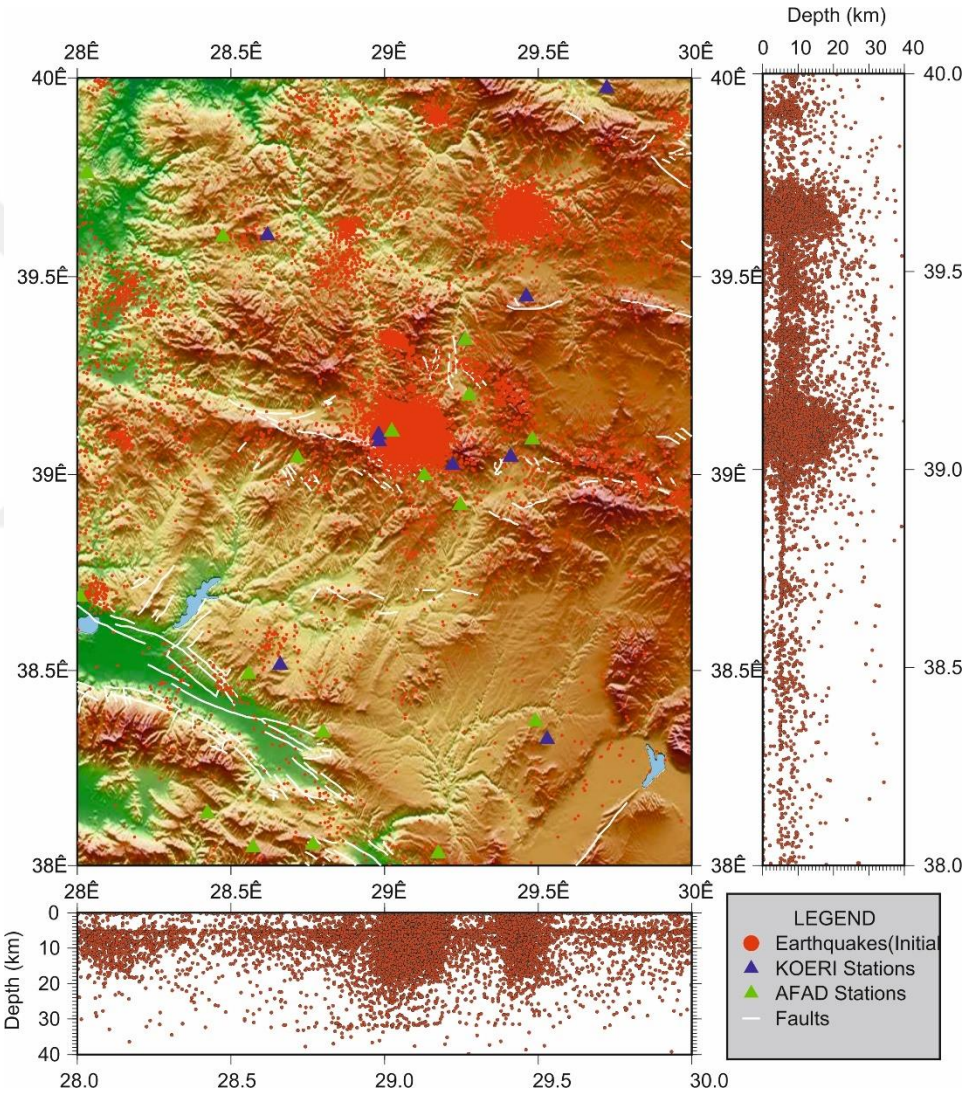


Figure 6.2. Initial (original) seismicity distribution for the combined data.

The seismicity distribution shows that particularly earthquakes in the study area, display clustering and a linear distribution in associated with the fault lines. The common

characteristic observed in all data sets is that the Simav earthquake and its aftershocks occurred by clustering. While the AFAD data cover a period of two years, the KOERI and KOERI+AFAD data has a period of 5.5 years. Comparing the depth distribution in all three data sets, most of earthquakes generally occurred at shallower depths than 20 km, only the AFAD data reach down to 40 km in depth. The lack of earthquakes in the region below the 38.70° is found in all data sets. The observation period is longer, a low seismicity activity would also not be expected in this region. The combined data displays clustering and linear distribution along some tectonic lines. The depth distribution of the data increases from west to east. The combined data contain some specific errors in terms of both distribution and error values obtained through location because two networks data is integrated without phase readings. On the other hand, the Simav main shock and aftershocks occurred in two very dense and small clusters. It was very difficult to obtain a high resolution velocity structure for the whole study area because of earthquakes concentrating in limited areas. In general tomographic nversion takes long computer calculation time. For efficient calculation generally 3-D inversion is applied into the selected earthquake set from the whole data set.

The earthquake selection criteria are given in Zhao 1991; and Zhao, et al., 1992. According to those criterias the study area is divided into a total of 768000 blocks with very small dimensions in latitude, longitude and depth directions and earthquakes are selected in a way that at least one ray would pass through each small block. I used the 4788 earthquakes selected from the combined data set for inversion, a total number of 123334 phases were obtained. This data has 93117 P phases and 30217 S phases. The selected earthquake distribution is given in Figure 6.3. As clearly observed that the general distribution of seismicity preserved after the event selection for the inversion.

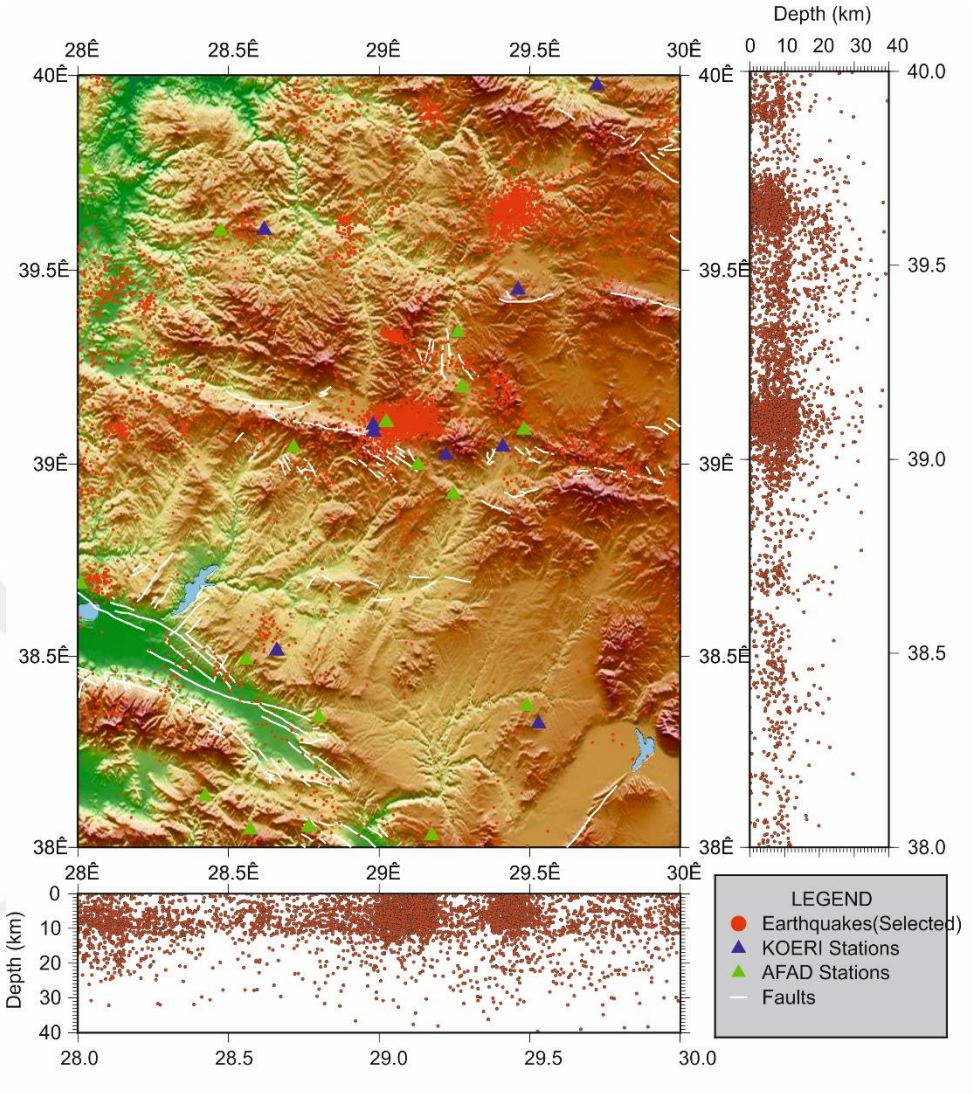


Figure 6.3. Seismicity map of selected events from the combined data set for inversion.

The seismicity maps shown in Figure 6.3 display the data distribution selected from the original data set for the local earthquake tomography in the study area. As seen in the Figure 6.3, the earthquakes preserved their clustering and linearity characteristics. Most of the earthquakes occurred at depths less than 30 km and the distribution of the depths of the earthquakes increased from west to east.

6.2. Velocity Model Parameterization

The study area was divided into blocks with a spatial dimension of 0.025°x0.025°x0.25km and a depth between 0-30 km. Earthquake selection criteria were based on the condition that at least one ray would pass through each small block.

While the synthetic checkerboard model was produced, different velocity models and various grid intervals were tried and the most suitable grid interval was selected. In particular, grid intervals are carefully selected because they represent the station distributions and frequent earthquake locations, in other words, the regions where the fault zones pass through.

As the number of stations and earthquake distribution were inadequate between longitudes 28.00-28.50° E in the west of the study area so thatthe grid interval was selected as 0.5°. The grid interval was taken as 0.25° and as 0.10° between 29.00-30.25°E and between 39.00-39.35°N. Different grid intervals were applied in the vertical direction. As a result, it was decided to place grid nodes at depths of 0, 5, 10, 15, 20, 25 and 30 km.

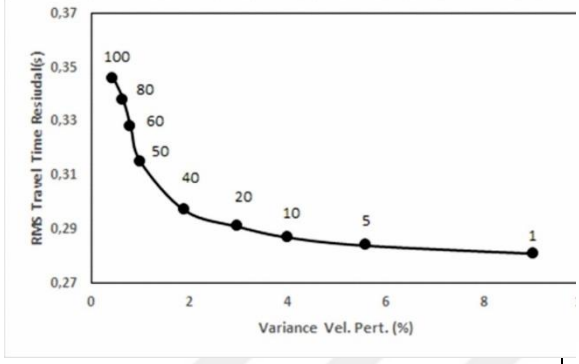
KOERI's minimum one-dimensional velocity model used in determining the locations of earthquakes was selected to minimize the location errors in total and represent the region best. This model given in Table 6.2 was entered into the inversion as an initial velocity model. An additional velocity model was determined via VELEST and AFAD and combined data were subjected to the relocation process again with both this velocity models.

6.3. Control Parameters

One of the most important control parameters in LET is the damping factor applied to velocity values because damping affects both results and resolution estimates. High damping

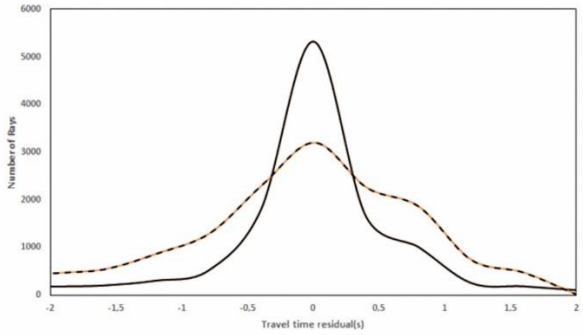
values yield low model perturbations and low resolution estimates, whereas low damping yields high model perturbations and high resolution estimates.

Damping depends mainly on model parametrization of the average observational error (Kissling *et al.*, 2001). It can be determined by analysing trade-off curves between model variance and data variance for a single iteration inversion run in TOMOG3D (Zhao, 1992). Appropriate damping values show a significant decrease in data variance without a strong increase in model variance.



Damping parameter	Rms Travel Time Residual	Variance Velocity Perturbation
1	0.281	9
5	0.284	5.6
10	0.287	4.01
20	0.291	2.99
40	0.297	1.90
50	0.315	1.00
60	0.328	0.80
80	0.338	0.65
100	0.346	0.45

(a)



Data order	Travel Time Residual	Number of rays
1	-2.0	180
2	-1.6	201
3	-1.2	303
4	-0.8	512
5	-0.4	1783
6	0.0	5325
7	0.4	1655
9	0.8	1010
10	1.2	255
11	1.6	184
12	2.0	105

(b)

Figure 6.4. (a) Damping factor (b) Travel Time Residuals.

Figure 6.4 shows the selection of the damping factor, which is one of the most important parameters in 3-D tomography, used in the study area, and the effect of the selected parameter on the location resolution. As stated by Eberhart-Phillips (1986) and Huang and Zhao (2004), different damping parameters were applied to the data set to determine the most appropriate damping factor and the optimum damping factor was

selected as 40 for this study, just as in Nakamura et al. (2002), Barış et al. (2005), Aslan (2008), Tunç et al. (2009). This damping factor was used in all data sets. The velocity variation obtained for different damping factors and the rms travel time residuals are shown in Figure 6.4(a). Figure 6.4(b) shows the travel time residual with number of rays obtained from the data set prior to 3-D inversion and the rms distribution obtained after inversion. This figure shows that the rms errors recovered significantly after the 3-D inversion.

6.4. Resolution Tests

6.4.1. Synthetic Checkerboard Resolution Test

In order to assess the adequacy of the ray coverage and resolution degree of tomographic inversions would be, I built synthetic models and enforced the checkerboard resolution tests (CRT). Figure 6.5 displays the distribution of the grids whose checkerboard test and local earthquake tomography were calculated. Here, the point to take into consideration is the distribution of stations and earthquakes. In the areas where the earthquake and station number is intense grid size is smaller, otherwise it would be bigger. 3-D velocities to be calculated by tomography are applied for each block. These grid sizes are the most important parameters when determining the resolution of the tomography results. Different grid sizes were used to find the optimum grid dimensions. The best grid distribution shown in Figure 6.5 is selected according to various CRT tests and ray paths for horizontal and vertical directions.

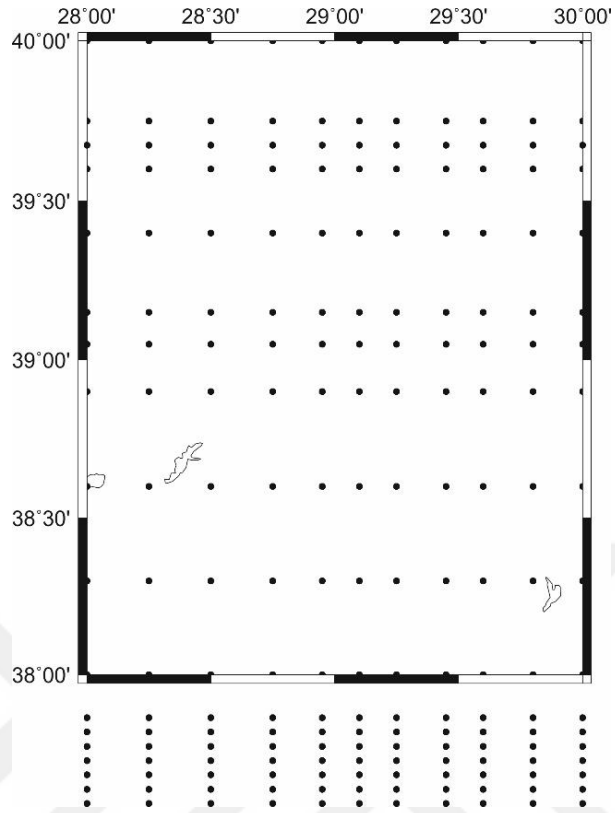


Figure 6.5. Plan (above map) and E-W cross sectional view(below) of variable grid distribuiton.

Figure 6.5 shows the checkerboard resolution test pertaining to the combined data set. It is expected that the checkerboard test given as the initial model should show almost the same patterns after inversion. However, in the TOMOG3D algorithm, the test model is expected to yield more accurate results by adding noise to P and S waves instead of using the checkerboard model alone. The results show that resolution tests are reliable in the areas where earthquake and station distribution are frequent, while pattern results are much more different than the initial data in the areas where stations and earthquakes are scarce. Also, in these areas grid dimensions are much larger than those in areas where earthquakes occurred intensively. In these areas the resolution of the velocity distribution is not high and the velocity values acquired are not as reliable.

Figure 6.6 shows the distribution of grids for which the local earthquake tomography is to be calculated. What must be considered is the distribution of stations and earthquakes:

in areas where the earthquake and station number is intense, grid size is smaller. 3-D velocities to be calculated by tomography are applied for each block. The grid sizes are the most important parameters when determining the resolution of the tomography results. Different grid heights were used to find the optimum grid dimensions. Calculated checkerboard results are given for each horizontal cross section indicated in Figure 6.6.

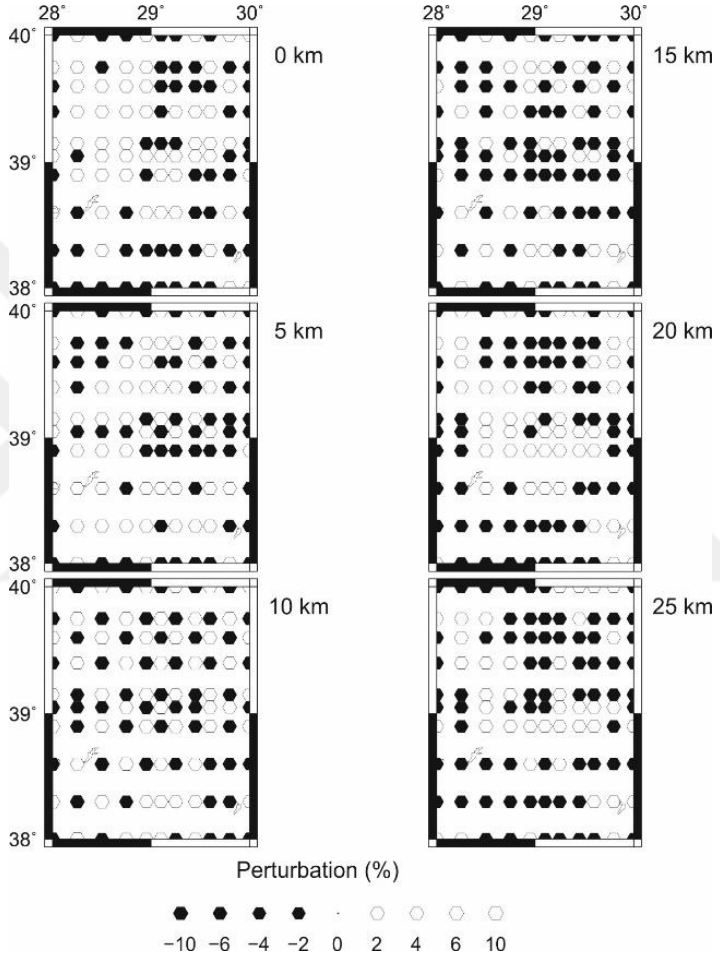


Figure 6.6. Results for the checkerboard resolution test for P wave. The depth of each layer is shown on the upper right of each map.

6.4.2. Ray Density

The number of rays passing through each block is used as an important parameter to calculate the velocity of the block more accurately. The numbers of rays which are calculated

with different depth cross-sections are displayed below in Figure 6.7. In local earthquake tomography, the number of rays is used as another important parameter of resolution and it was reported that, results acquired from the grids with dense rays had higher resolution.

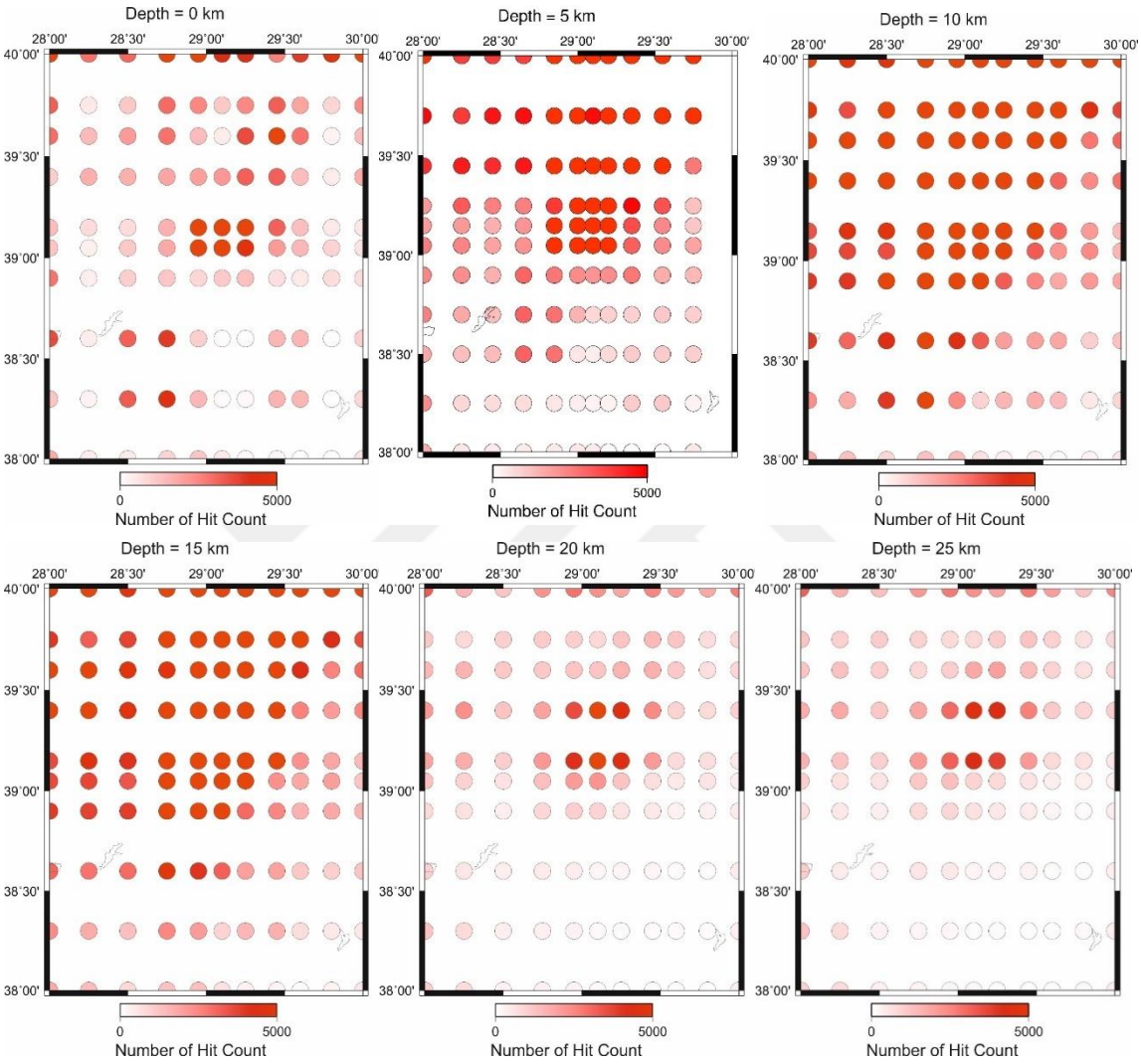
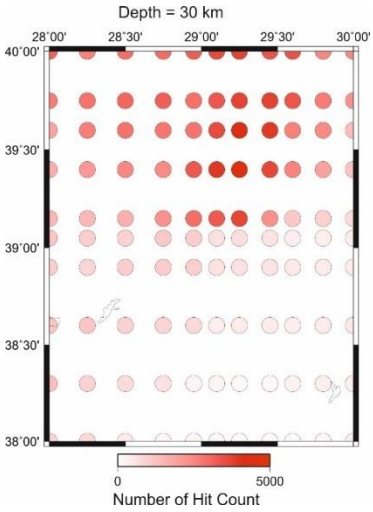


Figure 6.7. Ray density for each grid for the combined data.



Cont. Figure 6.7. Ray density for each grid for the combined data

Figure 6.7 shows the distribution of rays passing through the grids with different depths selected on the study field for the combined data set. The number of rays passing through one grid determines the resolution of velocity distribution. When the figures are analyzed -especially at shallow depth - it is observed that the area where the Simav earthquake occurred has a dense ray distribution, whereas the deeper areas –north of the areas where the Simav earthquake occurred- having also a denser ray distribution.

6.5. Results of 3-D Tomographic Inversions

In this thesis, three different data sets are used to calculate 3-D inversion. The following section includes the results of combined data set only. The results of AFAD and KOERI data sets together with combined data set's results are given in Appendix of this thesis.

6.5.1. P Phase Results

The tomographic inversion was performed with 5 iterations of simultaneous inversion. We provided final outcomes and the relocated hypocenters. For the travel times the rms

decreased from 0.139 sec to 0.117 sec for the *P* wave and 0.143 sec to 0.125 sec for the *S* wave. I also obtained Vp/Vs ratio values from the results of P and S wave inversion. All results will be displayed in horizontal and vertical cross section and interpret our results in the following sections. In Figs. 6.8, 6.9, 6.11 and 6.12, the blue perturbations indicate that the positive deviation of velocity from the initial 1-D model and the red perturbations indicate the negative deviation of velocity from the initial 1-D model. I showed Vp/Vs ratio values in Fig. 6.10, Fig. 6.11 and Fig. 6.12.

The horizontal cross-sections in Figure 6.8 below show the 3-D velocity distributions obtained from different depths for P phases. When all depth cross-sections are analyzed, the velocity distribution shows a significant change both laterally and vertically. It is important to note here that, similar to the 1999 Kocaeli earthquake, the main shock occurred near a cluster and like some other earthquakes the main shock occurred between the high velocity and low velocity zones.

Horizontal cross-sections of velocity perturrbation for combined data set is given with locations in Figure 6.8.

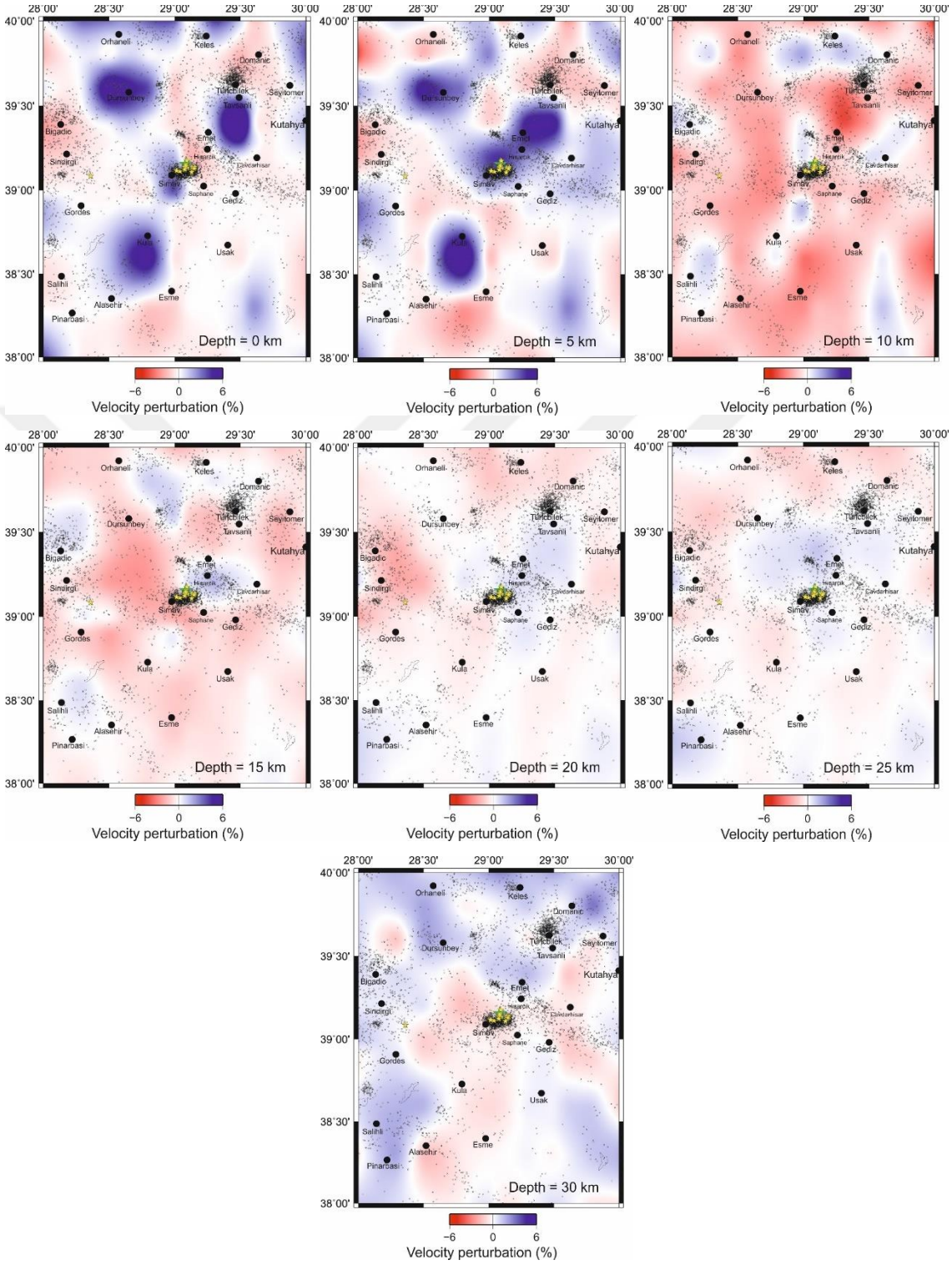


Figure 6.8. P wave velocity perturbations perturbations.obtained by the inversion for the integrated data and location. Blue and red colors represent high and low velocity perturbations.

In bove figure, large black dots show the location of town and city centers, red star shows main shock of the Simav earthquake, yellow stars show moderate size aftershocks and small black circles represent epicenters. The depth of each layer is given in the lower right corner of each map.

When the P velocity perturbations of the study area is examined, it is high perturbation regions are found in 0 km depth (surface layer) cross-section, namely east of Simav, Dursunbey, Kula, Emet and south of Tunçbilek. Also low velocity areas are seen around Domaniç, Şaphane and Gediz. A high velocity P zone in 5 km cross-section is clearly observed around Simav, Hisarcık, Emet, Dursunbey and Kula as well as in a large area including east of Gediz and Çavdarhisar and south of Kütahya. At this depth low velocity zones are seen in the area between Tunçbilek and Domaniç and alsoin the area between Seyitömer and Kütahya. The 10 km depth cross-section shows high velocity areas in a small area north of the main shock of the Simav earthquake, in a narrow area south of Simav, and Çavdarhisar as well as southwest and southeast of Keles. In this depth cross-section, low-velocity areas are the area between Emet, Tavşanlı and Tunçbilek, Seyitömer and Gediz, between Sındırgı and Simav and northwest of Simav. The 15 km velocity cross-section of P wave shows high velocity areas around northeast of Simav; Emet and Hisarcık, in the area northeast of Dursunbey. The low-velocity zones at these depths are observed in the region between Dursunbey and Simav. Simalar pattern is found inthe area between Emet, Tavşanlı and Tunçbilek; Keles and Seyitömer and west of Gördes. A high velocity zone in the 20 km depth cross-section is seen in the Simav, Emet, Gediz, and Şaphane areas and southwest of Tavşanlı. A low velocity zone in this cross-section is prevalently seen in the area between Simav, Bigadiç and Dursunbey and in the area between Keles, Tunçbilek and Domaniç. High velocity areas in 25 km depth cross-section are seen in Simav and the area between Dursunbey and Emet; Hisarcık, Şaphane; west of Gediz; south of Tavşanlı; north of Çavdarhisar; south of Kütahya. In this depth cross-section, a low-velocity zone is seen prevalently and with a low rate of change. The 30 km depth cross-section of P wave velocity shows that low-density with high-velocity zones are found in Simav, Şaphane, Keles, Dursunbey, Çavdarhisar and eastern parts of Kütahya. These high velocity bodies may correspond hard asperities. But, the depth distribution of seismicity show that seismicity is

very low in this depth and also resolution of tomographic results are very poor. So, these two factors effect the quality of the results. The low resolution result are not reliable in tomographic inversions and interpretation of these results lead us to wrong assumptions. So, it is adviced that it is better not to interpret these result (Eberhart-Philips, 1990 and 1993; Nakamura et al., 2002 and Baris et al., 2005).

Salah et al., (2007) concluded that two large 1999 Kocaeli and Duzce events occurred in highly heterogeneous zones namely distinctive zones characterized by average P velocity, low S wave velocity and high Poisson's Ratio. Zhao et al. (2007) concluded that the mainshock hypocenters of large interplate 12 large earthquakes M≥7.0 mainly cluster near the boundaries of high and low velocity zones on the subducting Pacific slab. Huang and Zhao (2004) studied seismic tomograpy including large crustal earthquakes in the Beijing region, such as the 1679 Sanhe earthquake (M8.0), the 1976 Tangshan earthquake (M7.8) and its two large aftershocks (the M6.9 Ninghe and the M7.1 Luanxian earthquakes). Vlahovic et al. (2003) indicated also larger earthquakes of magnitude ≥ 4 occurred along the edge of the high-velocity region.

On the other hand, in many different tomography studies conducted in subduction zones different velocity patterns have been observed than those in the above results. These studies include Kato et al., 2005; Wang and Zhao, 2006b; Xia et al., 2008, Wang and Zhao 2006b; Xia et al. 2008; Zhao et al. 2011b, Padhy et al. 2011; Zhao et al. 2010, 2011b).

6.5.2. S Phase Results

The horizontal cross-sections in Figure 6.9 show the 2-D velocity distributions for S phases taken at different depth cross-sections of the study area. It is observed that the velocity distributions differ in both lateral and vertical directions.

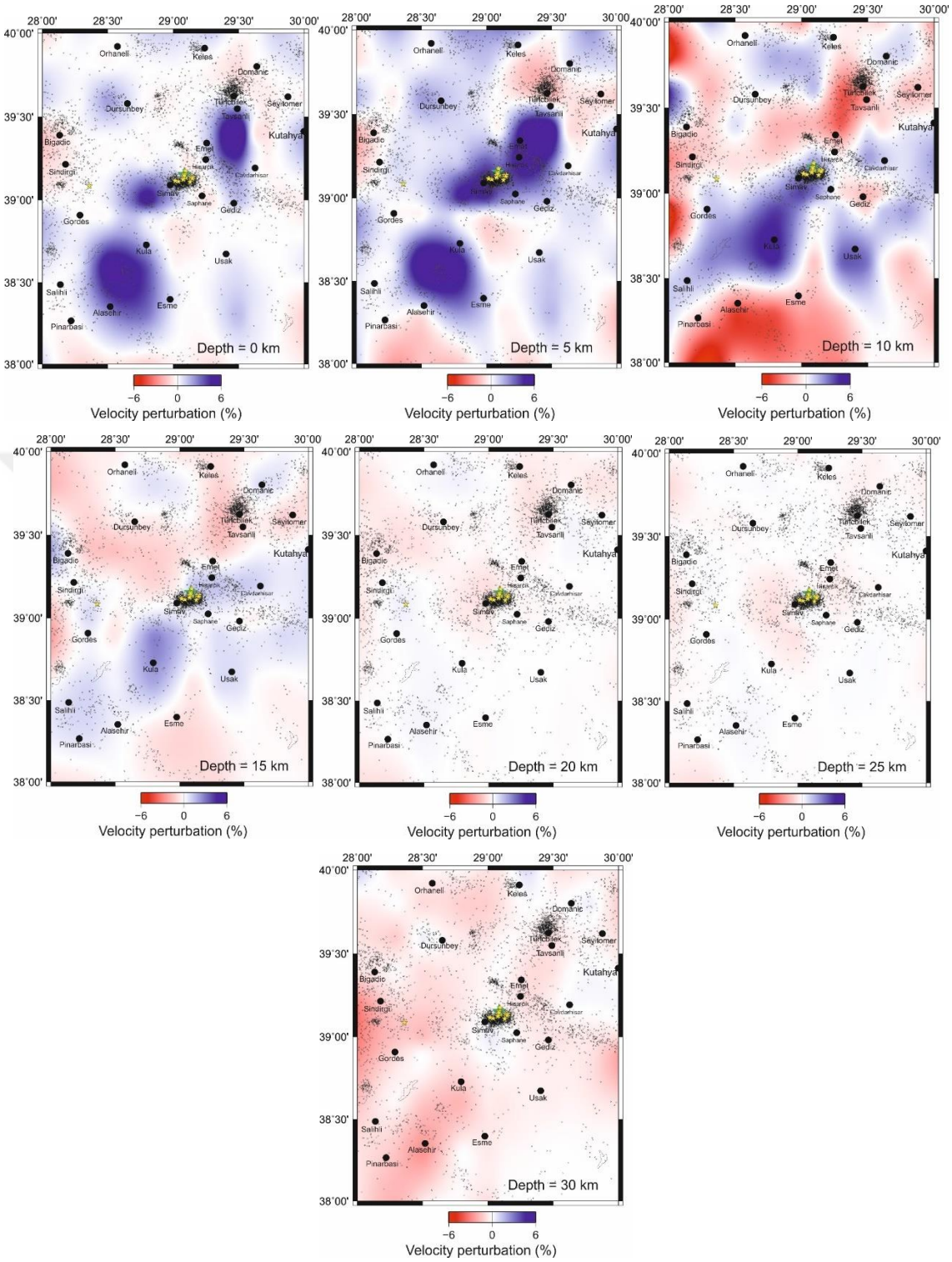


Figure 6.9. S wave velocity perturbations got by the inversion for the integrated data.

In above figure, large black dots show location of the town and city centers, red star shows main shock of the Simav earthquake, yellow stars show moderate size aftershocks and small black circles show epicenters relocated by the inversion. Resolution is poor in the 30 km depth slices due to low earthquake occurrence and also large grid nodes.

When considering the S velocity structure of the study area, at the 0 km depth (surface layer) cross-section, the high velocity region is located east of Simav, Dursunbey, Kula, Emet and south Tunçbilek. The low velocity region is located at Şaphane and Gediz. At the 5 km depth cross-section, the high velocity S zone specifically are marked Simav, Hisarcık, Emet, Dursunbey and Kula surroundings. Also high velocity perturbations are observed east of Gediz and Çavdarhisar, and south Kütahya. At this depth, low velocity zones are observed between Seyitömer and Kütahya, between southwest Tunçbilek, and Domaniç. At the 10 km depth cross-section, high velocity regions are observed at a small area north of the Simav main shock, a narrow area of south Simav and Çavdarhisar. At this depth cross-section, low velocity zones are observed between Emet, Tavşanlı and Tunçbilek, Seyitömer and Gediz, between Sındırgı and Simav, and northwest Simav. At the 15 km velocity cross-section, high velocity areas are observed northeast of Simav, Emet and Hisarcık surroundings. At the same depth, low velocity zones are located between Dursunbey and Simav, between Emet, Tavşanlı and Tunçbilek, between Keleş and Seyitömer, and West of Gördes. At the 20 km velocity cross-section of S wave, high velocity areas are observed between Simav, Emet, Gediz and Şaphane, southwest of Tavşanlı. Low velocity zones are located between Simav, Keles and Tunçbilek. At the 25 km velocity cross-section, high velocity areas are found between Simav, Dursunbey and Emet, between Hisarcık, Şaphane and west of Gediz, south of Tavşanlı, and south of Kütahya. At the same depth, low velocity zones are commonly observed and with a low variation rate. At the 30 km depth cross-section, low-density high-velocity zones are found between east of Simav, Şaphane, Keles, Dursunbey, Çavdarhisar, Kütahya. Due to low seismicity and poor resolution of the results belongs to the 30 Km cross section will not be interpreted.

6.5.3. Vp/Vs Results

Figure 6.10 cross-sections shows horizontal distribution from different depths for Vp/Vs ratio. Orange regions show higher value than 1.73 (entry data), dark blue regions show lower rates. When considering all depth cross-sections, Vp/Vs ratio shows significant change in the vertical and lateral directions.

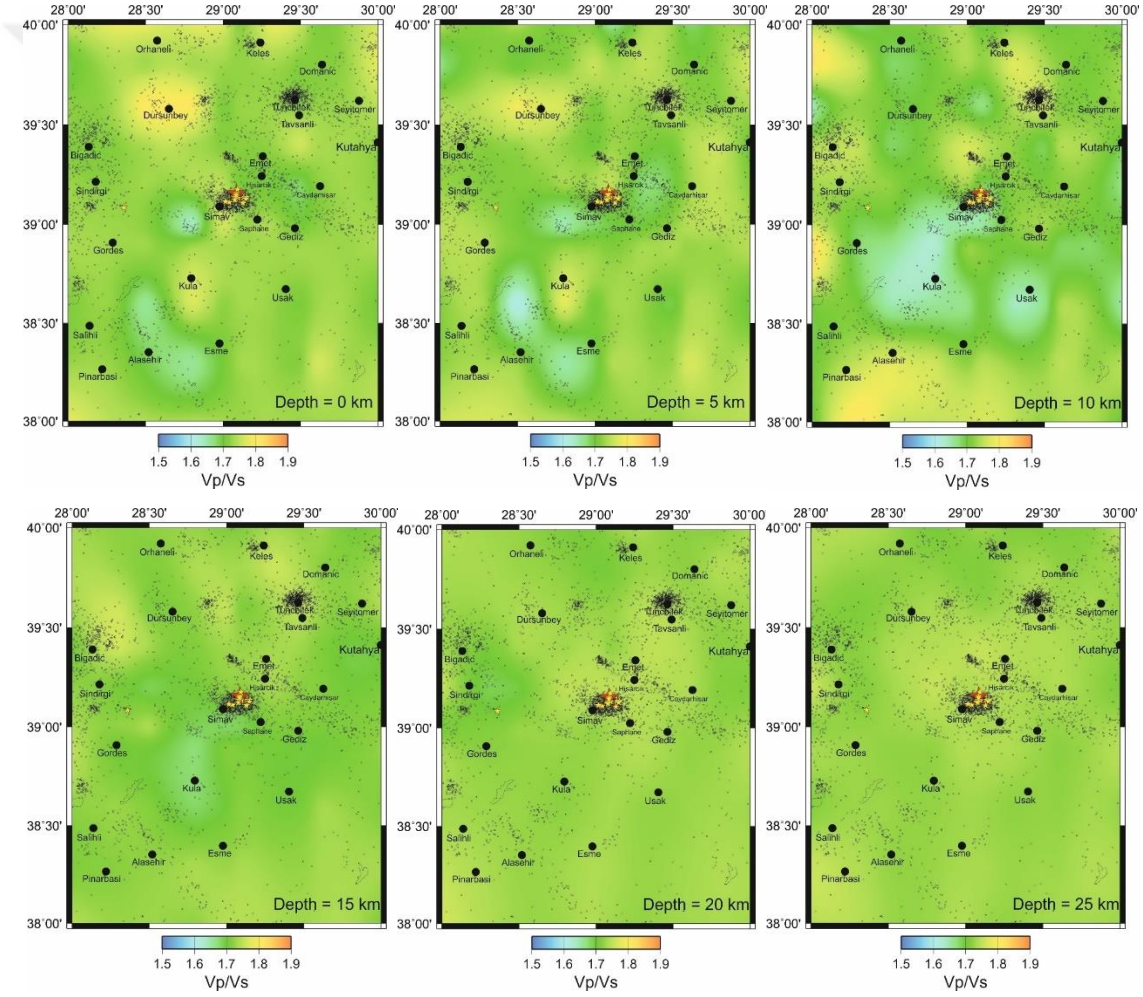
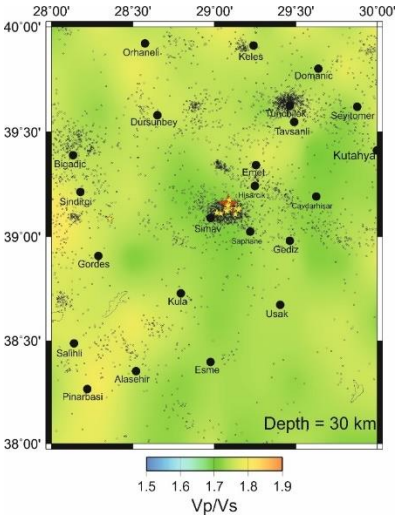


Figure 6.10. Horizontal cross section of Vp/Vs ratio's values obtained by the inversion. Blue and yellow colors show low and high Vp/Vs ratio.



Cont. Figure 6.10. Horizontal cross section of Vp/Vs ratio's values obtained by the inversion. Blue and yellow colors show low and high Vp/Vs ratio.

In above figure, red star shows the epicentre of the Simav mainshock, yellow stars show moderate aftershocks, small dots show the epicentres relocated by the inversion. Large black circles respresent location of the town and city centers.

When the Vp/Vs ratio of the study area is examined, high values are found in 0 km depth (surface layer) cross-section, namely east of Simav, Dursunbey, Kula, Emet and south of Tunçbilek. Also low value areas are seen around southwestern part of Simav. A high values in 5 km cross-section is clearly found around Dursunbey, North of Simav, Gediz and western part of Çavdarhisar and South of Kütahya. At this depth low value areas are seen Simav, the area between western part of Simav and Hisarcık-Çavdarhisar regions. The 10 km depth cross-section shows high values areas in Dursunbey and in a narrow area between the north of Simav and Hisarcık. In this depth cross-section, low-value areas are the region between the mainshock of Simav and southwestern part of Simav and Şaphane regions. The 15 km velocity cross-section of Vp/Vs ratio shows high value areas found between Tavşanlı-Tunçbilek and Keles, east of Seyitömer. The low-value zones at this depth is found only in a narrow area south of Simav. The high value areas seen in 15km depth cross section can be seen in also 20, 25 and 30 km cross sections. These regions are Emet-Tavşanlı and area

between Orhaneli and Dursunbey. Normal and smaller value zones are seen almots all over the region in these depths.

I examined the cross sections of velocity perturbation in the E-W direction and in the N-S directions crossing the mainshock regions. In Figures 6.11 and 6.12, I show the east-west cross sectional view of velocity perturbation along 39.15°N for (a) the *P* wave, (b) the *S* wave and (c) *Vp/Vs*. Figure 6.11 shows the cross sections along 39.15°N. Another important feature is that the Simav mainshock and most of the aftershocks including moderate aftershocks occurred in the high velocity region of P and S waves, and lower Vp/Vs regions. The Simav main shock occurred between a high-velocity and low-velocity area. A similar pattern was seen in 1999 Kocaeli earthquakes and many inner-crust earthquakes in Japan (Nakamura et al., 2002, Barış et al., 2005, Salah et al., 2007; Zhao et al., 2007). The seismogenic zone reaches up to 20 km depth. Below this depth there are not many earthquake occurred.

Also, I obtained cross sections in the N-S direction for P wave, S wave and Vp/Vs, especially for the Simav mainshock area. In Figure 6.12, I show the cross sections along 29.10°E. Another important feature is that most of the aftershocks, moderate aftershocks and the Simav mainshock occurred in the high velocity region of P and S waves, and lower Vp/Vs regions.

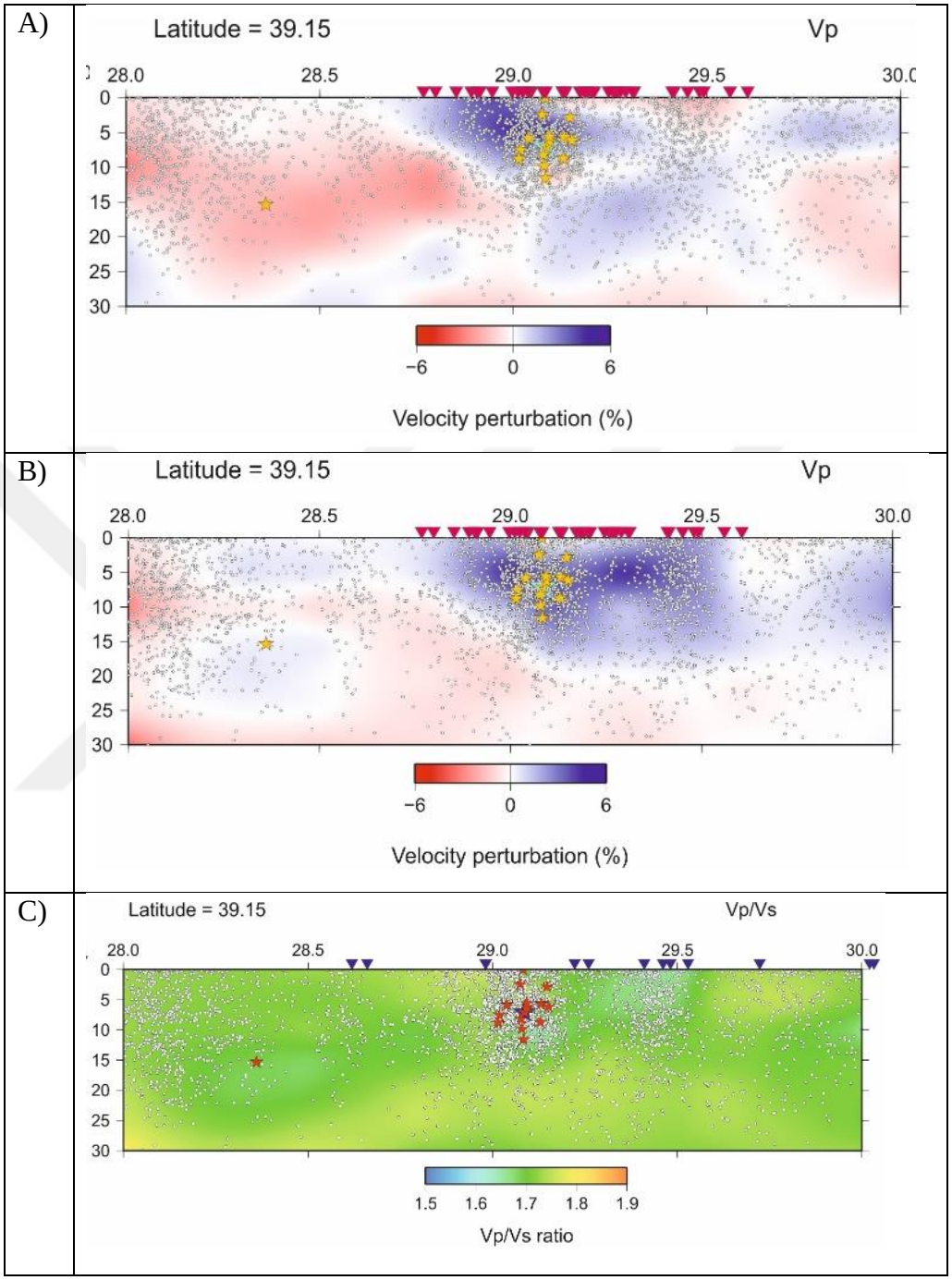


Figure 6.11. In the E-W direction along 39.15°N vertical cross section of velocity perturbation for (a) the P wave, (b) the S wave and (c) Vp/Vs.

When these cross-sections are examined, where the Simav earthquake occurred, a layer having a low-velocity zone on top probably indicates an alluvial layer probably Simav

Plain. As the earthquake distribution is concentrated shallower than 20 km, resolution of the velocity distribution is thought to be high until this depth and the velocity structure at depths below 20 km is expected to be not very accurate because of the low resolution. The Simav main shock occurred between a high velocity and low velocity area. On the other hand, the distribution of aftershocks and moderate aftershocks show almost vertical distribution Most of the aftershocks occurred in high-velocity areas. A similar pattern was seen in 1999 Kocaeli earthquakes and many inner crust earthquakes in Japan (Nakamura et al., 2002, Barış et al., 2005, Salah et al., 2007; Zhao et al., 2007).

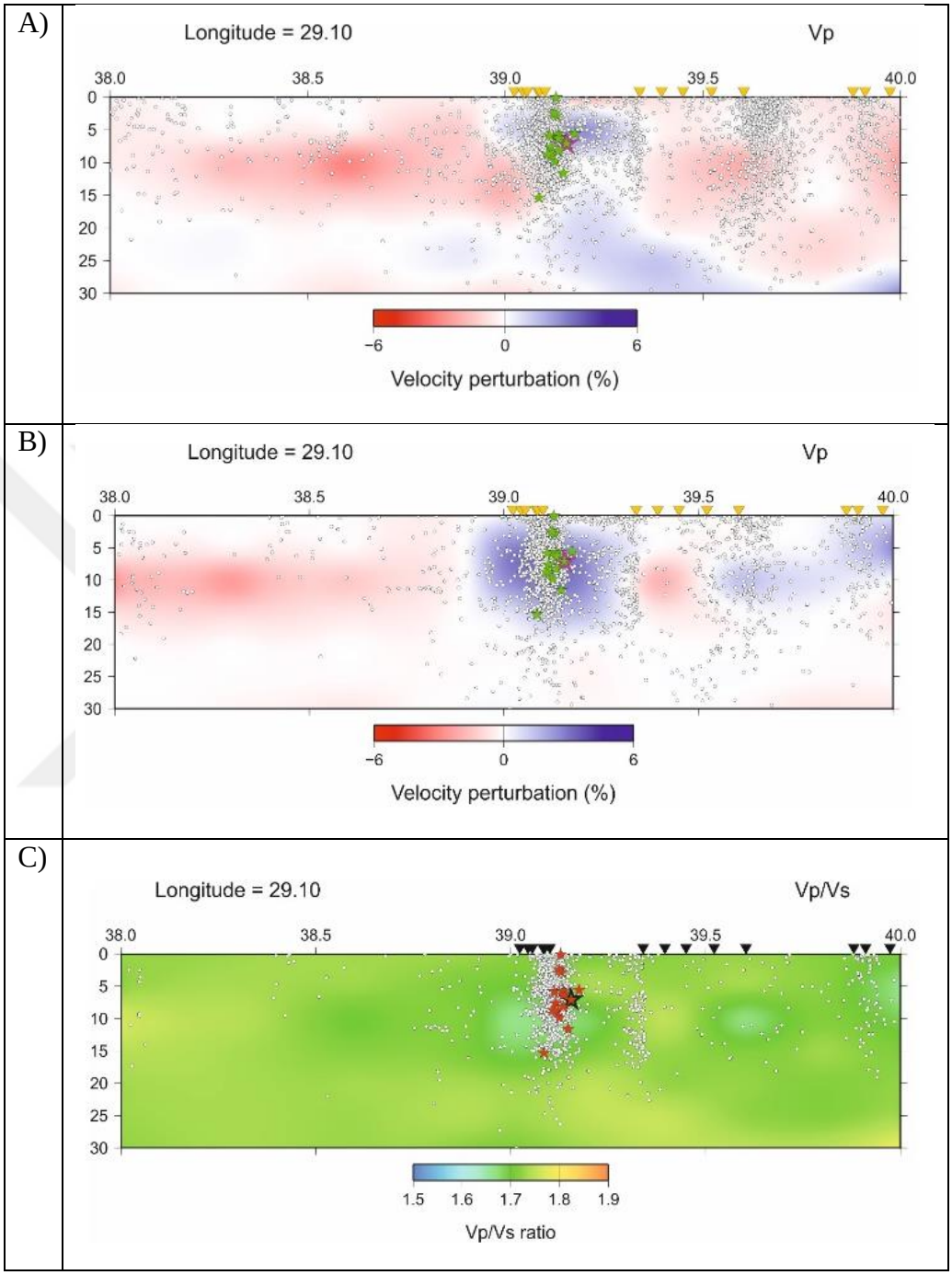


Figure 6.12. In the N-S direction along 29.10°E vertical cross section of velocity perturbation for (a) the P wave, (b) the S wave and (c) Vp/Vs ratio.

7. DISCUSSION AND CONCLUSIONS

Local earthquake tomography (LET) has become a relatively routine application for a region covered by a dense seismic network. In this study, I built a 3-D P-wave velocity model by iterating a minimum 1-D P-wave velocity model for the Simav (Kütahya) region and surroundings in southwestern Turkey. Data from a five-year (Januray 2010 - July 2015) field experiment was used to compute 1-D and 3-D P-wave velocity models beneath the Kütahya region and surroundings in southwestern Turkey. The resulting 3-D P-wave velocity model yields high quality earthquake locations with average location errors of 1 km horizontally. Although the 1-D P-wave velocity model can be used as an earthquake location procedure, a 3-D P-wave velocity model can be used in comparative studies. The distribution of seismicity is apparently linked to active faults in the region, notably the Simav Fault-Zone. Resolution and stability tests demonstrate that the 1-D and 3-D P-wave velocity structure at 20 km depth is well resolved in this study.

Since the main aim of this study is to resolve the upper crustal model of the Simav (Kütahya) region and surroundings, the local earthquake tomography method has been used. The Simav region and surroundings is an active region in terms of seismicity. However, mostly shallow depth earthquakes occur here so the observed phases are mostly the direct arrivals (Pg, Sg). This makes the region compatible to study the LET method. The dense network also makes this region reasonable to study the LET method properly.

The use of local earthquakes as sources of seismic arrival time tomography has advantages and disadvantages. Their spatial 3-D distribution makes it feasible to use them to determine a 3-D velocity model of the crustal structure. However, the lack of control of their distribution and knowledge of their exact locations and origin times are disadvantages. Compared with the other seismic travel time tomography types, LET can usually offer much higher spatial resolution of structure due to the higher density of ray sampling, higher wave frequency and closer station spacing. The depth extent of LET is limited due to including subsurface events and higher wave frequency. The a priori 1-D P-wave velocity model was generated by using more than 15,400 well locatable events, station coordinates and 1-D

preliminary P-wave velocity models generated by a trial and error process. This model was improved by combining adjacent layers with similar velocities. A 1-D P-wave velocity model and final earthquake locations were used as input to the 3-D tomography process. With the LET method, the 3-D P-wave velocity structure of the upper crust was resolved. Careful analysis of resolution capabilities of the data set demonstrates that the velocity model in the central part of Simav and surroundings is well resolved on a 20x20 km horizontal grid to a depth of about 20 km. The hypocentral distribution of the events indicates that peak seismicity for the region occurs at depths of about 15 km. The earthquake locations used in this study basically focus on three points: the central part of Simav, Emet and along some fault lines in the study region. The depth of earthquakes varies from 10 km to 25 km. The depth range of the earthquakes illustrates the recent and active deformation zones in the region. There are also deeper earthquake locations; however the ray density is relatively low for these regions.

The resulting 3-D P-wave velocity model was sampled by cross-sections across constant latitudes, cross-sections perpendicular to the main discontinuity systems and cross-sections that cut across earthquake locations high in magnitude. E-W oriented depth-cross-sections show that P-wave velocity below the 17 km depth increases from west to east. The western and eastern part of the region display seismic heterogeneity and different velocity perturbations.

The P wave velocity of sedimentary layers is slow and the P wave velocity of volcanic rocks is higher. In the study area, high velocity regions were located at depths of 0, 5, 10 and 15 km, and usually in areas of volcanic and metamorphic rocks. Geologically, Simav and Kula volcanos located in the region. When P wave velocity variation examined at 20, 25 and 30 km depths of 3-D depth cross-sections, shows the velocity to be low at these depths. The reason is may be the pore pressure and the presence of some liquids at these depths. Variation of velocity caused by the temperature and physical structure of rocks can also be interpreted. In the 0, 5, 10 and 15 km depth cross-sections, high velocity and low Vp/Vs ratio in regions such as Simav, Kula, Uşak and Emet may indicate the presence of metamorphic rocks. Same results are given Li et all., 2009. The tectonic and geological formation process of these regions occurred with active volcanism and as a result of this formation, metamorphic

structures have been mapped widely in the region (Gündüz et all., 2010; Belonko, O., 2013; Okay, A., 2004; Gemici and Tarcan, 2002; Oberhänsli et all., 1997. On the other hand, Powell, C. A., (2011) identified that low Vp/Vs values can explain the presence of composition in quartz-rich rocks and quartz-rich rocks can show a ductile feature. It can be said that this evaluation is concerned with the composition of the rocks in the area.

The Nafe-Drake (1963) curve that gives the relationship between the P-wave velocity and density of water-saturated sediments and sedimentary rocks, supports the hypothesis that quartz-rich metamorphic rocks have high velocity and low Vp/Vs values.

The Vp/Vs ratio significantly depends on the mineral composition of rocks, size and distribution of the particles that constitute the rock texture, porosity, the type and amount of the pore water, compression degree, cement degree, medium volume and as a result, the age of rocks related to geological history. The growth of the Vp/Vs ratio indicates plenty of porous loose sedimentary layers, if rocks are magmatic it indicates joint and fracture systems in the medium (Açık, 2006).

Ercan (2001) identified the solid-liquid status of the rocks classified by Vp/Vs ratio. According to this classification, if the Vp/Vs ratio is between 1.87-1.71, rocks are solid-liquid. If the Vp/Vs ratio is between 1.71-1.50, rocks are solid and if Vp/Vs ratio is greater than 1.87, rocks are loose. According to this classification, at depth cross-section of 0 km, regions such as Simav, Kula, Dursunbey and Tunçbilek have a loose rocks structure. In this depth cross-section, southwest of Simav and southern region have solid features. It can be said that solid-liquid soils are related to sedimentary layers of the area. In this study, the Vp/Vs ratio is calculated to be greater than 1.87. This ratio shows that as loose rocks are quite low or smaller volume in the region. At the 5 km of depth cross-section, Simav, Hisarcık, Emet area has solid structure, north Simav, Dursunbey and many regions have loose structure. At 10 km depth cross-section, a wide region between Simav and Kula has solid rocks. At 15 km depth cross-section, structural features are the same as at 10 km depth cross-section but rates decrease. At depths of more than 15 km, the region shows the presence of rocks with tight-solid features. Probably, this can be related to ongoing tectonics and geothermal activity.

This study is the first 1-D velocity model and 3-D seismic tomography study conducted for Simav and surrounding regions. Data obtained by two national data centres were used to derive the 3-D crustal structure. Both data centres have used different 1-D models and location programs. When three data sets are examined, P and S phases that belong to Simav earrhquake and aftershocks, there are many earthquakes were used than other tomography studies in Turkey. I believe that using a very large data set including many S phases can be regarded as improving the reliability of the results obtained. The VELEST 1-D velocity model was used for the location of a new data set that was produced by combining the two data sets.

To conclude, tomographic results reveal that there are lateral velocity variations beneath central Simav and surroundings. Shallow low velocity zones interpreted as alluvium deposits, and relatively higher velocity below 25 km depth can be explained as the transition from upper crust to lower crust.

No previous tomography results from this region could be obtained and therefore comparison of my results was not possible. Magnetotellurics (MT) measurements that can provide deep crustal information, and cross-section results of magnetic and gravity profiles could also not be obtained. I noticed in the internet a TUBİTAK project using integrated geophysical methods are completed for this region, the results could not be accessed. No publication showing the results of MT or other geophysical measurement made in this project could be found. This is probably because a publication is still under preparation. Three seismic stations were established in the region by COMU (Bekler, T., personel communication) and aftershocks of Simav earthquake were recorded. However, phase readings from this study were also not used. Using phase readings from these data together with existing data sets and obtaining a new data set and 1-D velocity model would be a great benefit. For the region, creating a new crustal model from the new dat set and obtaining a new 3-D velocity model are of great benefit. During combination of AFAD and KOERI data, seismic phases did not read from the seismograms, but only phase readings belongs to the same earthquake was used. These data were relocated with the obtained VELEST velocity model. Such a process can accommodate possible erroneous readings. However, 3-

D velocity models were examined for each of the three data sets and similar results were obtained in all depth cross-sections. In a future study, reading phases belonging to different data centres with a similar program and relocation using only the same 1-D velocity model would be of great benefit. Furthermore, comparing the tomography results with other geophysical observation results in the region and other earthquake tomography results, has great importance. In this study, the 3-D velocity and crustal structure obtained is based on the data and the station distribution, defined grid sets and accepted damping parameters. In conclusion, the obtained velocity model is one of the possible velocity models for his region. The 3-D velocity structure of the region maybe obtained with a new data set that has been more denser station distribution and including seismic phases recorded by COMU stations.

REFERENCES

1. Açık, Ö., *Sıcak çermik travertenleri ve Ulaş-Akkaya Sölestr Madeninin(Sivas) Sismik Kırılıma yöntemi kullanılarak Araştırılması*, Master Tezi, Cumhuriyet Üniversitesi Fen Bilimleri Enstitüsü, 2006.

2. Akdeniz, N. and N. Konak, *Simav- Emet- Tavşanli- Dursunbey-Demirci yörelerinin jeolojisi (Geology of Simav -Emet –Tavşanli-Dursunbey- Demirci area).* MTA report no: 6547, 1979.

3. Aki, K., A. Christoffersson, E. S. Husebye, *Three-dimensional seismic-velocity anomalies in the crust and upper-mantle under the U.S.G.S. California seismic array (abstract),* Eos. Trans. Am. Geophys. Union, 56, 1145,1974.

4. Aki K. and W. H. K. Lee, *Determination of three-dimensional velocity anomalies under a seismic array using first P arrival times from local earthquakes: 1. A homogeneous initial model.* Journal of Geophysics Research Volume 81, Solid Earth and Planets Pages 4381- 4399, 1976.

5. Ambraseys N. N. and J. S. Tchalenko, *Seismotectonic aspects of Gediz, Turkey, Earthquake of March 1970.* Geophysical Journal of the Royal Astronomical Society Volume 30, Issue 3, pages 229–252, 1972.

6. Ardos M., *Türkiye Ovalarının Jeomorfolojisi*, Cilt I, 2. Baskı, Çantay Yayınevi, İstanbul, 1995.

7. Aslan, Ö., *Armutlu - Gemlik civarının 3 boyutlu Sismik hız yapısı*, Master Thesis, Kocaeli University, 2008.

8. Ateş Ö. and S. Z. Tutkun, *Hydrochemical Changes in Geothermal Systems with Simav (Kütahya) Earthquakes*, Geological Bulletin of Turkey Volume 57, Number 3, 2014.

9. Aydan, Ö. and H. Kumsar, *A Preliminary Report The May 19, 2011 Simav, Turkey Earthquake*, Pamukkale University, 2011.

10. Barış, Ş., J. Nakajima, A. Hasegawa, Y. Honkura, A. Ito, S. B. Üçer, *Three-Dimensional Structure of Vp, Vs and Vp/Vs in the upper Crust of the Marmara Region, NW Turkey*, Earth Planets Space, 57, 1019–1038, 2005.

11. Bekler, T., A. Demirci, S. Özden, D. Kalafat, *Simav Ve Emet Fay Zonlarındaki Depremlerin Optimum Kaynak Parametrelerinin Analizi*, 1. Türkiye Deprem Mühendisliği ve Sismoloji Konferansı, Orta Doğu Teknik Üniversitesi, Ankara, 2011.

12. Bello A. O., *Simav ve Yakın Çevresi Jeotermal Sularının Hidrojeolojik, Hidrojeokimyasal ve İzotop Jeokimyasal Özellikleri,* Master Tezi, Süleyman Demirel Üniversitesi Fen Bilimleri Enstitüsü, 2013.

13. Biryol, C.B., S. L. Beck, G. Zandt, and A.A. Özacar, *Segmented African Lithosphere beneath the Anatolian Region Inferred from Teleseismic P-wave Tomography*, Geophys. J. Int., Vol. 184, pp. 1037-1057, 2011.

14. Bozkurt, E., *Late Alpine evolution of the central Menderes Massif, western Anatolia, Turkey.* International Journal of Earth Sciences, 89, 728-744, 2011.

15. Cambaz, M.D., and H. Karabulut, *Love-wave Group Velocity Maps of Turkey and Surrounding Regions*, Geophys. J. Int., Vol. 181, pp. 502-520, 2010.

16. Çakır E., *3-D Crustal Structure Of The Isparta Angle Regıon From Local Earthquake Tomography*, Master Thesis, KOERI Boğaziçi University, 2011.

17. Çiftçi N.B. ve E. Bozkurt, *Anomalous Stress Field and Active Breaching at Relay Ramps: A Field Example from Gediz Graben, SW Turkey.* Geological Magazine, 144: 687-699, 2007.

18. Cheng, B., S. Cheng, G. Zhang, D. Zhao, *Seismic structure of the Helan-Liupan-Ordos western margin tectonic belt in North-Central China and its geodynamic implications*. J. Asian Earth Sci. 87, 141-156, 2014.

19. Cheng, B., D. Zhao, G. Zhang, *Seismic tomography and anisotropy in the source area of the 2008 Iwate-Miyagi earthquake (M 7.2).* Phys. Earth Planet. Inter. 184, 172–185, 2011.

20. Demirci A., *Seismicity And Seismotectonic Characteristics Of Simav (Kutahya) Fault,* Ph.D. Thesis, Çanakkale 18 Mart University, 2013.

21. *Preliminary Report on Kütahya - Simav Earthquake Western Turkey,* AFAD, 2011.

22. Doğan, A., Ö. Emre, *Ege Graben Sistemi'nin Kuzey Sınırı: Sındırgı-Sincanli Fay Zonu*. 59. Türkiye, 2006.

23. Eberhart-Philips, D., *Three-Dimensional Velocity Structure in Northwestern California Coast Ranges from Inversion of Local Earthquake Arrival Times,* Bulletin of the Seismological Society of America, Vol. 76, No. 4, pp. 1025-1052, 1986.

24. Eberhart-Phillips, D., and A.J. Michael, *Three-dimensional Velocity Structure, Seismicity and Fault Structure in the Parkfield region, Central California*, Journal of Geophysical Research, Vol. 98, pp. 15737-15758, 1993.

25. Eberhart-Phillips, D., *Local earthquake tomography: earthquake source regions.* In: H.M. Iyer and K. Hirahara (Editors), Seismic Tomography: Theory and practice. Chapman & Hall, London, pp. 613-643, 1993.

26. Eberhart-Phillips, D., *3D P and S velocity structure in the Coalinga region, California*, J. Geophys. Res., 95, pp. 15343-15363, 1990.

27. Emre, Ö., T. Y. Duman, *19 Mayıs 2011 Kütahya (Simav) Depremi (Mw=5.8) Ön Değerlendirmesi*, Jeolojik Etüdler Dairesi, MTA, Ankara, Türkiye, 2011.

28. Emre, Ö., T. Y. Duman, S. Özalp, A. Doğan, *Simav Fayı ve 19 Mayıs 2011 Simav Depremi (Mw=5.8)*, 65. Türkiye Jeoloji Kurultayı, MTA, Ankara, Türkiye, 2012.

29. Ercan A., *Kıran bölgeelrinde Yeraraştırma Yöntemleri,* Kardeşler Yayınevi, İstanbul, 2001.

30. European Macroseismic Scale, EMS-98, *European Seismological Commission, Subcommission on Engineering Seismology*, Working Group Macroseismic Scales, Luxembourg, 1998.

31. Eyidoğan, H., J. Jackson, *A seismological study of normal faulting in the Demirci. Alaşehir and Gediz earthquakes of 1967-70 in western Turkey: implications for the nature and geometry of deformation in the continental crust*. Geophysical Journal of the Royal Astronomical Society. London. 81. 569-607, 1985.

32. Gemici Ü. and G. Tarcan, *Hydrogeochemistry of the Simav geothermal field, Western Anatolia, Turkey*. Elsevier Journal of Volcanology and geothermal research, 116 (2002) 215-233, 2002.

33. Glover, C., and A. Robertson, *Neotectonic Intercross-section of the Aegean and Cyprus Tectonic Arcs: Extensional and Strike-slip Faulting in the Isparta Angle, SW Turkey,* Tectonophysics, Vol. 298, pp. 103-132, 1998.

34. Gökalp, H., *Local earthquake tomography of the Erzincan Basin and the surrounding area in Turkey*, Annals Of Geophysics, Vol. 50, N. 6, pp 707-724, 2007.

35. Gökkaya G., *Denizli ve Dolayının Üç Boyutlu Sismik. Hız Yapısının Yerel Deprem* Tomografisi *Yöntemi ile Belirlenmesi,* Master Tezi, Ankara University, 2008.

36. Güleç, N. and D. R. Hilton, *Helium and Heat Distribution in Western Anatolia, Turkey: Relationship to Active Extension and Volcanism. In: Dilek, Y. and Pavlides, S. (eds.) Post-Collisional Tectonics and Magmatism in the Eastern Mediterranean Region*, GSA Special Paper 409, Geological Society of America, p.305-319, 2006.

37. Gündüz, O., C. Simsek, A. Hasozbek, *Arsenic Pollution in the Groundwater of Simav Plain, Turkey: Its Impact of on Water Quality and Human Health,* Water Air Soil Pollut, 205:43-62, DOI 10.1007/s11270-009-0055-3, 2010.

38. Hasegawa, A., D. Zhao, *Deep structure of island arc magmatic regions as inferred from seismic observations.* In: M. P. Ryan (ed.) Magmatic Systems pp. 179–195, Academic Press, Burlington, 1994.

39. Hasegawa, A., J. Nakajima, N. Umino, S. Miura, *Deep structure of the northeastern Japan arc and its implications for crustal deformation and shallow seismicity*. Tectonophysics 403, 59–75, 2005.

40. Hawley, B.W., G. Zandt, and R.B. Smith, *Simultaneous Inversion for Hypocenters and Lateral Velocity Variations: An Iterative Solution with Layered Model*, J. Geophys. Res., Vol. 86, pp. 7073-7076, 1981.

41. Hirahara, K., *Seismic Tomography: Theory and Practice: Tomography using both local earthquake and teleseisms: velocity and anisotropy-theory*, Iyer H.M. ve Hirahara, K., Chapman & Hall, London, 493-518, 1993.

42. Horiuchi, S., H. Ishii and A. Takagi, *Two-dimensional depth structure of the crust beneath the Tohoku District, I. Method and Conrad Discontinuity*, J. Geophys. Res., Vol. 30, pp. 47-69, 1982.

43. Huang, J., D. Zhao, *Crustal heterogeneity and seismotectonics of the region around Beijing, China*, Tectonophysics v. 385, pp. 159–180, 2004.

44. Huang, J., D. Zhao, *Seismic imaging of the crust and upper mantle under Beijing and surrounding regions.* Phys. Earth Planet. Inter. 173, 330–348, 2009.

45. Işık V., *Micro-tectonic Features of Simav Shear Zone, Northern Menderes Massif, Western Turkey*. Bulletin of Geological Society of Turkey, 47:49-91, 2004.

46. İnan S., Z. Pabuçcu, F. Kulak, S. Ergintav, O. Tatar, E. Altunel, S. Akyüz, O. Tan, C. Seyis, R. Çakmak, R. Saatçılar ve H. Eyidoğan, *Microplate Boundaries as Obstacles to Pre-earthquake Strain Transfer in Western Turkey: Inferences from Continuous Geochemical Monitoring*, Journal of Asian Earth Sciences, 48:56-71, 2011.

47. Kahraman, M., *Crustal structure of Isparta Angle surrounding regions using P-receiver function analysis*, Master Thesis, Boğaziçi University, 2008.

48. Kalafat, D., C. Gürbüz, ve S. B. Üçer, *Batı Türkiye'de kabuk ve üst manto yapısının araştırılması.* Deprem Araştırma Bülteni, 59, 43-64, 1987.

49. Kato, A., T. Igarashi, K. Obara, S. Sakai, et al., *Imaging the source regions of normal faulting sequences induced by the 2011 M9.0 Tohoku-Oki earthquake*. Geophys. Res. Lett. 40, 273–278, 2013.

50. Kato, A., E. Kurashimo, H. Hirata, T. Iwasaki, T. Kanazawa, *Imaging the source region of the 2004 Mid-Niigata prefecture earthquake and the evolution of the seismogenic thrust related fold*. Geophys. Res. Lett. 32, L07307, 2005.

51. Kaypak, B., *Erzincan havzası 3-D hız yapısının yerel deprem tomografisi yöntemi ile belirlenmesi,* Doktora Tezi, İstanbul Teknik Üniversitesi, 224 s., İstanbul, 2002.

52. Kissling E., VELEST User's Guide, ftp://ftp.ingv.it/pub/mario.anselmi/. 31 pages, 1995.

53. Kissling, E., W.L. Ellsworth, D. Eberhart-Philips, and U. Kradolfer, *Initial Reference Models in Seismic Tomography,* J. Geophys. Res., Vol. 99, pp. 19635-19646, 1994.

54. Kissling E., *Geotomography with local earthquake data,* Rev. Geophys., 26, 659-698, 1988.

55. Koçyiğit A., *Güneybatı Türkiye ve Yakın Dolayında Levha İçi Yeni Tektonik Gelişim*. TJK Bülteni, 27:1-16, 1984.

56. Koçyiğit, A., *Tectono-stratigraphic characteristics of Hoyran Lake Region,* Inter. Symp. on the geology of the Taurus belt., 53-67, Ankara, 1984.

57. Koçyiğit, A., Ş. Deveci, *Akşehir-Simav Fault System: commencement age of neotectonic regime and seismicity, SW Turkey*. Deprem Sempozyumu Kocaeli 2005, Özler Kitabi, s.26, 2005.

58. Koçyiğit, A., Ş. Deveci, *Çukurören- Çobanlar Afyon) arasindaki deprem kaynaklarinin (Aktif faylarin) belirlenmesi*, TÜBİTAK, Proje No: 106Y209, 71s., Ankara, 2007.

59. Konak, N., *Simav grabeni ve getirdiği kent sorunları (Simav graben and related ·problems of urbanisation).* Türkiye Jeoloji Mühendisliği. 1. Bilimsel ve Teknik Kongresi. Bildiriler. 157-164, 1979.

60. Konak, N., *Simav dolayının jeolojisi ve metamorfik kayaçlanma evrimi, Geology of Simav and the evolution of metamorphic rocks*. İ.Ü.M.F. Yerbilimleri Dergisi. 3. 313-337, 1982.

61. Lee, W. H. K. and J. C. Lahr, *HYP071: A computer program for determining hypocenter, magnitude, and first motion pattern of local earthquakes*, *Open File Report, U. S. Geological Survey*, 100 pp, 1972.

62. Li, Z., Y. Xu, T. Hao, J. Liu, L. Zhang, *Seismic Tomography and Velocity Structure in the Crust and Upper Mantle Around Bohai Sea Area,* Chineese Journal of Geophysics, Vol. 49, Issue 3, Pages 698–706, 2006.

63. Li, Z., B. Tian, S. Liu, J. Yang, *Asperity of the 2013 Lushan earthquake in the eastern margin of Tibetan Plateau from seismic tomography and aftershock relocation,* Geophys. J. Int. 195, 2006-2022, 2013.

64. Lienert, B.R., E. Berg, and N. Frezer, *HYPOCENTER: An Earthquake Location Method Using Centered, Scaled and Adaptively Damped Least Squares*, BSSA, Vol .76, No. 3, pp. 771-783, 1986.

65. McClusky, S., S. Balassanian, A. Barka, C. Demir, S. Ergintav, I. Georgiev, O. Gurkan, M. Hamburger, K. Hurst, H. Kahle, K. Kastens, G. Kekelidze, R. King, V. Kotzev, O Lenk, S. Mahmoud, A. Mishin, M. Nadariya, A. Ouzonis, D. Paradissis, Y. Peter, M. Prilepin, R. Reilinger, I. Sanli, H. Seeger, A. Tealeb, M. N. Toksöz, G. Veis, *Global Positioning System constraints on plate kinematics and dynamics in the eastern Mediterranean and Caucasus*, J. Geophys. Res., 105: 5695-5720, 2000.

66. McKenzie, D., *Active tectonics of the Alpine-Himalayan belt: the Aegean Sea and surrounding regions*, Geophys. J. R. astr. Soc., 55, 217–254, 1978.

67. Mercier et al., *Principal results of a neotectonic study of the Aegean arc and its location within the Eastern Mediterranean,* Proc. VI Coll. Geol. Aegean Region Athens, Volume 3, Pages 1281-1291, 1976.

68. Nafe, J. E., and C. L. Drake, *Physical properties of marine sediments. In Hill, M. N. (Ed.) The Sea* (Vol. 3): New York (Interscience), 794-815, 1963.

69. Nakamura, A., A. Hasegawa, A. Ito, S. B. Üçer, Ş. Barış, Y. Honkura, T. Kono, S. Hori, R. Pektaş, T. Komut, C. Çelik and A. M. Işıkara, *P-Wave Velocity Structure of the Crust and Its Relationship to the Occurrence of the 1999 İzmit, Turkey, Earthquake and Aftershocks*, Bull. Seismol. Soc. Am. 7 92, 1, pp. 330-338, 2002

70. Oberhänsli, R., O. Candan, O. Ö. Dora, S. Dürr, *Eclogites within the Menderes Massif, Western Turkey*, Lithos 41, 135-150, 1997.

71. Okada, T., N. Umino, A. Hasegawa, *Deep structure of the Ou mountain range strain concentra-tion zone and the focal area of the 2008 Iwate-Miyagi Nairiku earthquake, NE Japan—Seismo-genesis related with magma and crustal fluid*, Earth Planets Space 62, 347–352, 2010.

72. Okay A.I., *Tectonics and high pressure metamorphism in Northwest Turkey*. 32nd Geological Congress. Field trip guide book, İstanbul, 2004.

73. Oygür, V., A. Erler, *Metallogeny of the Simav Graben (Inner-Western Anatolia, Turkey),* Geological Bulletin of Turkey Vol.43, No. 1, 7-19, 2000.

74. Öner Z., D. Yıldırım, *Supradetachment basin evolution during continental extension: The Aegean province of western Anatolia, Turkey,* Geological Society of America Bulletin, November 2011, v. 123, no. 11-12, p.2115-2141, Miami University, 2011.

75. Padhy, S., O. P. Mishra, D. Zhao, W. Wei, *Crustal heterogeneity in the 2007 Noto-Hanto earthquake area and its geodynamical implications*. Tectonophysics. 509, 55–68, 2011.

76. Paige, C.C. and M. A. Saunders, *LSQR: an algorithm for sparse linear equations and sparse least squares,* ACM Trans. Math. Software, 8, 43–71, 1982.

77. Powell, A.C., *Low Vp/Vs ratios and Earthquake Occurrence in Intraplate Seismic zones,* American Geophysical Union, Fall Meeting 2011, abstract #S22A-08, 2011.

78. Poyraz, S.A., *Isparta Büklümünü Oluşturan Tektonik Yapıların Sismolojik Yöntemlerle Araştırılması,* Ph.D. Thesis, Istanbul University, 2009.

79. Qi, C., D. Zhao, Y. Chen, *3-D P and S wave velocity structures and their relationship to strong earthquakes in the Chinese capital region*. Chin. J. Geophys. 49, 805–815, 2006.

80. Reilinger, R., S. McClusky, D. Paradissis, S. Ergintav and P. Vernant, *Geodetic constraints on the tectonic evolution of the Aegean region and strain accumulation along the Hellenic subduction zone*. Tectonophysics, 488: 22–30, 2010.

81. Robertson, A.H.F., *Mesozoic–Tertiary Sedimentary and Tectonic Evolution of Neotethyan Carbonate Platforms, Margins and Small Ocean Basins in the Antalya Complex, SW Turkey,* Spec. Publ. Int. Assoc. Sedimentol., Vol. 20, pp. 415–465, 1993.

82. Salah, M., S. Sahin, C. Destici, *Seismic velocity and Poisson's ratio tomography of the crust beneath southwest Anatolia: an insight into the occurrence of large earthquakes*. J. Seismol. 11, 415–432, 2007.

83. Seyitoglu, G., B. C. Scott, *Age of the Alaşehir graben (West Turkey) and its tectonic implications,* Geological Journal Vol 31, Issue 1, pg 1–11, 1996.

84. Seyitoglu, G., *The Simav Graben: An example of young E-W trending structure in the late Cenozoic Extensional systemof western Turkey*, Tr. J. Of earth Sciences, 6, 135-141, 1997.

85. Şaroğlu,F., Ö. Emre, İ. Kuşçu, *Active Fault Map of Turkey, 2 sheets*. General Directorate of Mineral Research and Exploration -GDMRAE, Ankara, Turkey, 1992.

86. Tezel, T., T. Shibutani, and B. Kaypak, *Crustal Structure Variation in Western Turkey Inferred from the Receiver Function Analysis,* Tectonophysics, Vol. 492, pp. 240-252, 2010.

87. Tokay, M., ve V. Doyuran, *Gediz ve Dolaylarının Sismotektonik Özellikleri*. Türkiye Jeoloji Kurumu Bülteni, 22: 209-211, 1979.

88. Tong, P., D. Zhao, D. Yang, *Tomography of the 2011 Iwaki earthquake (M 7.0) and Fukushima nuclear power plant area.* Solid Earth 3, 43–51, 2012.

89. Thurber, C.H., *Earthquake Locations and Threee Dimensional Crustal Velocity Structure in the Coyota Lake Area, Central California,* J. Geophys. Res, Vol. 88, pp. 8226-8236, 1983.

90. Thurber, C.H., *Hypocenter-velocity Structure Coupling in Local Earthquake Tomography,* Phys. Earth Planet. Inter., Vol. 75, pp. 55-62, 1992.

91. Thurber, C.H., *Seismic Tomography,* Chapman and Hall, London, pp. 563-583, 1993.

92. Um, J. and C. H. Thurber, *A fast algorithm for two-point seismic ray tracing,* Bull. Seismol. Soc. Am. 77: 972–986, 1987.

93. Üçer, S.B., N. Kafadar, D. Kalafat, Z. Öğütcü, *Orta ve Doğu Anadolu Deprem Ağının Kurulması,* Araştırma Fonu Raporu, 90T1030, 15 sayfa, Boğaziçi Üniversitesi, 1990.

94. Vlahovic, G., C. Powell, M. Lamontagne, *A three-dimensional P wave velocity model for the Charlevoix seismic zone, Quebec, Canada*, Geophys. J. Int., 08, B9 DOI: 10.1029/2002 JB002188, 2003.

95. Wang, J., D. Zhao, Z. Yao, *Crustal and uppermost mantle structure and seismotectonics of North China craton*, Tectonophysics, 582, 177-187, 2013.

96. Wang, Z., D. Zhao, *Seismic images of the source area of the 2004 Mid-Niigata prefecture earth- quake in Northeast Japan.* Earth Planet. Sci. Lett. 244, 16–31, 2006.

97. Wei, W., D. Zhao, *The 2008 Iwate-Miyagi earthquake (M 7.2) and arc volcanism: Insight from irregular-grid tomography*. Earth Sci. Frontiers 20, 155–171, 2013.

98. Xia, S., D. Zhao, X. Qiu, *The 2007 Niigata earthquake: Effect of arc magma and fluids*. Phys. Earth Planet. Inter. 166, 153–166, 2008.

99. Westaway R., *Present-day kinematics of the plate boundary zone between Africa and Europe, from the Azores to the Aegean,* Phys. Earth Planet. Inter. Volume 96, Issues 3–4, Pg 393–406, 1990.

100. Yoshida, K., A. Hasegawa, T. Okada, T. Iinuma, Y. Ito, Y. Asano, *Stress before and after the 2011 great Tohoku-oki earthquake and induced earthquakes in inland areas of eastern Japan*. Geophys. Res. Lett. 39, L03302, 2012.

101. Yükünç M., *Hisarcık (Kütahya) Çevresindeki Neojen Birimlerinin Stratigrafisi, Mineralojisi, Petrografisi ve Jeokimyası,* Master Tezi, Dokuz Eylül University, İzmir, 2007.

102. Zeng, X., Y. Luo, L. Han, Y. Shi, *The Lushan Ms 7.0 earthquake on 20 April 2013: A high-angle thrust event.* Chinese J. Geophys. 56, 1418–1424, 2013.

103. Zeschke, G., *Der Simav graben und seine gestine*. Bulletin of the Geological Society of Turkey. 5. 179-189, 1954.

104. Zhao, D., S. Horiuchi and A. Hasegawa, *3-D Seismic velocity structure of the crust and the uppermost mantle in the northeastern Japan,* Tectonophys., 181, 135-49, 1990.

105. Zhao, D., *A tomographic study of seismic velocity structure in the Japan Islands*, Ph.D Thesis, Tohoku University, Sendai, Japan, 301, 1991.

106. Zhao, D., A. Hasegawa and S. Horiuchi, *Tomographic imaging P and S wave velocity structure beneath northeastern Japan*, J. Geophys. Res, Vol. 97, pp. 19909-19928, 1992.

107. Zhao, D., *TOMOG3D Manual*, 1999.

108. Zhao, D., F. Ochi, A. Hasegawa, A. Yamamoto, *Evidence for the location and cause of large crustal earthquakes in Japan*. J. Geophys. Res. 105, 13579–13594, 2000.

109. Zhao, D., O. P. Mishra, R. Sanda, *Influence of fluids and magma on earthquakes: seismological evidence*. Phys. Earth Planet. Inter. 132, 249–267, 2002.

110. Zhao, D., M. Santosh, A. Yamada, *Dissecting large earthquakes in Japan: role of arc magma and fluids*. Island Arc 19, 4–16, 2010.

111. Zhao, D., H. Kitagawa, G. Toyokuni, *A water wall in the Tohoku forearc causing large crustal earthquakes*, Geophys J. Int. 200, 149-172, 2015.

112. Zhao, D., Z. Wang, N. Umino, A. Hasegawa, *Tomographic imaging outside a seismic network: Application to the northeast Japan arc*. Bull. Seismol. Soc. Am. 97, 1121–1132, 2007.

113. Zhao, D., Z. Huang, N. Umino, A. Hasegawa, T. Yoshida, *Seismic imaging of the Amur-Okhotsk plate boundary zone in the Japan Sea.* Phys. Earth Planet. Inter. 188, 82–95, 2011.

114. http://udim.koeri.boun.edu.tr, Boğaziçi Üniversitesi Kandilli Rasathanesi ve Deprem Araştırma Enstitüsü (Boğaziçi University Kandilli Observatory and Earthquake Research Institute).

115. www.deprem.gov.tr, AFAD Deprem Dairesi Başkanlığı, (Prime Ministry Diaster&Emergency Management Presidency).

116. www.mta.gov.tr, Maden Tetkik Arama (General Directorate of Mineral Research and Exploration).

APPENDIX A

Data Selection Criterias:

Table A.1. Initial 1-D velocity model for relocation procedure for AFAD(left), KOERI(middle), Combined data set(right)

Depth	Vp (km/s)	Vs (km/s)
0	3.750	2.020
3.0	5.800	3.410
13.0	6.330	3.930
35.0	7.180	4.650

Depth (km)	Vp (km/s)	Vs (km/s)
0	4.500	2.601
5.4	5.910	3.416
31.6	7.800	4.508
89.2	8.300	4.797

Depth (km)	Vp (km/	Vs (km/s)
0	4.850	2.600
5.0	5.700	3.295
11.0	6.300	3.642
32.0	7.450	4.306

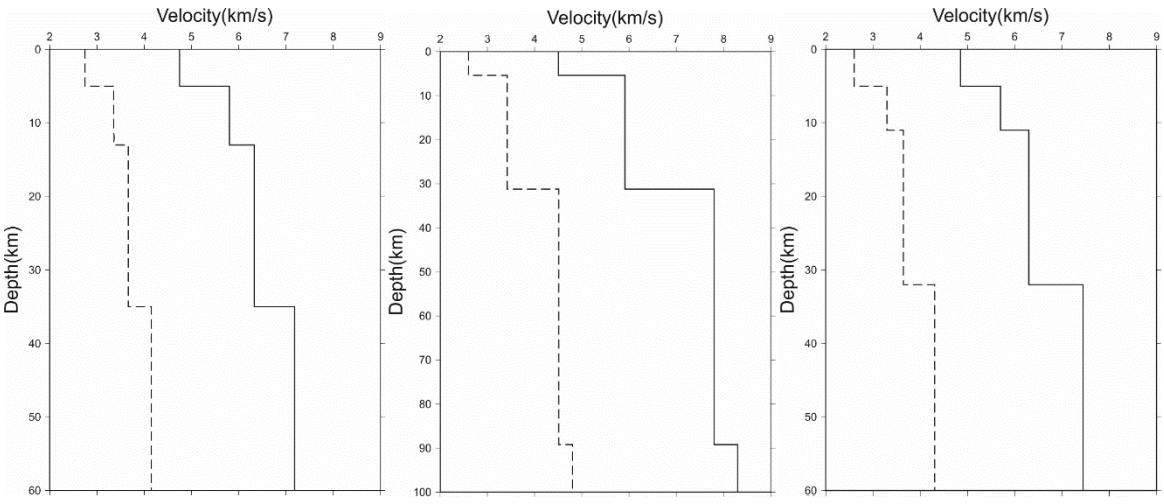


Figure A.1. Schematic view of used 1-D velocity models for location of earthquakes for AFAD(left), KOERI(middle), and Combined data set(right). Solid lines denote P-wave velocity, dashed lines denote the S-wave velocity.

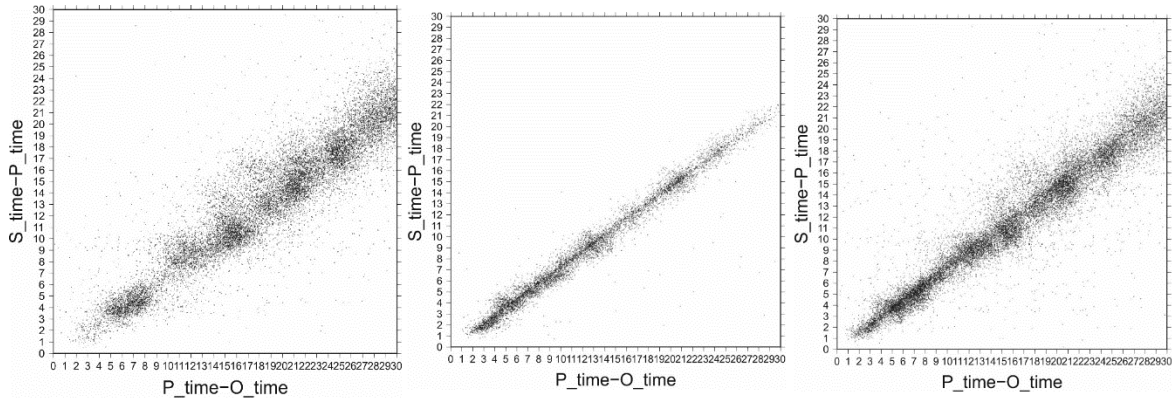


Figure A.2. Schematic view of Wadati diagram for AFAD(left), KOERI(middle), and Combined data set(right).

Station Distributions For 3 Different Data Sets:

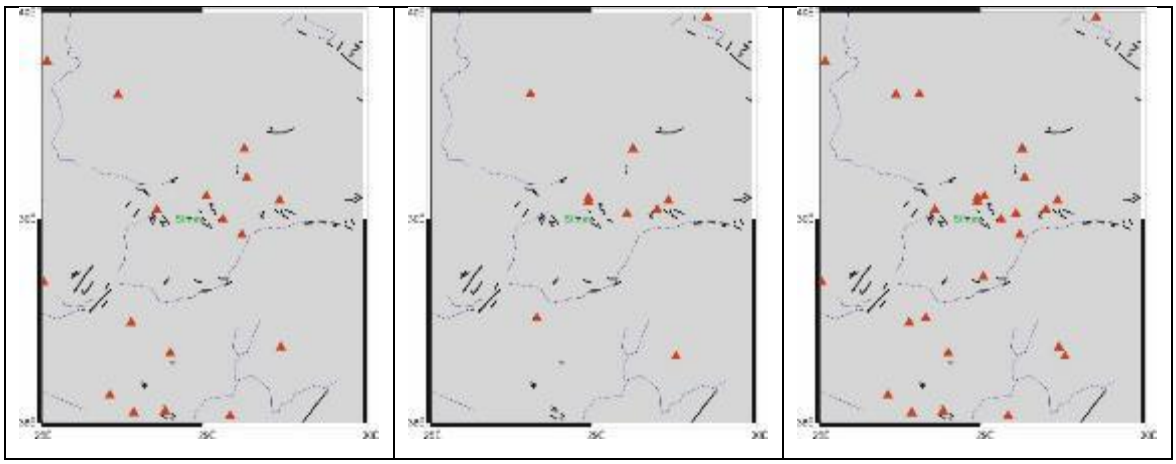


Figure A.3. Map view of the station distribution of the study region for AFAD(left), KOERI(middle), Combined data set(right)

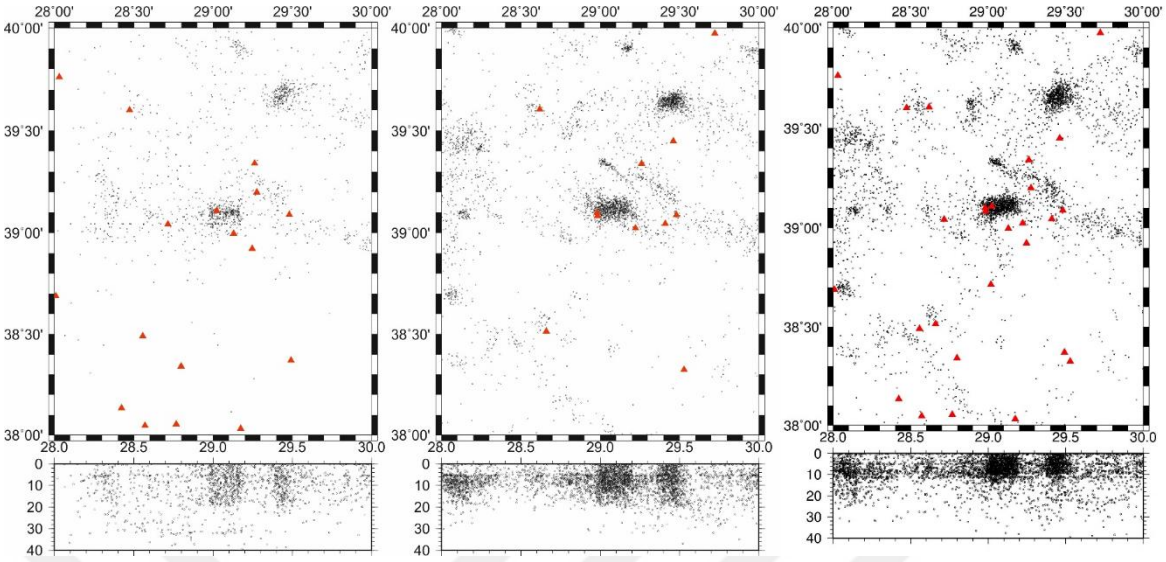


Figure A.4. Seismicity and station distribution of original data for AFAD(left), KOERI(middle), Combined data set (right). Red triangles show seismic stations and black dots show earthquakes.

Original Data Sets For 1-D Relocation:

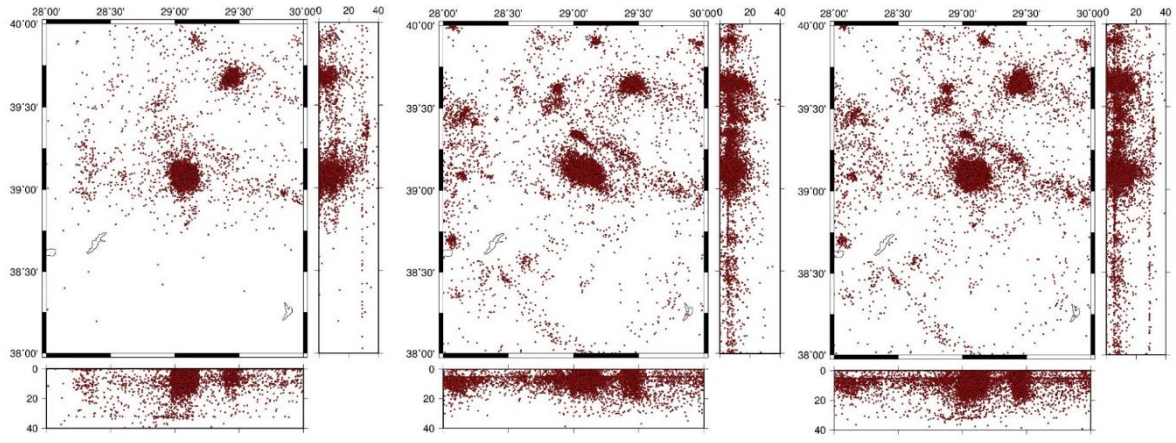


Figure A.5. Initial data sets for AFAD(left), KOERI(middle), Combined data(right).

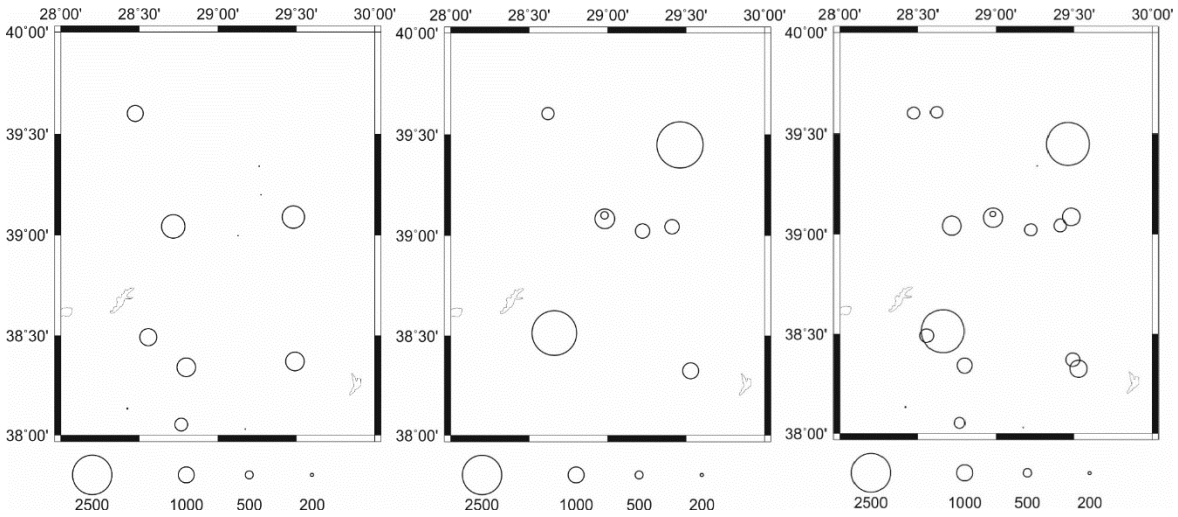


Figure A.6. Number of recorded earthquakes by each seismic station for AFAD(left), KOERI(middle), Combined data set(right).

Selected Earthquake Distribution For 3-D Inversion:

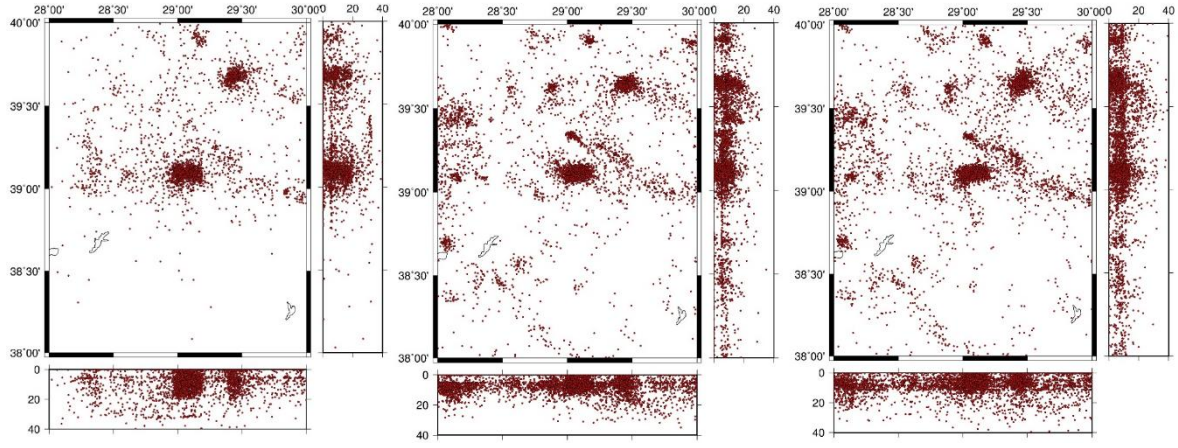


Figure A.7. Selected earthquakes for inversion AFAD(left), KOERI(middle), Combined earthquake data(right).

Grid Distribution Results:

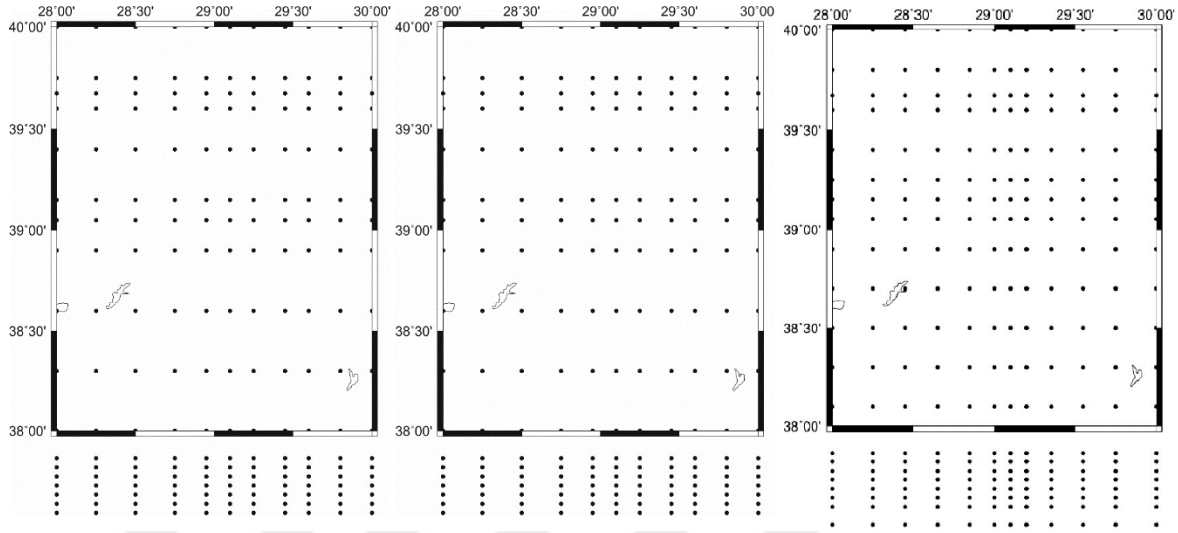


Figure A.8. Map view of horizontal and vertical grid distributons for AFAD(left), KOERI (middle), Combined data(right).

Checkerboard Resolution Test Results:

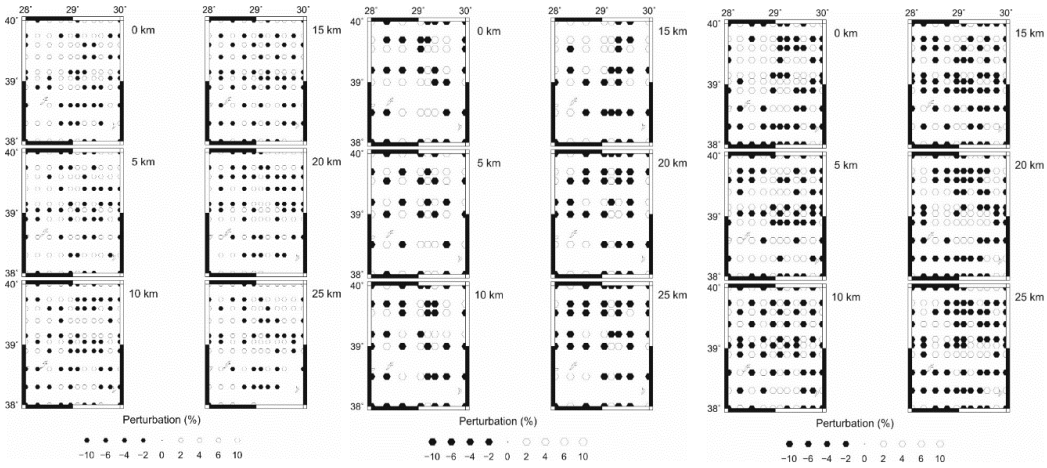


Figure A.9. Map view of checkerboard resolution tests for AFAD(left), KOERI (middle), Combined data(right).

Ray Density Results:

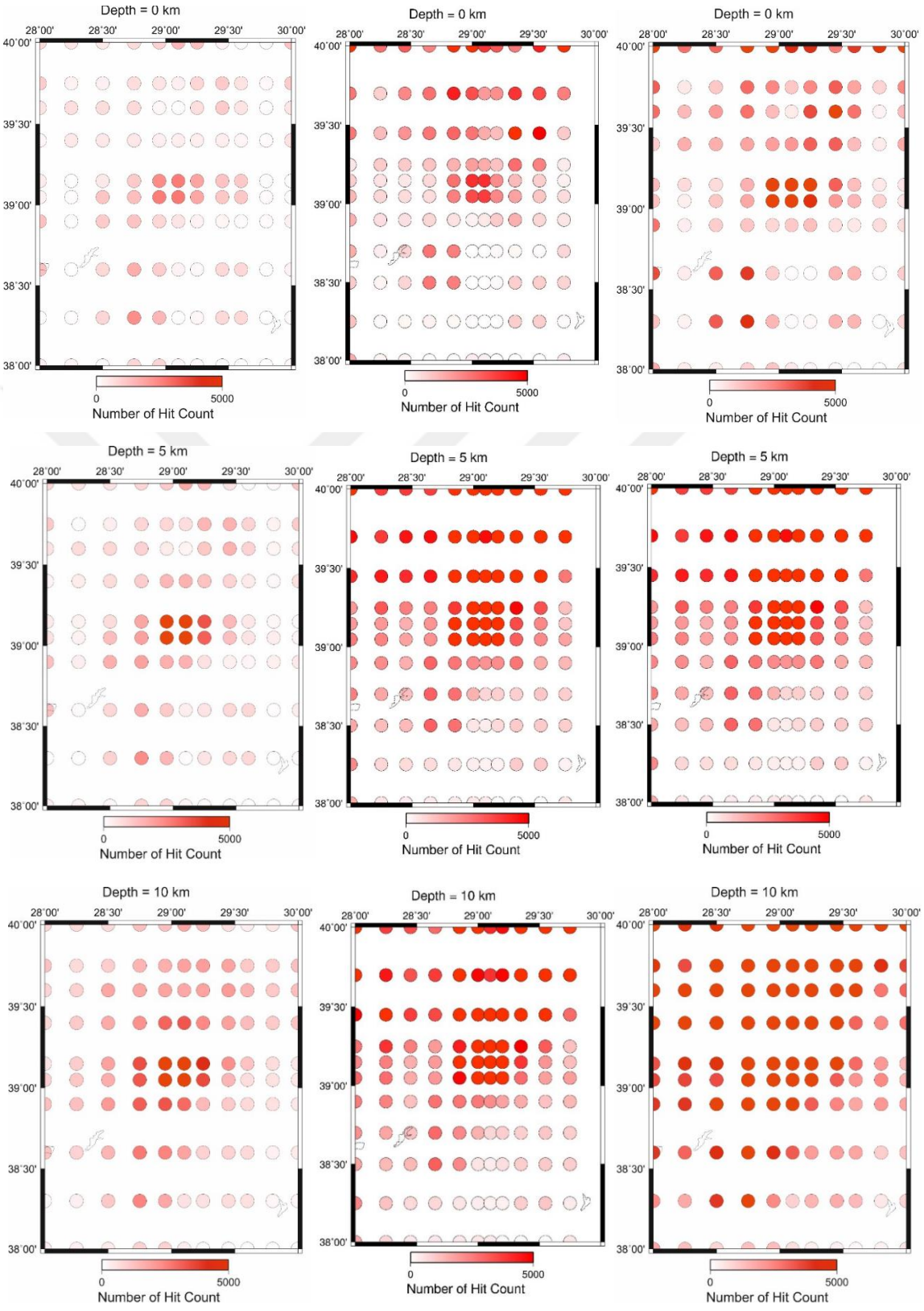
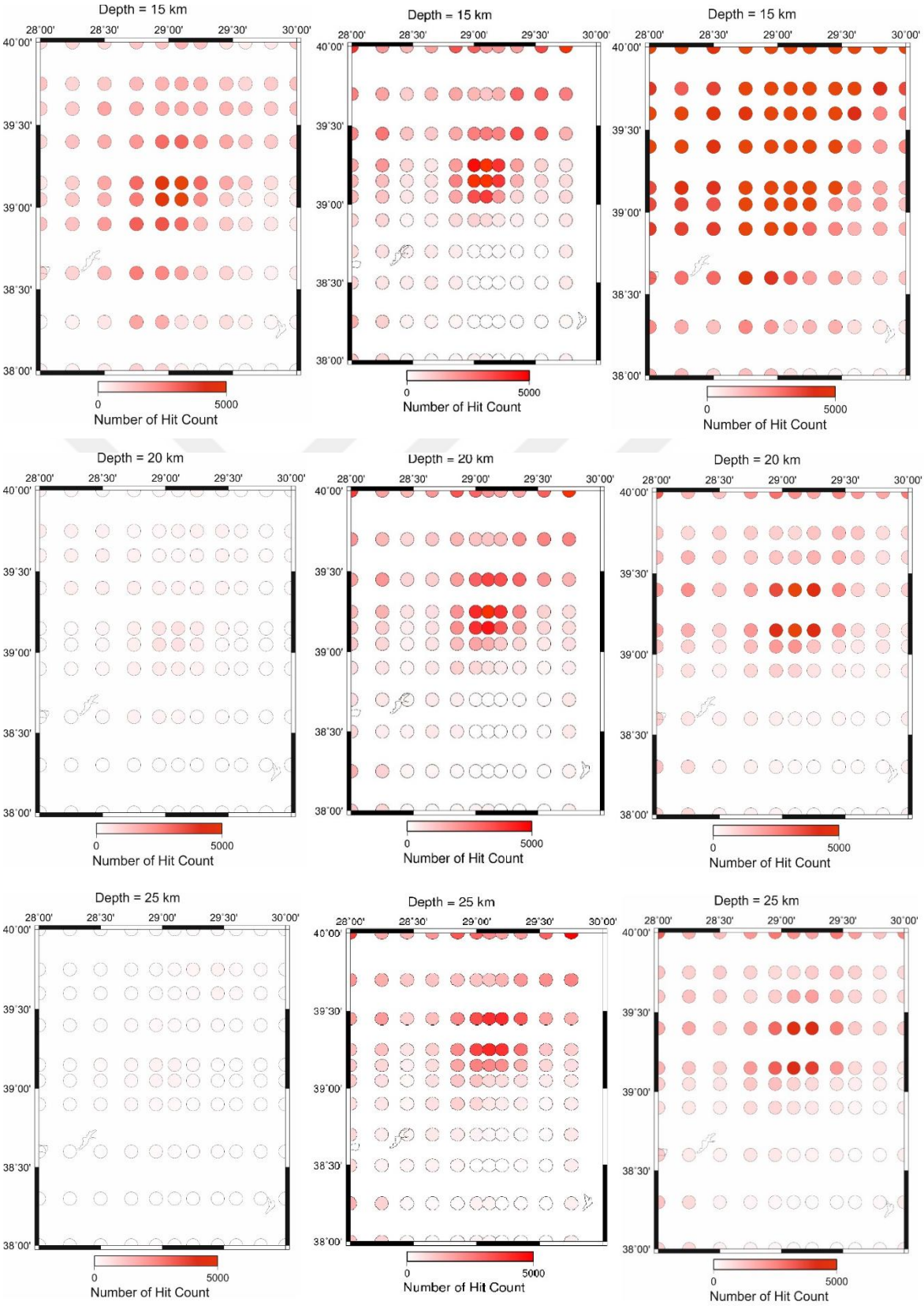
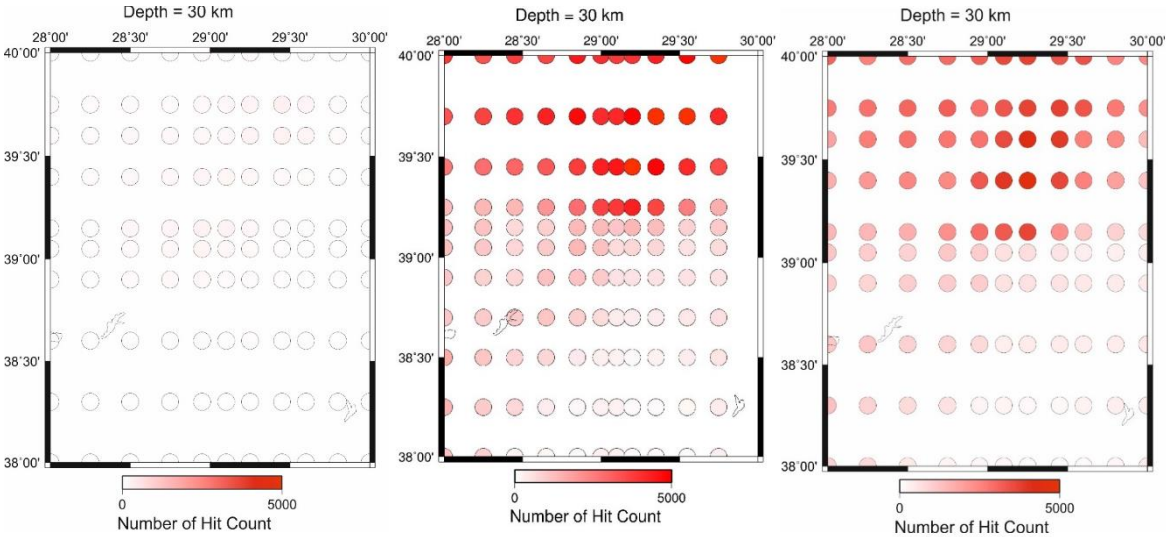


Figure A.10. (a) AFAD (b) KOERI (c) Combined data ray density for each grids.



Cont. Figure A.10. (a) AFAD (b) KOERI (c) Combined data ray density for each grids.



Cont. Figure A.10. (a) AFAD (b) KOERI (c) Combined data ray density for each grids.

P Wave 3-D Tomography Results:

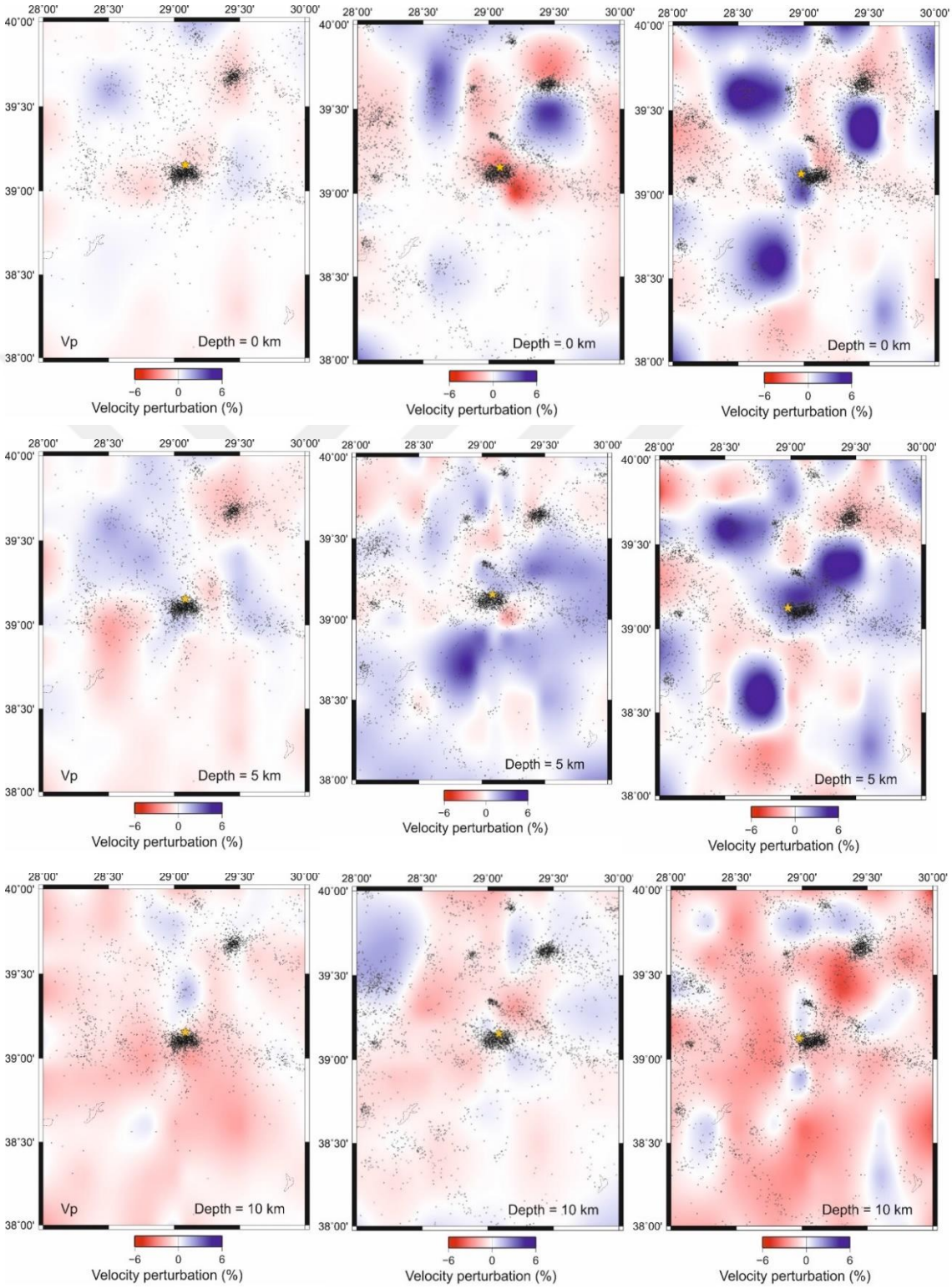
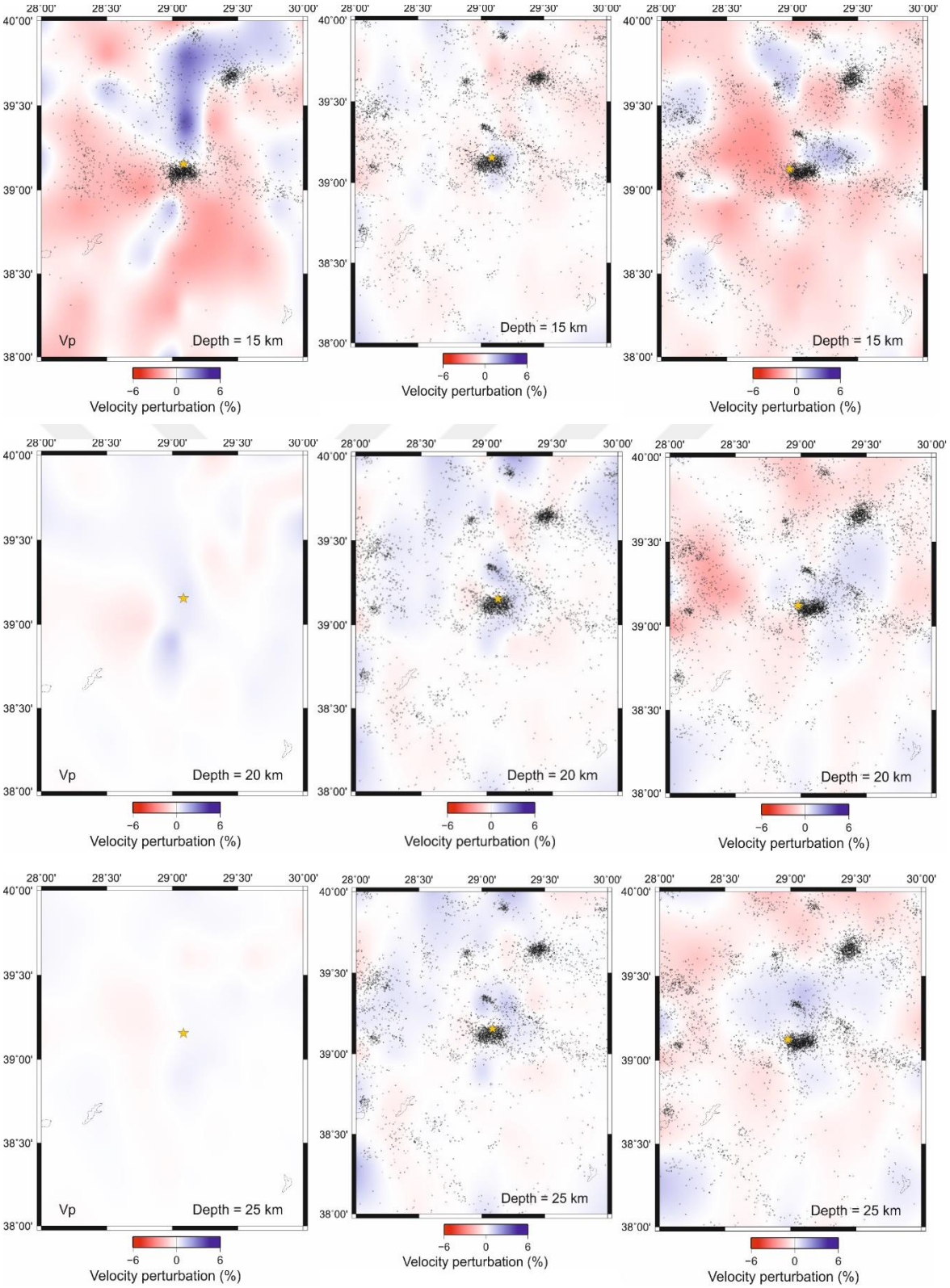
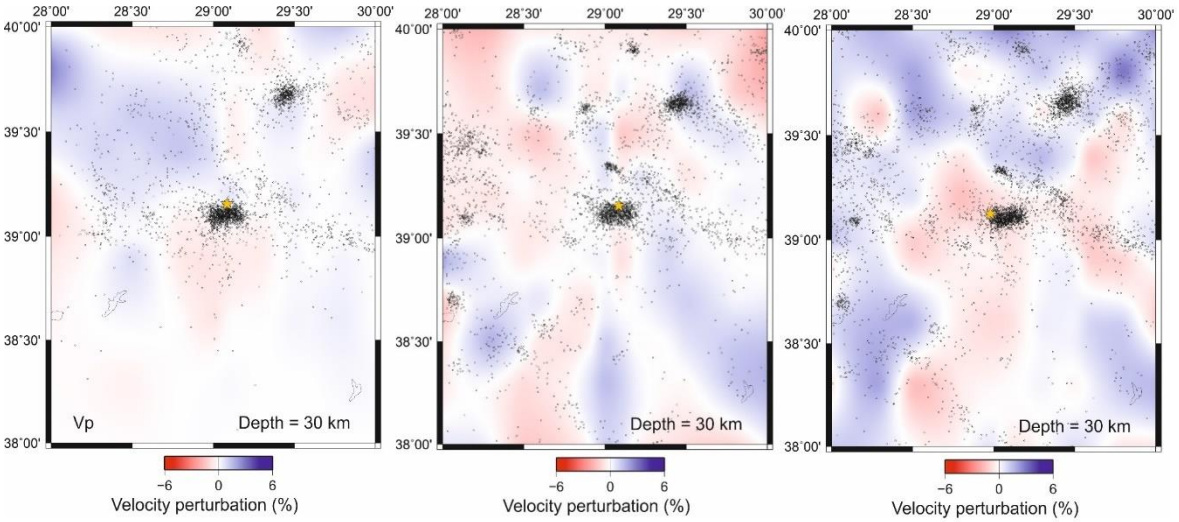


Figure A.11. (a) AFAD (b) KOERI (c) Combined data horizontal cross-section of Vp distribution



Cont. Figure A.11. (a) AFAD (b) KOERI (c) Combined data horizontal cross-section of Vp distribution



Cont. Figure A.11. (a) AFAD (b) KOERI (c) Combined data horizontal cross-section of Vp distribution

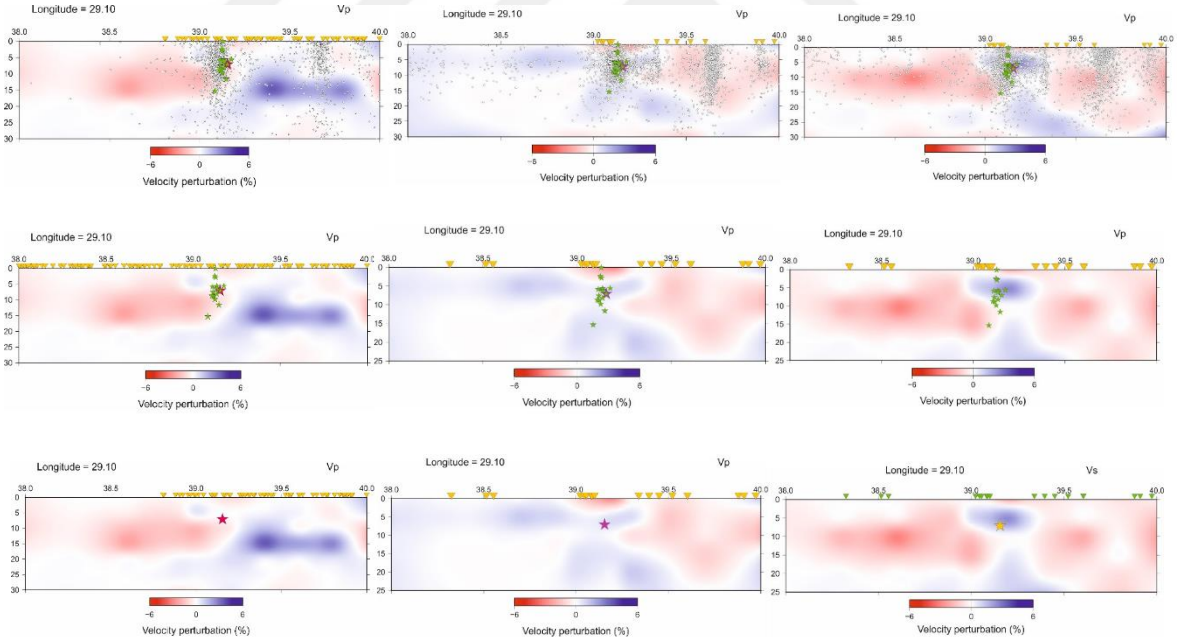


Figure A.12. (a) AFAD (b) KOERI (c) Combined data vertical cross-section of Vp distribution along 29.10°E longitude

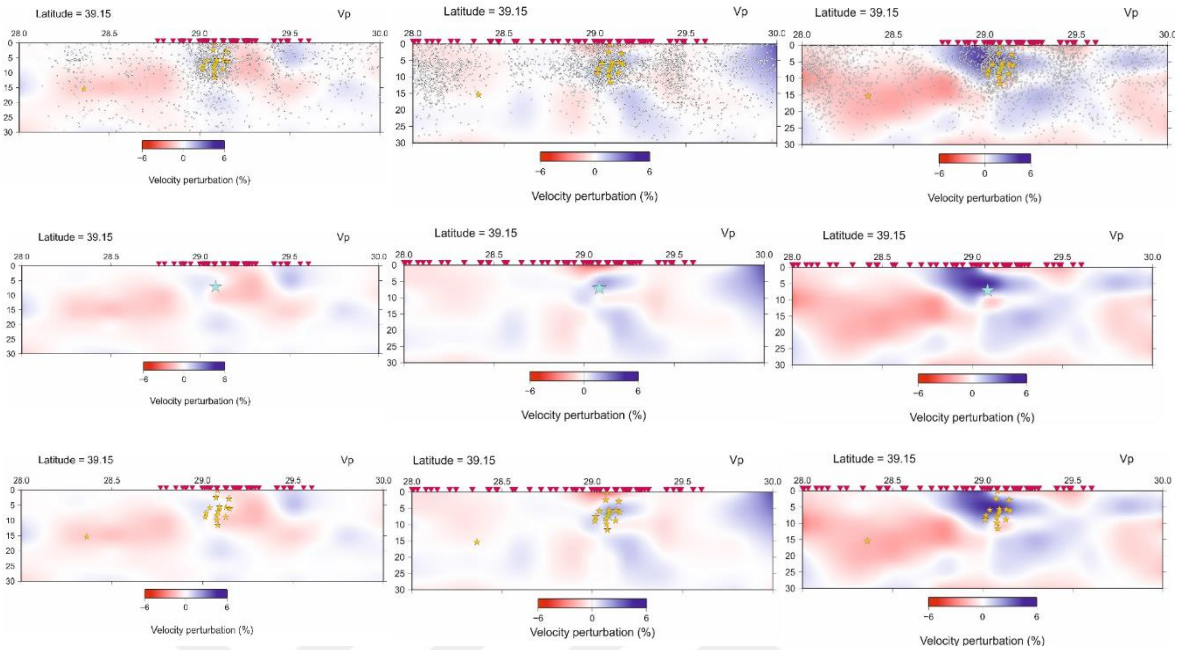


Figure A.13. (a) AFAD (b) KOERI (c) Combined data vertical cross-section of Vp distribution along 39.15°N latitude

S Wave 3-D Tomography Results:

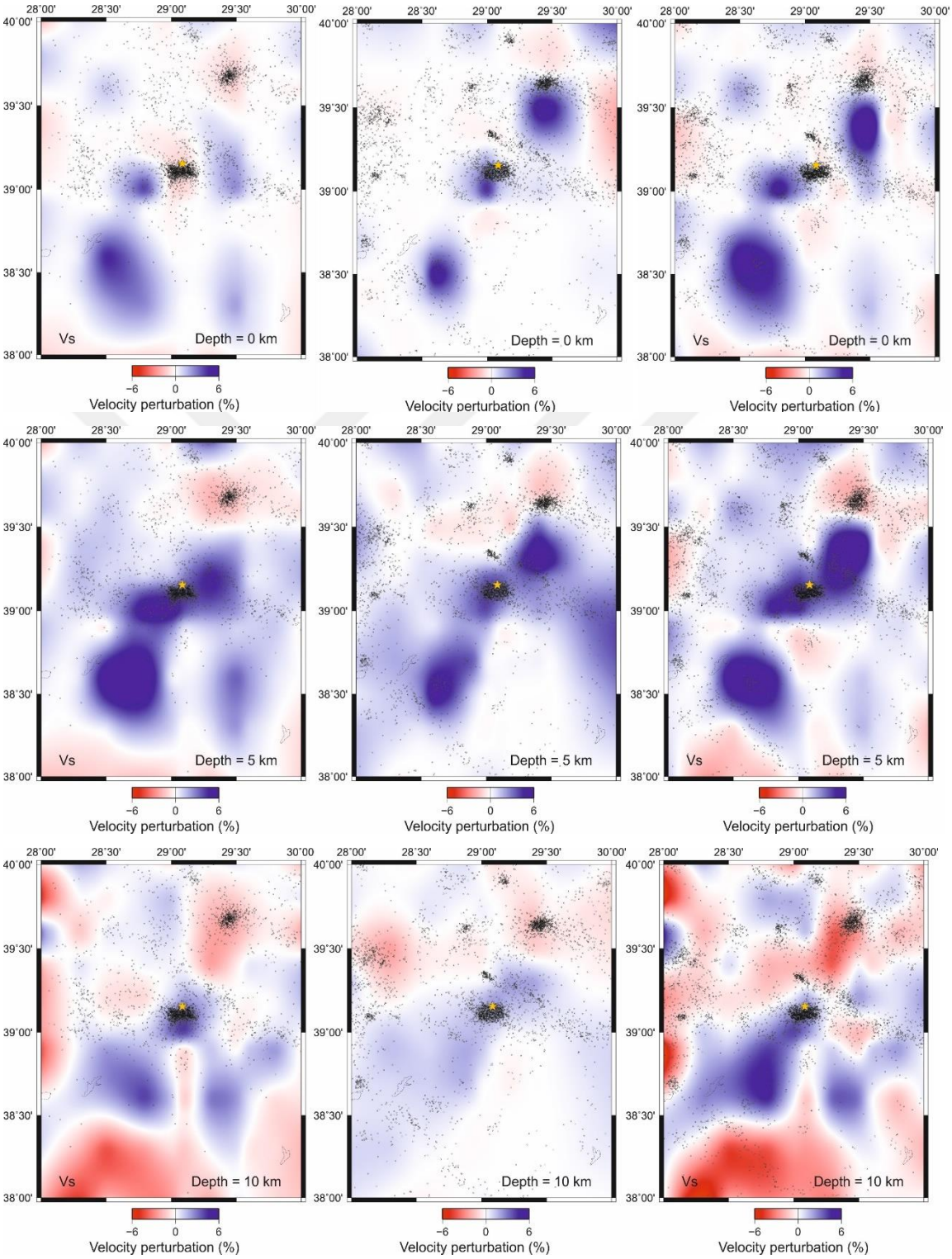
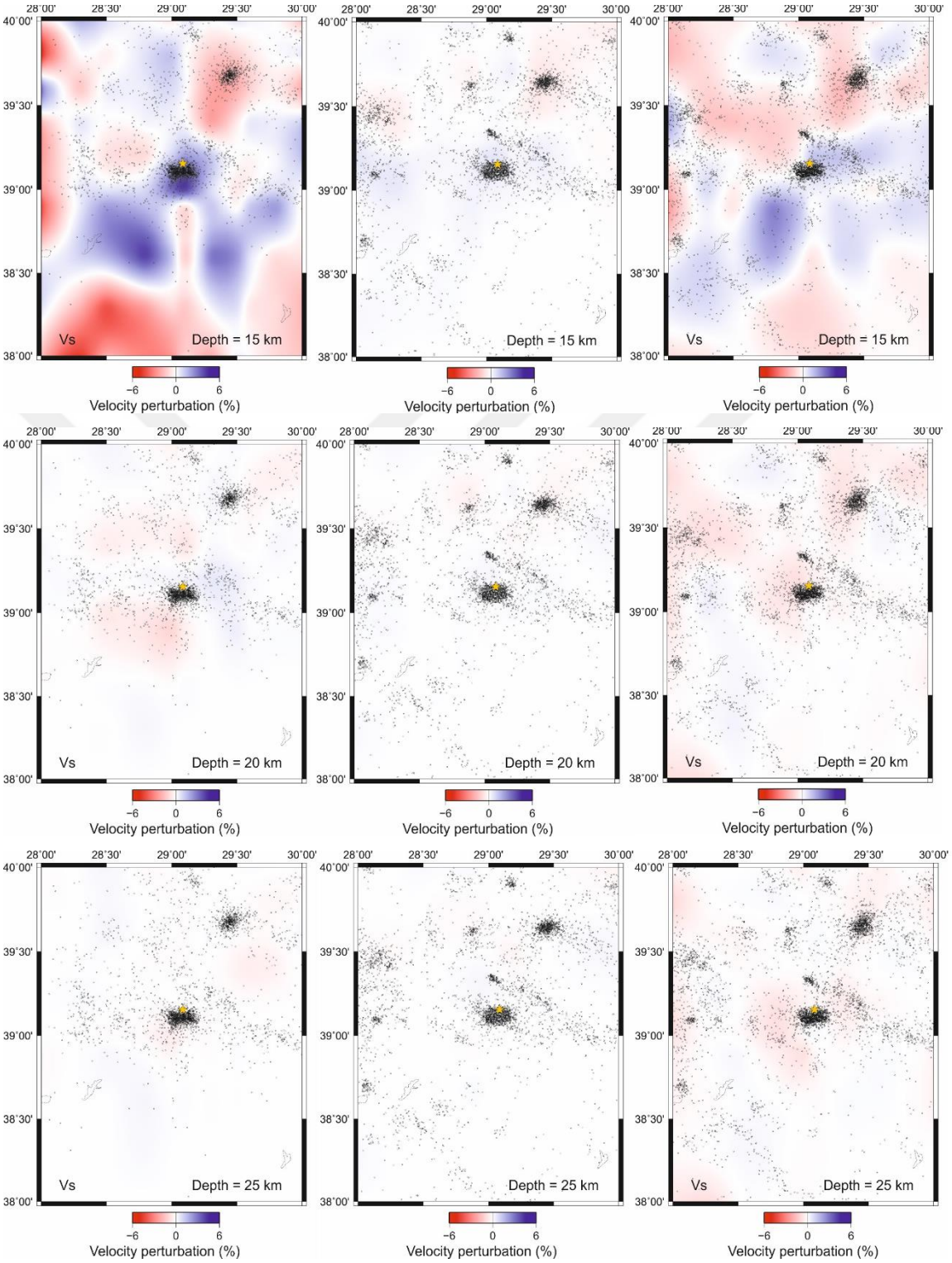
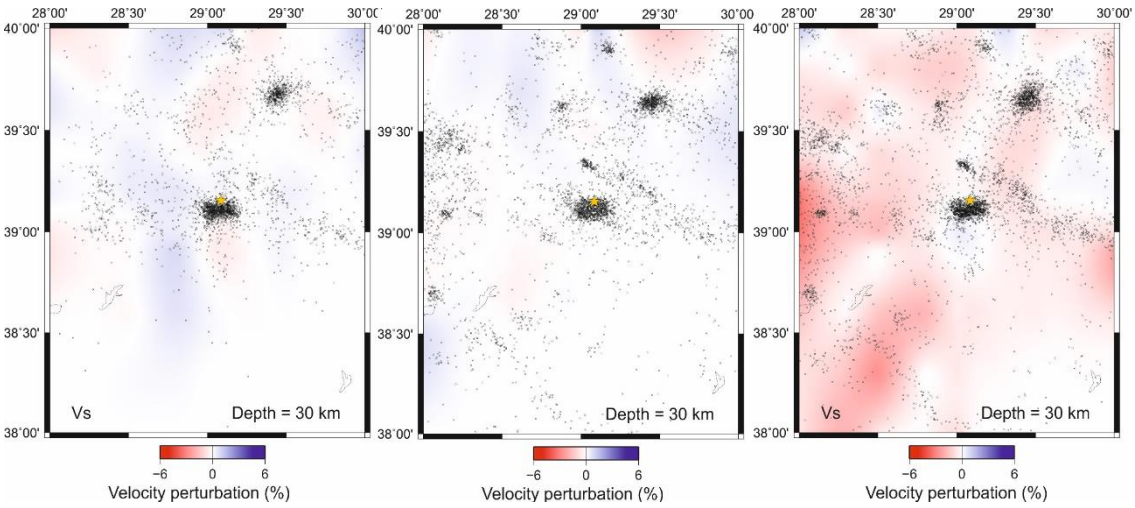


Figure A.14. (a) AFAD (b) KOERI (c) Combined data horizontal cross-section of Vs distribution.



Cont. Figure A.14. (a) AFAD (b) KOERI (c) Combined data horizontal cross-section of Vs distribution.



Cont. Figure A.14. (a) AFAD (b) KOERI (c) Combined data horizontal cross-section of Vs distribution.

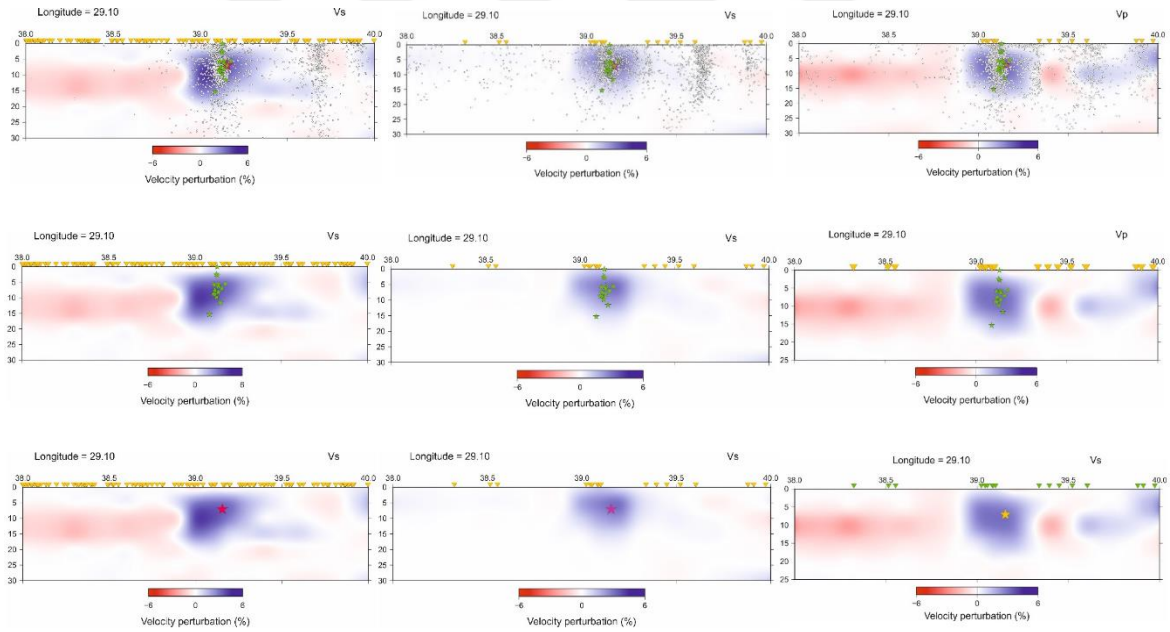


Figure A.15. (a) AFAD (b) KOERI (c) Combined data vertical cross-section of Vs distribution along 29.10° E longitude

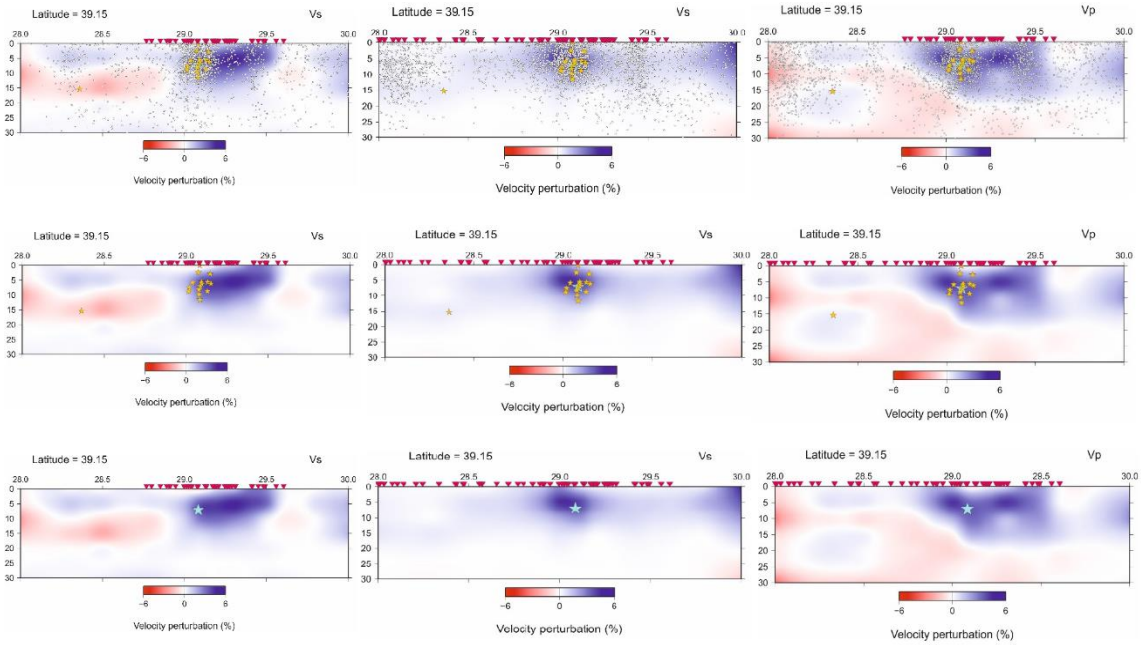


Figure A.16. (a) AFAD (b) KOERI (c) Combined data vertical cross-section of Vs distribution along 39.15°N latitude.

Vp/Vs Ratio 3-D Tomography Results:

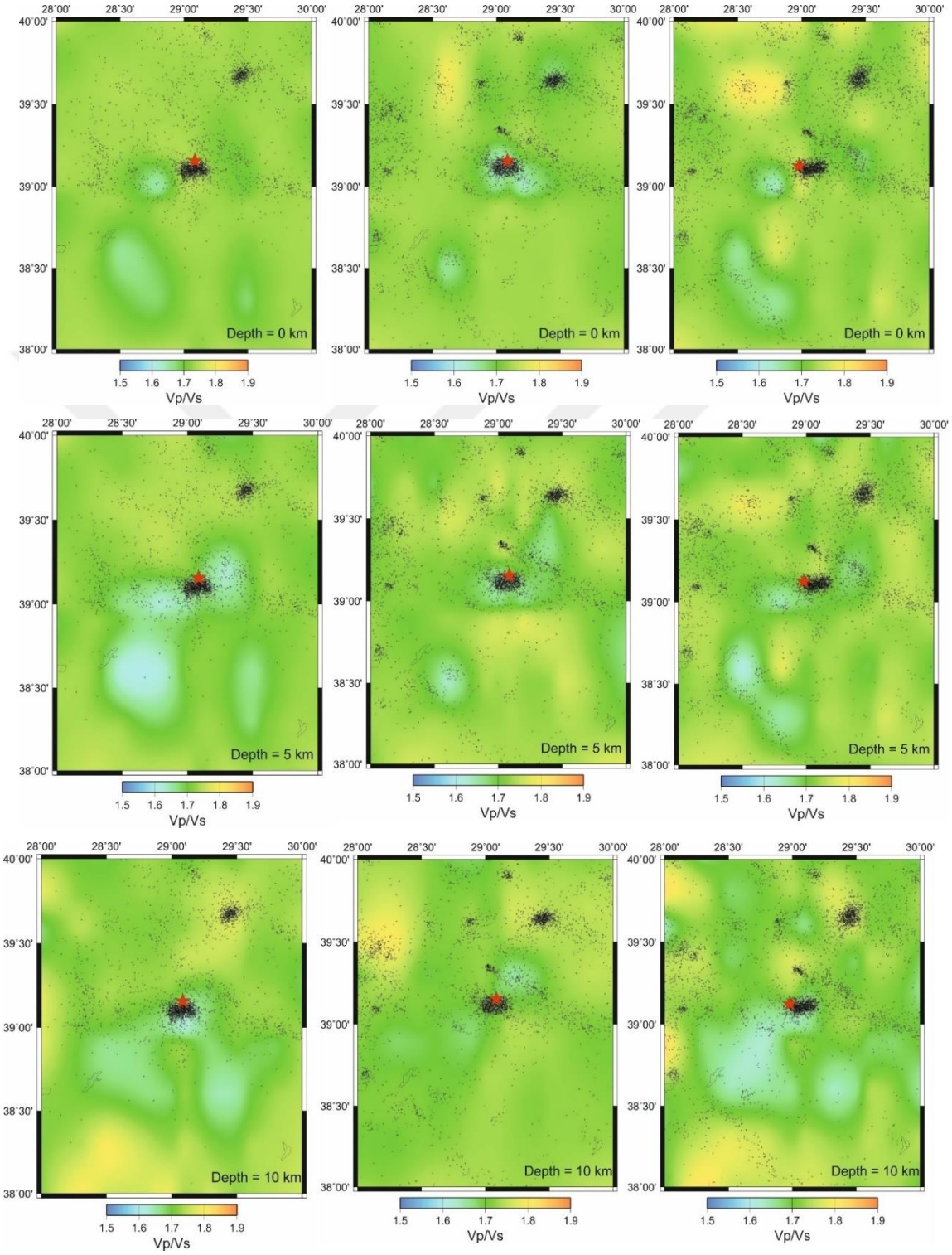
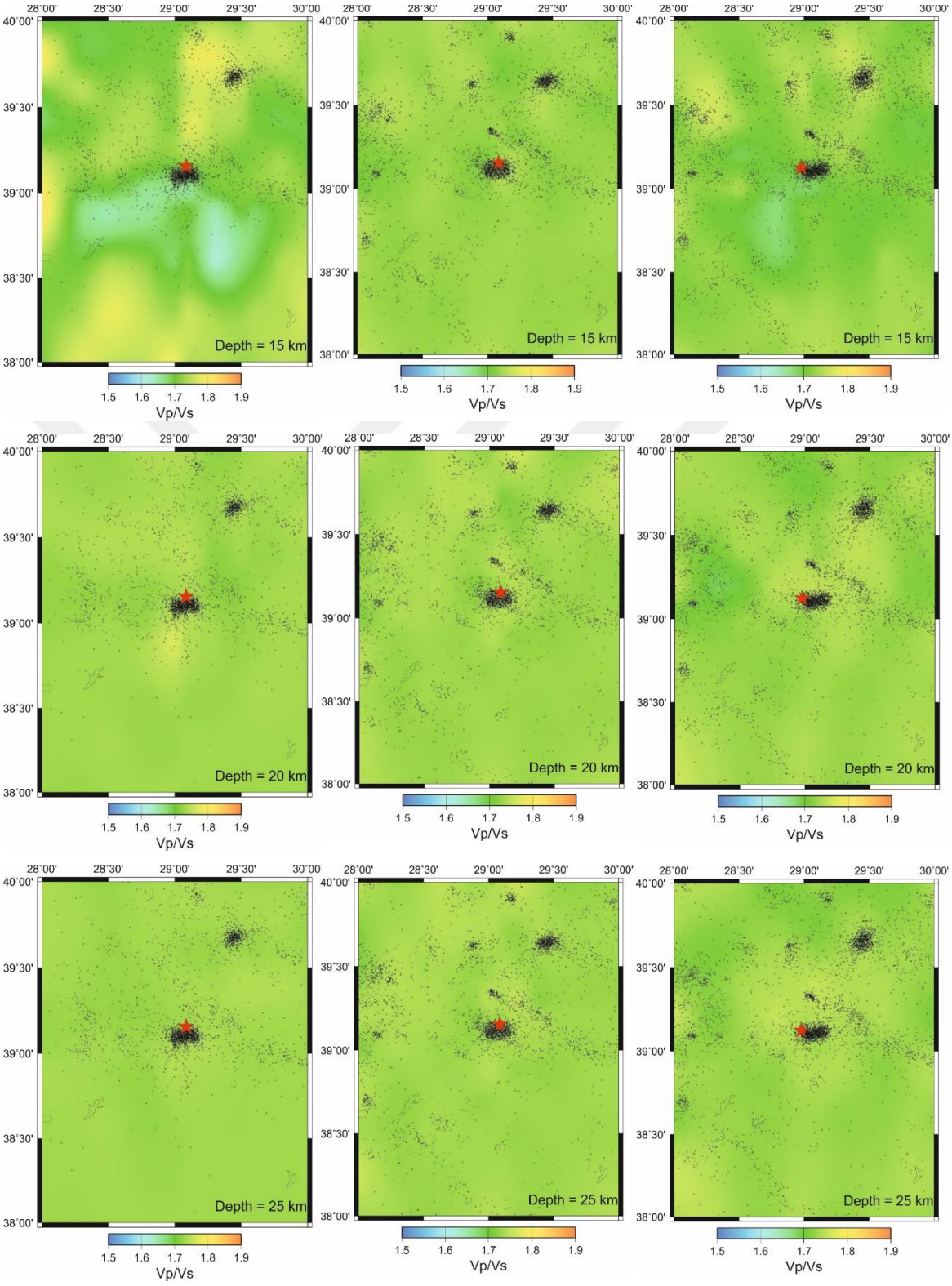
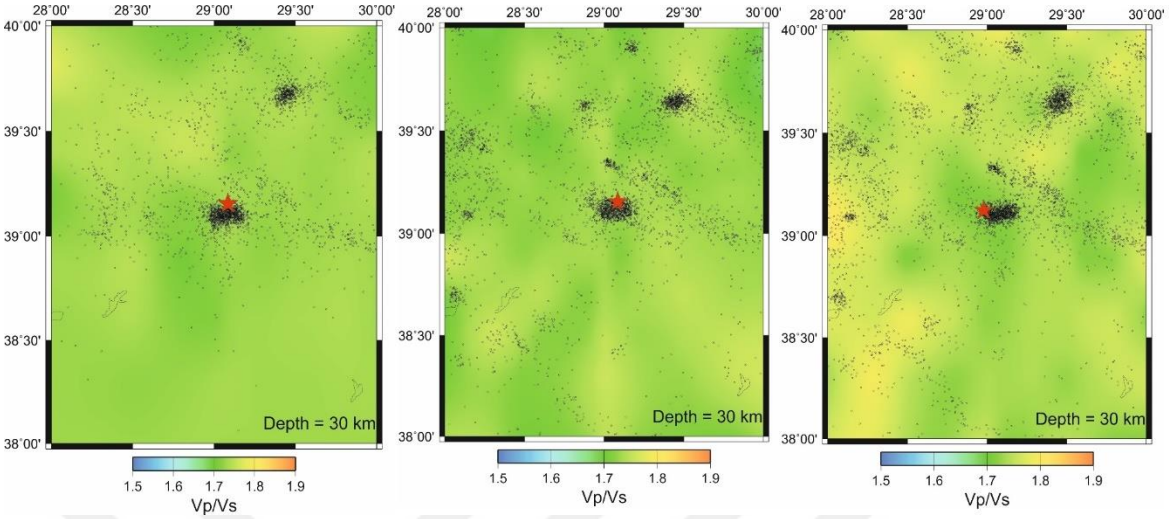


Figure A.17. (a) AFAD (b) KOERI (c) Combined data horizontal cross-section of Vp/Vs ratio distribution.



Cont. Figure A.17. (a) AFAD (b) KOERI (c) Combined data horizontal cross-section of Vp/Vs ratio distribution.



Cont. Figure A.17. (a) AFAD (b) KOERI (c) Combined data horizontal cross-section of Vp/Vs ratio distribution.

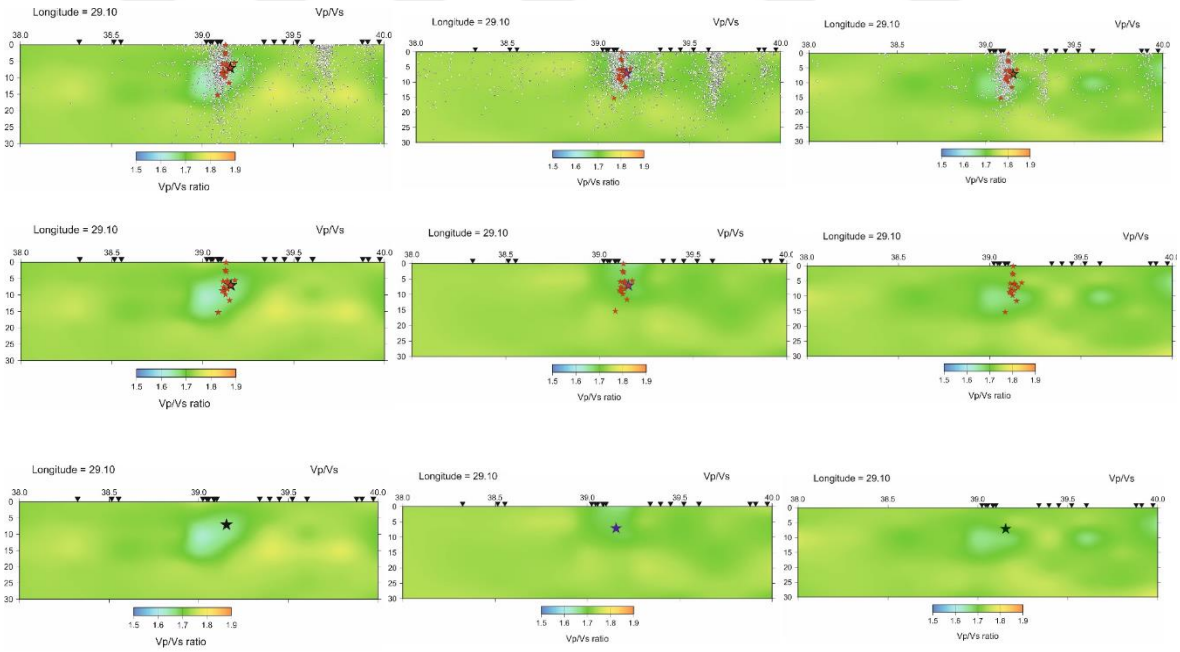


Figure A.18. (a) AFAD (b) KOERI (c) Combined data vertical cross-section of Vp/Vs ratio distribution along 29.10°E longitude

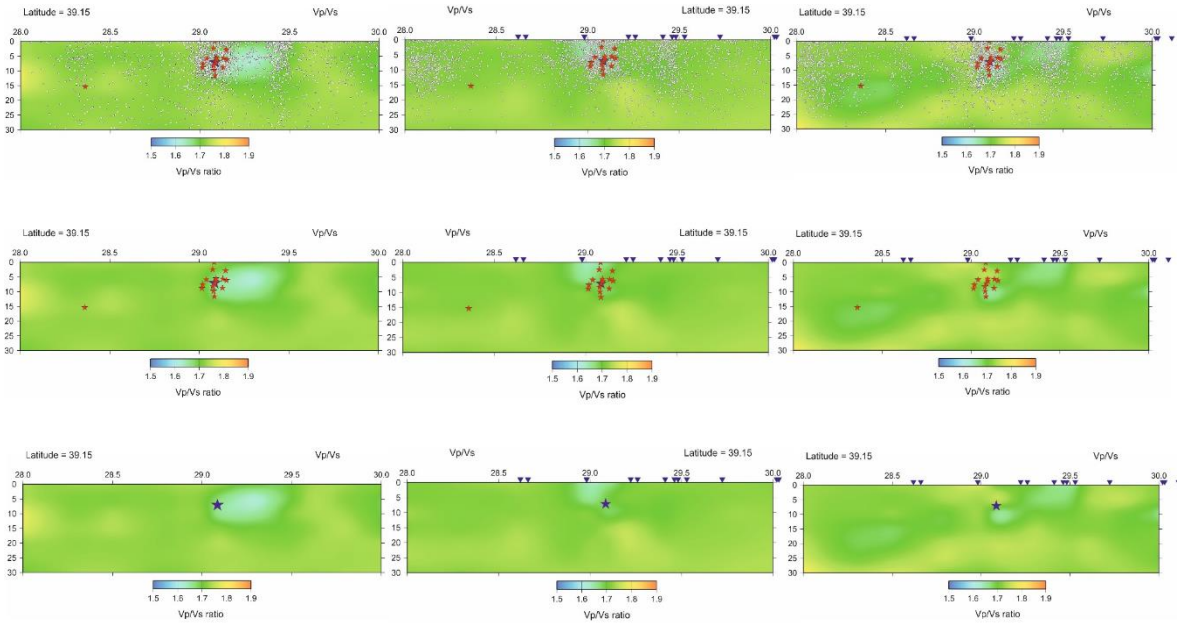


Figure A.19. (a) AFAD (b) KOERI (c) Combined data vertical cross-section of Vp/Vs distribution along 39.15°N latitude